PAUL SCHERRER INSTITUT

PSI

UNIVERSITÄT BERN

LABOR FÜR RADIO- UND UMWELTCHEMIE
DER UNIVERSITÄT BERN UND
DES PAUL SCHERRER INSTITUTS

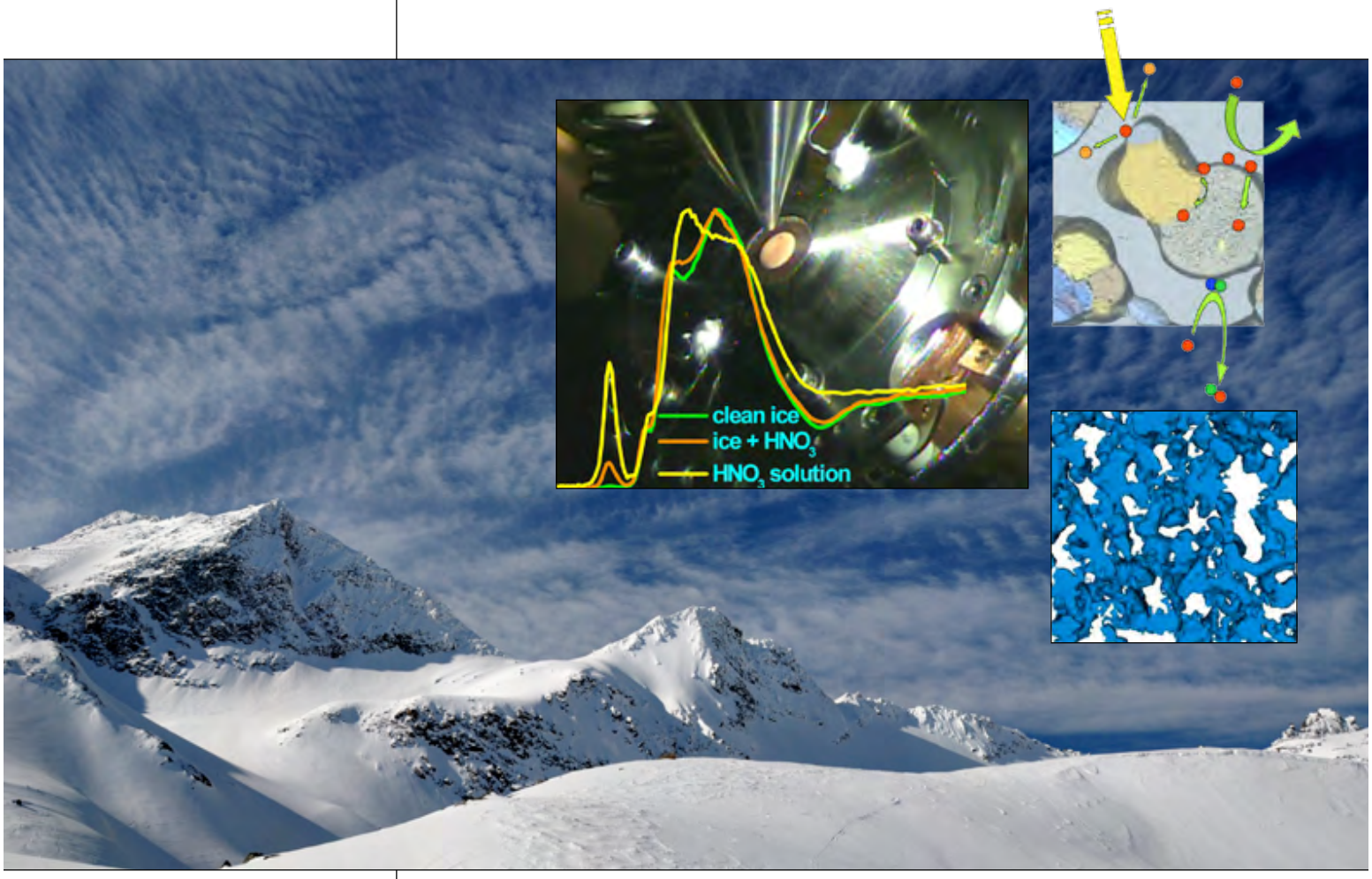

Annual Report 2010

January 2011

COVER:

Ice exists in various forms throughout the atmosphere. The background image shows two of them: Cirrus clouds in the upper troposphere and snow on the ground (Photo by Uta Philipp). On the surface of ice, heterogeneous chemical reactions relevant for atmospheric chemistry can take place. The 3D-reconstruction of data from X-ray microtomography of a snow sample at the lower right clearly shows the porous structure and high surface area of ice in snow (Photo from WSL/SLF Davos, Pinzer et al., J. Geophys. Res., 2010). The picture in the upper right, taken with a polarization microscope, illustrates the polycrystalline nature of ice grains, as the different crystal orientations result in different colors (Image by F. Riche, WSL/ SLF Davos). Symbols and arrows represent possible interactions for trace gases such as adsorption, diffusion into the bulk and along grain boundaries, photolysis and heterogeneous surface reactions. The upper left photograph is taken from an X-ray photoelectron spectroscopy experiment performed at the Advanced Light Source in Berkeley (USA) that provides direct information on the chemical composition and structure of the ice surface in the presence of trace gases (Křepelová et al., Phys. Chem. Chem. Phys., 2010). Electron yield O K-edge X-Ray absorption spectra are shown for a clean ice sample (green line), an ice with nitric acid sample (red line), and a nitric acid solution (yellow line). Research related to these topics is presented on pages 14–17 of this report.

PAUL SCHERRER INSTITUT

UNIVERSITÄT BERN

LABOR FÜR RADIO- UND UMWELTCHEMIE
DER UNIVERSITÄT BERN UND
DES PAUL SCHERRER INSTITUTS

Annual Report 2010

January 2011

Editors: A. Türler
M. Schwikowski
A. Blattmann

Reports are available from:
Angela Blattmann (angela.blattmann@psi.ch), Paul Scherrer Institut, 5232 Villigen PSI, Switzerland (See also our web-page: http://lch.web.psi.ch/)

Paul Scherrer Institut
Labor für Radio- und Umweltchemie
5232 Villigen PSI
Switzerland

Durchwahl +41 (0)56 310 24 04
Sekretariat +41 (0)56 310 24 01
Fax +41 (0)56 310 44 35

Universität Bern
Departement für Chemie und Biochemie
Labor für Radio- und Umweltchemie
Freiestrasse 3, 3012 Bern, Switzerland

Durchwahl +41 (0)31 631 42 64
Sekretariat +41 (0)31 631 42 42
Fax +41 (0)31 631 42 20

TABLE OF CONTENTS

Analytical Chemistry

Radwaste Analytics

Radionuclide Development

Environmental Radionuclides Universität Bern

EDITORIAL

At the end of 2010 I take the opportunity to let the past year pass in review and appreciate what we have accomplished, but also look ahead to the challenges that we will have to master in the future.

Our annual report summarizes the so far unpublished scientific results of ongoing research in our unit, but also gives the audience an impression what our mission is and where we are heading.

After one year the Laboratory for Radiochemistry and Environmental Chemistry is well integrated into the new department "Biology and Chemistry" at PSI which is headed by Prof. Gebhard F.X. Schertler (simultaneously head of the Laboratory of Biomolecular Research (BMR)). Prof. Roger Schibli officially became head of the Center of Radiopharmaceutical Sciences (ZRW) also belonging to the BIO department, with which we already entertain close collaborations.

In 2010 we initiated several new projects that all have been funded by various institutions. Just before Christmas I was able to sign a collaboration agreement with the Laboratory of Ion Beam Physics at ETHZ (Prof. Hans-Arno Synal) which will allow us to purchase and operate a MICADAS accelerator mass spectrometer at Bern University for ultralow level ^{14}C measurements. This world class instrument combined with the know-how at LCH and LIP will boost our efforts in aerosol- and climate research. Credit for this superb accomplishment goes to PD Dr. Sönke Szidat who coordinated the consortium of applicants and did a fantastic job in writing the successful R'equip proposal. The project will be financed by three main contributors, the University of Bern with its Oeschger Centre, which will coordinate the research, the Swiss National Science Foundation (SNF), and the Bundesamt für Gesundheit (BAG) that has expressed its continued interest in ^{14}C measurements in the environment. Another project approaching almost the same financial dimension within the next few years was successfully proposed by Dr. Markus Ammann to the PSI Forschungskommission. His group will be involved in setting up a near ambient pressure photo electron spectrometer at one of the SLS beam lines, in collaboration with Prof. J. van Bokhoven (ETHZ/SLS/ENE). This method will be used for surface chemistry applications in environmental science and catalysis. Last, but not least, our efforts to contribute to radiopharmaceutical research with our radiochemical know-how have been met with great support. In collaboration with SWAN Isotopen AG at the Insel Hospital of Bern University we have been charged to equip and operate a research and development laboratory for the production of novel radiopharmaceuticals. Thanks to the excellent work of Dr. Konstantin Zhernosekov and the generous support of Bern University we were able to place an order for research hot cells and associated equipment under great time pressure. We are looking forward to start operating the new laboratory already by mid 2011! All three projects underline the excellent reputation that LCH is having at PSI and Bern University, but will require all our dedication and skills to make them a success.

LCH is not only very successful scientifically, but also very competitive in sports. At the Sola-Staffette our team "Chemie-Fäger" (14 team members) reached rank 91 out of 729 teams with an average of 4:45 min/km. A bit less successful was the choice of the date for our social event which should have taken us to the Plaine Morte glacier, but had to be cancelled due to weather conditions. Thanks to an excellent idea by Silvia Köchli a last minute change of plans took us to Basel instead, where we visited the city and the exposition "2 Grad" about climate and climate change, followed by a tour on the river Rhine. Despite the short notice almost the entire staff of LCH was participating and after lots of rain in the morning enjoyed some sunshine in the late afternoon.

It is rewarding to see LCH continue to thrive. On the one side this is due to the excellent conditions that PSI and Bern University are providing, on the other side it is due to the dedication of every member of LCH to accomplish the extraordinary as a team. In this respect I am proud to be the leader and happy to be a member of this team.

Andreas Türler

THERMAL RELEASE OF p-ELEMENTS FROM METAL MATRICES

D. Wittwer, R. Eichler, H.W. Gäggeler, A. Türler (Univ. Bern & PSI), R. Dressler, D. Piguet, A. Vögele (PSI)

Thermal release properties of group 13 and 14 elements from metal foils and from Si, and Ge were studied.

INTRODUCTION

Nowadays gas-jet transport is instrumental to investigate short-lived, volatile transactinides [1], but it has some drawbacks. The first drawback is a possible aerosol particle transport affecting the experimental outcome. A second drawback is a possible contamination of the gas and hence of the stationary chromatography surface. A lowered energy resolution of the alpha spectroscopic measurement in the gas is a third drawback. Therefore, a change to vacuum chromatography is envisaged in our project. However, the gas-free setup requires some new ideas to stop the incoming evaporation residues (EVR) produced in nuclear fusion reactions. In the gas-jet system the EVR's are thermalized in the transport gas. In vacuum, a medium must be provided which stops the EVR. A possible solution would be the recoil implantation in a thin metal foil, which can be heated up quickly or is permanently held at high temperatures. Dependent on the material-implant combination a fast release of the EVR is possible, which is then injected into the directly coupled vacuum chromatographic system. Here, we try to elaborate release data for volatile p-elements of group 13 and 14 from metal matrices and from the semiconductor materials silicon and germanium.

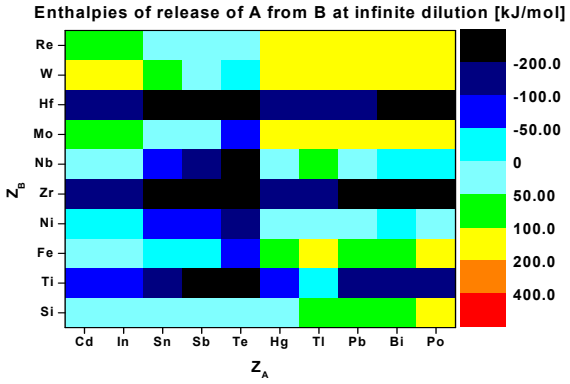

Fig. 1: Miedema release enthalpies for heavy p-elements.

EXPERIMENTAL

MIEDEMA model calculations [2,3] were performed to deduce the best performing materials for the thermal release of p-elements. (see Fig.1). A zinc, cadmium, and mercury alloy target was prepared on a 20 micrometer gold backing foil and irradiated at the Philips Cyclotron at PSI, Villigen, Switzerland with 35 MeV He^{2+} and a beam current of about 120 nA_{el}. Behind the target, catchers were installed to collect the EVR's. After irradiation the catchers were immersed into concentrated nitric acid (65 %) to remove all absorbed and not implanted activities and sputtered target material. Subsequently, the samples were measured using an HPGe-γ-detector in conjunction with an acquisition and analysis system based on standard electronics and data acquisition system (Canberra's Genie2k®). Afterwards, the foils were heated in a setup as shown in Fig. 2. The heating times and temperatures were varied to gain different data points (see e.g. Fig. 3). The sample was cooled down and measured again to determine the relative release yield.

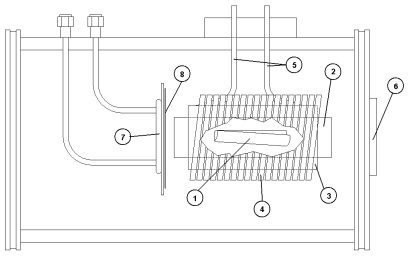

Fig. 2: Schematic of the vacuum release setup. Implantation foil (1) in a tantalum crucible (2) centered by a corundum space holder (3) which is wrapped by the copper coil (4) of the induction furnace. Water cooling of the induction furnace (5). The closed end of the tantalum crucible points towards the vacuum window (6) to measure its temperature with the pyrometer. The open end of the tantalum crucible points towards the cooled carrier (7) holding the tantalum foil (8) to collect the released products.

RESULTS

The experiments were conducted using Si, Ni, Ge, Y, Zr, Nb, Mo, Hf, W, Re, and steel as catching materials. Promising release results were found for heating times of 15 min or 60 min. The relative release increases within the group towards the heavier homologues of elements 113 and 114, see Fig. 3. More experiments, especially with shorter release times will be performed.

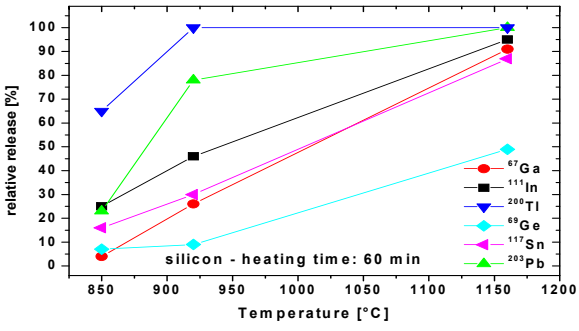

Fig. 3: Relative release of group 13 and 14 elements from silicon at different temperatures. Heating time: 60 min.

REFERENCES

[1] R. Eichler et al., Radiochim. Acta, **98**, 133 (2010).
[2] A. R. Miedema, J. Less-Common Met., **45**, 237 (1976).
[3] D. Wittwer et al., Ann. Rep. Lab. of Radio- & Environ. Chemistry, Uni. Bern & PSI (2009), p. 9.

THE THERMAL RELEASE OF SCANDIUM FROM TITANIUM METAL – A SIMPLE WAY TO PRODUCE PURE ^{44}Sc FOR PET APPLICATIONS

D. Wittwer, R. Eichler, H.W. Gäggeler, A. Türler (Univ. Bern & PSI), R. Dressler, D. Piguet, A. Vögele (PSI)

Thermal release properties of scandium from titanium were studied.

INTRODUCTION

Despite the increasing number of cyclotron installations at medical centers, the delivery of radionuclides by generator systems is still considered the most convenient way to provide isotopes to medical installations located away from nuclear reactors or accelerators. The ^{44}Ti/^{44}Sc system gains importance, since trivalent metals are frequently discussed for labeling of radiopharmaceuticals. The ideal half-life of ^{44}Sc ($T_{1/2}$= 3.97 h) permits the use of this isotope for labeling slow biological processes. Its big positron emission branch of 94.3 % [1] allows for smaller doses to be used for labeling. Moreover, ^{44}Ti with a half-life of 58.9 ± 0.3 y [2] yields an almost constant ^{44}Sc activity over several decades. An efficient procedure must be elaborated to gain the daughter activity with high yields and purity. The obtained product must be in a chemical state to be easily available for further processing, while the parent nuclide should remain completely in the radionuclide generator. Simple handling in terms of security as well as chemical and mechanical stability of the radionuclide generator systems is a further important point. Several attempts were undertaken to design ^{44}Ti/^{44}Sc generators, e.g. [3]. First clinical studies were performed using this kind of radionuclide generator system [4,5]. These methods comprise liquid separation using ion exchange, liquid extraction or distillation of thionylchloride adducts. We propose here another convenient way to separate the desired scandium from its titanium matrix by thermal release in vacuum.

EXPERIMENTAL

The irradiated samples [6] were immersed for 5 min in HNO_3 (65 %) trying to dissolve all adsorbed and not implanted activities. Subsequently, the titanium foil was cut into small pieces. Each piece was measured to determine the scandium content using a HPGe-γ-detector in conjunction with an acquisition and analysis system based on standard electronics and data acquisition system (Canberra's Genie2k®). The activities of the whole irradiated samples were typically some 100 kBq. Afterwards the metal foil was placed into tubular tantalum crucible where one side was closed, see Fig. 1 from [6]. The crucible containing the irradiated titanium samples was heated up to a defined temperature between 900°C and 1420°C and kept at this temperature for a certain time between 15 and 60 min. The heating was switched off and the crucible was cooled down for 15 min. The extracted titanium foil was measured again on the HPGe-γ-detector to determine the remaining scandium. This data was used to determine the relative release yield. The tantalum foil, which collected the evaporated products, was also measured on the detector to monitor the separation factor. Finally, this tantalum foil was washed with HCl (36%) to recover the released scandium isotopes.

RESULTS

The separation of scandium from a titanium matrix by thermal release appears possible. Quantitative yields are achievable without any problems above certain temperatures. Fig. 1 shows, for example, the release plot of ^{46}Sc for different heating times. At temperatures around 1200°C and heating times of 60 min an almost complete release was observed. This means that no scandium activity was found in the titanium foil after the heating process above the background of the detection system. Below 1000°C the release of the scandium decreases. Presumably, almost no release can be expected at heating temperatures below 600°C. As seen in Fig. 1, the heating time is of minor importance at high temperatures.

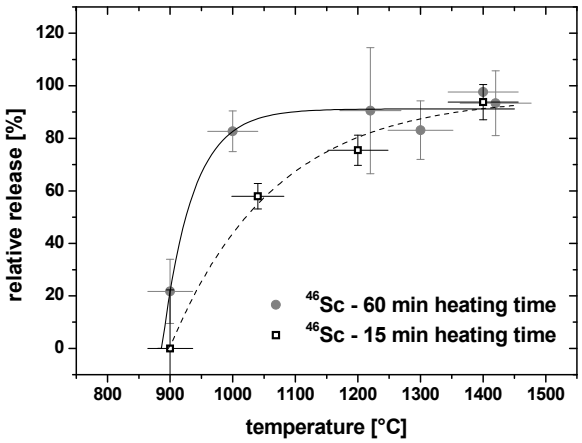

Fig. 1: The relative amount of scandium released from titanium metal versus the temperature at varied heating times 15 min (black open squares) and 60 min (grey points). A distinct heating time dependence and a maximum release above 1200°C are observed. The horizontal error bars are showing the temperature uncertainty in the sample during the heating time. The vertical error bars are calculated 1σ errors from the γ-measurements. Lines were drawn to guide the eye.

REFERENCES

[1] J.A. Cameron et al., Nucl. Data Sheets **88**, 299 (1999).
[2] I. Ahmad et al., Phys. Rev. C **74 (6)**, 065803-1 (2006).
[3] D.V. Filosofov, D.V. et al., Radiochim. Acta **98**, 149 (2010).
[4] N. Loktionova et al., The J. of Nucl. Med. **51**, 590 (2010).
[5] M. Pruszynsk et al., The J. of Nucl. Med. **51**, 1534 (2010).
[6] D. Wittwer et al., this report, p. 3.

INTERACTION OF ASTATINE SPECIES WITH QUARTZ AND GOLD SURFACES

A. Serov, R. Eichler, H.W. Gäggeler, A. Türler, D. Wittwer (Univ. Bern & PSI), R. Dressler, D. Piguet, A. Vögele (PSI), N. Aksenov, G. Bozhikov, V. Lebedev, O. Petrushkin, S. Shishkin, E. Tereshatov (FLNR)

Astatine isotopes were prepared by heavy ion induced nuclear fusion reactions using Tm- targets and Ar beam as well as in nuclear transfer reactions irradiating bismuth targets with argon beams. Their adsorption properties on quartz and gold were investigated by gas chromatography at varied experimental conditions.

INTRODUCTION

Astatine is a radioactive element, which can be found in three natural radioactive decay series. However, only the following short-lived isotopes can be detected: ^{218}At ($T_{1/2}$= 1.5 s) from the $^{234/238}$U-decay series; ^{215}At ($T_{1/2}$= 0.1 ms) as well as ^{219}At (most long-lived isotope with $T_{1/2}$= 56 s) occur in the ^{235}U-decay series. Astatine is claimed to be the rarest naturally-occurring element. The first confirmed discovery of astatine was made in 1940 by Dale R. Corson and co-workers during the irradiation of bismuth with alpha particles [1]. This new element in the periodic table was reported by several researchers as "eka-iodine" and names like alabamine, dakin, helvetium, and anglohelvetium were suggested [2]. The existence of astatine in the uranium-decay series was discovered in 1943 by Karlik and Bernert [3,4]. The successful synthesis of the so far missing element with the atomic number 117 was recently reported at the JINR, Dubna, Russia [5]. In preparation of a chemical investigation of element 117 (E117), the main goal of the present research was the investigation of the formation of volatile astatine species and their adsorption interaction with quartz and gold surfaces.

EXPERIMENTAL

The nuclide ^{201}At ($T_{1/2}$ = 89.0 s) was produced in the heavy ion induced nuclear fusion reaction ^{169}Tm(^{40}Ar, 4n)^{205}Fr ($T_{1/2}$ =3.9 s, α)→^{201}At and was used for online experiments. The long-lived ^{209}At ($T_{1/2}$ = 5.4 h) was produced in nuclear transfer reactions via irradiation of a ^{209}Bi target with ^{40}Ar at the PSI PHILIPS cyclotron. Therefore, a 0.1 mm thick metallic bismuth target was irradiated with ^{40}Ar entering the target with an energy of 220±3 MeV. This isotope was used for offline experiments. The fast online gas phase chemical separation technique – In-situ Volatilization and Online detection system (IVO) was used to perform on-line isothermal gas chromatography experiments, whereas thermochromatography was used for a series of offline experiments.

RESULTS AND CONCLUSIONS

In online isothermal chromatographic experiments an extreme sensitivity of astatine to traces of oxygen and water in the carrier gas was observed. The presence of a getter in the system is essential for investigation of At in the elemental state (see Fig. 1). The determined adsorption enthalpy of the oxidized astatine species on gold is $-\Delta H_{ads}^{Au}(AtO_xH_y)$=110±15 kJ mol^{-1} (Fig. 1, Panel A), whereas astatine in its elemental state on gold has an adsorption enthalpy of $-\Delta H_{ads}^{Au}$(At)=147±15 kJmol^{-1} (Fig. 1, Panels B and C). A series of offline thermo-chromatographic experiments with various carrier gases on Au and SiO_2 surfaces revealed the existence of several astatine species. Their adsorption enthalpies can be summarized as:

$-\Delta H_{ads}^{Au}$(At)=160±10 kJ mol^{-1},
$-\Delta H_{ads}^{Au}(AtO_2)$=125±10 kJmol^{-1},
$-\Delta H_{ads}^{SiO2}$(At)=123±10 kJmol^{-1},
$-\Delta H_{ads}^{SiO2}(AtO_2)$=83±10 kJ mol^{-1},
$-\Delta H_{ads}^{SiO2}$(HAtO)=50±10 kJmol^{-1}.

The data for sublimation enthalpies were estimated from the correlation between the adsorption enthalpies and the macroscopic property sublimation enthalpy [6,7] as:
ΔH_{subl}(At)=150±30 kJmol^{-1},
$\Delta H_{subl}(AtO_2)$=110±20 kJmol^{-1},
ΔH_{subl}(HAtO)=55±20 kJmol^{-1}.

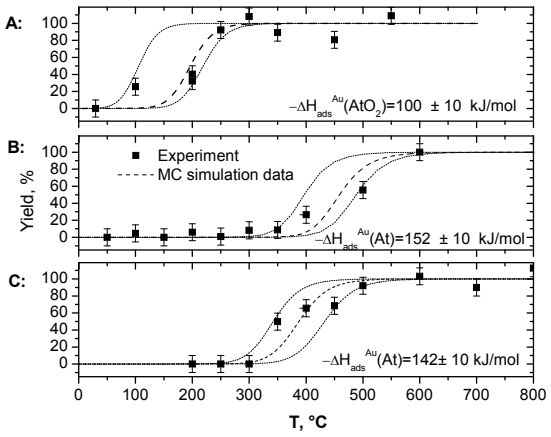

Fig. 1: External chromatograms of ^{201}At adsorption on the stationary gold surface (black squares) together with Monte Carlo simulation data (dashed lines). Experimental conditions: Panel A: argon flow rate 1.8 L min^{-1}, column length – 10 cm, without getter oven; Panel B: argon flow rate 1 L min^{-1}, column length – 10 cm, with getter oven; Panel C: argon flow rate 1 L min^{-1}, column length – 20 cm, with getter oven.

The authors kindly appreciate financial support by the SNF.

REFERENCES

[1] D.R. Corson et al., Phys. Rev. 58, 672 (1940).
[2] R.F. Trimble, J. Chem. Educ. 52, 585 (1975).
[3] B. Karlik, T. Bernert, Naturwissenschaften 298, 31 (1943).
[4] B. Karlik, T. Bernert, Zeitschrift für Physik 123, 51 (1943).
[5] Yu. Ts. Oganessian et al., PRL 104, 142502 (2010).
[6] B. Eichler, R. Eichler in "The Chemistry of Superheavy Elements" (M. Schädel, ed.), Kluwer Academic Publishers 2003).
[7] R. Eichler et al., J. Phys. Chem. B106, 5413 (2002).

INTERACTION OF THALLIUM SPECIES WITH QUARTZ AND GOLD SURFACES

A. Serov, R. Eichler, A. Türler, D. Wittwer, H.W. Gäggeler (Univ. Bern & PSI),
R. Dressler, D. Piguet, A. Vögele (PSI)

Thallium isotopes were prepared by heavy ion induced nuclear fusion reactions using gold targets and helium beams. Their adsorption interactions with quartz and gold surfaces were investigated by thermochromatography at varied experimental conditions.

INTRODUCTION

Recently, it was shown that the chemical behavior of so-called superheavy elements (SHE), Cn and element 114, is strongly influenced by relativistic effects [1-4]. Important experiments with some lighter homologues (Hg and Pb) were performed prior to real experiments with superheavy elements at the same experimental conditions. The experiments on the investigation of the chemical properties of element E113 have recently been started at the FLNR in Dubna, Russia. Recently, we have published a detailed study of adsorption properties of different indium species with quartz and gold surfaces [4]. In the present research, we report new data for two thallium species: metallic Tl and TlOH and their interaction with Au and SiO_2 surfaces.

EXPERIMENTAL

Long-lived ^{200}Tl ($T_{1/2}$ = 26.1 h) was produced in nuclear fusion reactions via irradiation of a ^{197}Au target with ^{4}He at the PSI PHILIPS cyclotron applying beam intensities between 10^{11}-10^{12} particles per second. Therefore, a 30 µm thick metallic gold target array was irradiated with ^{4}He entering the target with an energy of 80±1 MeV. Thermochromatography was used as the main method for the investigation of thallium species interaction with Au and SiO_2 surfaces.

RESULTS AND CONCLUSIONS

The deposition temperature determined for thallium on the gold surface using purified hydrogen as carrier gas was T_{dep}^{Au}(Tl)=944±25°C (Fig. 1, Panel A). The enthalpy of adsorption of elemental thallium on the gold surface was derived as $-\Delta H_{ads}^{Au}$(Tl)=285±5 kJ mol^{-1}. A series of experiments with pure oxygen resulted in deposition of thallium species at a significantly lower temperature $T_{dep}^{Au}(TlO_xH_y)$=340±25°C, yielding an enthalpy of $-\Delta H_{ads}^{Au}(TlO_xH_y)$=145±5 kJ mol^{-1} (Fig.1 Panel B). Later experiments with quartz as stationary surface allowed us to assign this deposition peak to TlOH. A series of experiments with SiO_2 as chromatographic surface resulted only in one deposition peak regardless of the reducing potential of the carrier gas (Fig. 2). The deduced adsorption enthalpy was $-\Delta H_{ads}^{SiO2}$(TlOH)=135±5 kJ mol^{-1} (Fig. 2, Panels A, B, and C, respectively). These data are in perfect agreement with the results obtained for the interaction of TlOH with gold surface. The sublimation enthalpy for TlOH was evaluated as ΔH_{subl}(TlOH)=177±3 kJ mol^{-1} using an empirical correlation between the adsorption enthalpies and the macroscopic property sublimation enthalpy [6,7]. These results will be certainly important for the data evaluation of experiments with element 113.

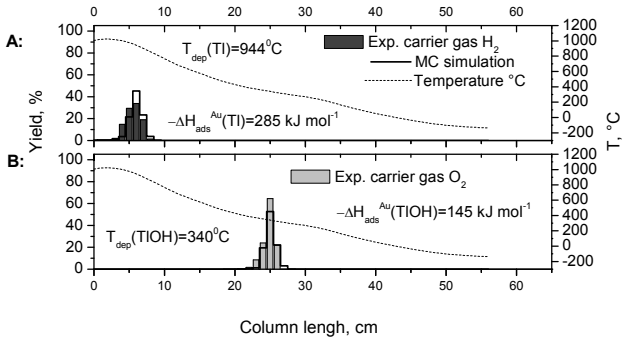

Fig. 1: Thermochromatograms of ^{200}Tl (dark grey bars, left hand axis) and ^{200}TlOH (light grey bars, left hand axis) on gold surface using as carrier gas: Panel A: 15 ml min^{-1} H_2; Panel B: 25 ml min^{-1} O_2. The solid stepped lines represent the results of Monte Carlo model simulations applying the adsorption enthalpies given in the panels. The temperature gradients are indicated (dashed line, right hand axis).

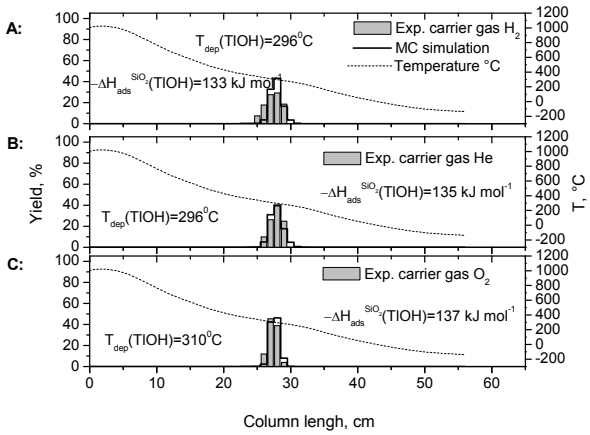

Fig. 2: Thermochromatograms of ^{200}TlOH (light grey bars, left hand axis) on quartz surface using as carrier gas: Panel A: 15 ml min^{-1} H_2; Panel B: 25 ml min^{-1} He; Panel C: 25 ml min^{-1} O_2. The solid stepped lines represent the results of the Monte Carlo simulations applying the adsorption enthalpies given on the panels. The temperature gradients are indicated (dashed line, right hand axis).

The authors kindly appreciate financial support by the SNF.

REFERENCES

[1] R. Eichler, et al., Nature **447,** 72-75 (2007).
[2] R. Eichler, et al., Angew. Chem. Int. Ed. **47(17),** 3262 (2008).
[3] D. Wittwer et al., Nucl. Instr. and Meth**. B. 268,** 28 (2010).
[4] R. Eichler et al., Radiochim. Acta, **38,** 133-139 (2010).
[5] A. Serov et al., Radiochimica Acta, accepted (2010).
[6] B. Eichler, R. Eichler in "The Chemistry of Superheavy Elements" (M. Schädel, ed.), Kluwer Academic Publishers (2003).
[7] R. Eichler et al., J. Phys. Chem. **B106,** 5413 (2002).

SIGNIFICANCE TEST OF LIFE-TIME MEASUREMENTS IN THE CASE OF POOR COUNTING STATISTICS

R. Dressler (PSI)

A one-sided parameter-free significance test of independent life-time measurements in the case of poor counting statistics is proposed.

INTRODUCTION

The confirmation of the synthesis of new isotopes is based on the reproduction of their primarily observed decay properties. Beside the simple comparison of decay energies only the approach from [1] merging all observed events and checking whether they originate from the decay of a single radioactive species is available.

We propose here a method to test two independently obtained data sets against the null-hypothesis – both data sets exhibit the same decay constant – in comparison to an alternative hypothesis – the second data set shows a smaller or greater decay constant.

METHOD

We use the method of total ignorance (MoTI) as proposed in [2], i.e. a Bayesian approach with a non-informative pseudo primer. Starting from p_t we get using MoTI p_λ:

$$p_t(\tau|M,\lambda) = \lambda \cdot M \cdot \frac{(\lambda \cdot M \cdot \tau)^{M-1}}{(M-1)!} e^{-\lambda \cdot M \cdot \tau}$$

(p_t – probability density function (pdf) to obtain a mean life-time of τ with M observed events if the decay-constant λ is known)

$$p_\lambda(\lambda|N,t_0) = t_0 \cdot \frac{(\lambda \cdot N \cdot t_0)^{N}}{(N-1)!} e^{-\lambda \cdot N \cdot t_0}$$

(p_λ – pdf that λ has a certain value if a mean life-time t_0 was observed within N events).
Combining both formula yields p_τ

$$p_\tau(\tau|M,N,t_0) = \int_0^\infty p_t(\tau|M,\lambda) \cdot p_\lambda(\lambda|N,t_0) \cdot d\lambda$$
$$= \binom{N+M}{N} \cdot \frac{M^2 \cdot (M \cdot \tau)^{M-1} \cdot (N \cdot t_0)^{N+1}}{(N \cdot t_0 + M \cdot \tau)^{N+M+1}}$$

(p_τ – pdf to get in an independently performed experiment a mean life-time of τ within M events if in a reference experiment the mean life-time t_0 was obtained by observing N events). This pdf does not anymore depend on a particularly chosen decay constant. Therefore, this significance test is free of additional parameters. The ratio of both life times (or half-lives) can be used as test variable for a one-sided hypothesis test. In the case that τ is smaller compared to t_0 the following equation must be solved with respect to x.

$$P\left(\frac{\tau}{t_0} < x|M,N\right) = \int_0^{x \cdot t_0} p_\tau(\xi \cdot t_0|M,N,t_0) \cdot t_0 \cdot d\xi =$$
$$\binom{N+M}{N} \cdot \left(\tfrac{M}{N}x\right)^M \cdot {}_2F_1\left(N+M+1, M; M+1; -\tfrac{M}{N}x\right) = \alpha$$

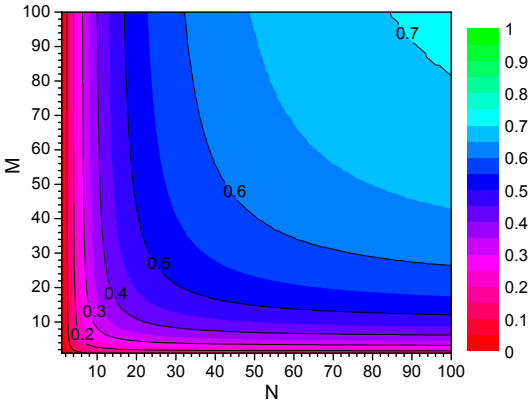

Fig. 1: Values of the test variable x for a shorter half-life at a significance level of 1%.

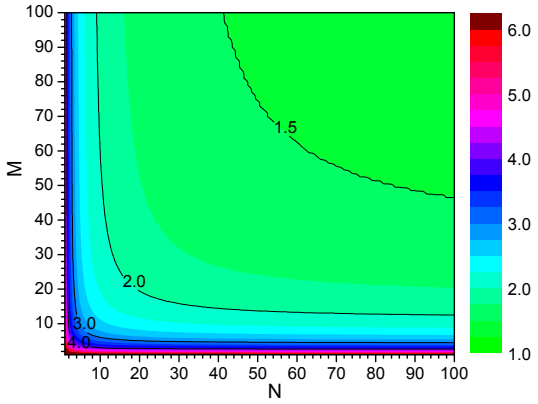

Fig. 2: Values of the test variable x for a longer half-life at a significance level of 1%.

The null-hypothesis that both observed life-times originate from the same statistical ensemble at a statistical significance level α (α is the error probability to incorrectly reject the null-hypothesis, the probability to accept the null-hypothesis will be 1-α) must be rejected if this ratio is smaller than x. The resulting values of x for event numbers between 1 and 100 of the events N in the reference experiment and M in the experiment under test are depicted in Fig. 1 for a 1% significance level, i.e. for a 99% correct acceptance of the null-hypothesis. A similar equation must be solved in the inverse case, where τ is larger compared to t_0. The obtained values of x are displayed in Fig. 2 for the same range of values of N and M and for a 1% significance level. Using this method it can be decided objectively whether in two independently performed experiments the observed half-lives are compatible or not.

REFERENCES

[1] K.H. Schmidt, Eur. Phys. J. **A 8,** 141–145 (2000).
[2] R. Dressler, et al., 1st Int. conf. on the chem. and phys. Of the transactinide elements TAN-99, Seeheim, Sept. 1999.

INFLUENCE OF SPIN-ORBIT EFFECTS ON THE VOLATILITY OF ELEMENT 114

A. Hermann (Univ. Auckland & Victoria Univ Wellington, New Zealand), J. Furthmüller (Friedrich-Schiller Univ. Jena, Germany), H.W. Gäggeler (on leave from PSI), P. Schwerdtfeger (Massey Univ. Auckland, New Zealand)

Spin-orbit effects become very important in the bonding of heavier p-group elements such as element 114. As a consequence, first-principles density functional calculations show a lowering of the cohesive energy for element 114 compared to that of its group homologue Pb. The resulting cohesive energy for element 114 amounts to 0.5 eV/atom, being significantly lower than that of Pb (2.02 eV/atom) and even lower than that of Hg (0.7 eV/atom).

INTRODUCTION

Recent investigations on the chemical properties of element 114 shows a surprisingly high volatility [1] – indicated by a low adsorption enthalpy on a Au surface. The measured data include the observation of three atoms of element 114 adsorbed inside of the Au-covered detector array COLD [1]. This observation is in line with a "historic" prediction by K.S. Pitzer back in 1975 [2], but also in line with an empirical extrapolation made by B. Eichler in 1974 [3].

Based on the idea that measured adsorption enthalpies of single atoms of p-elements on Au surfaces can be well correlated with their respective sublimation enthalpies [4], a sublimation enthalpy of element 114 may be estimated using this correlation as a proxy. The resulting experimental value for the sublimation enthalpy of element 114 is $0.23^{+0.22}_{-0.08}$ eV (1σ error bars).

CALCULATIONS

First-principles density functional calculations were performed for the group 14 elements C, Si, Ge, Sn, Pb, and element 114 [5]. As a consequence of the spin-orbit effects within the 7p shell, element 114 was found to exhibit a hexagonal-closed packed structure, deviating from the structure of its nearest group 14 neighbor Pb with a face-centered cubic structure. This implies, that unlike Pb with a cohesive energy of 2.02 eV/atom, element 114 is much more weekly bound with a cohesive energy of only 0.5 eV/atom. This is a consequence of the approx. 4 eV energy gap between the filled $7p_{1/2}$ and the empty $7p_{3/2}$ atomic electron levels of element 114.

Figure 1 depicts the calculated cohesive energies compared to the experimental values of the sublimation enthalpies. The left black arrows point to the values obtained excluding spin-orbit effects while the right black arrows show the values deduced including the spin-orbit effect. The blue arrows point to the experimental values. Following observations emerge:

- The accuracy of calculated values (including spin-orbit effects) compared to experimental values is about ± 0.5 eV.
- Spin-orbit effects become – as expected – increasingly important when moving down the members of group 14.
- Because carbon has fully degenerate $2p_{1/2}$ and $2p_{3/2}$ energy levels – which is the basis of the Hund rule – the cohesive energies are not influenced by spin- orbit effects.
- For Pb the difference between the calculated values including and excluding spin-orbit effects is already 1 eV while for element 114 it amounts to 2.5 eV.

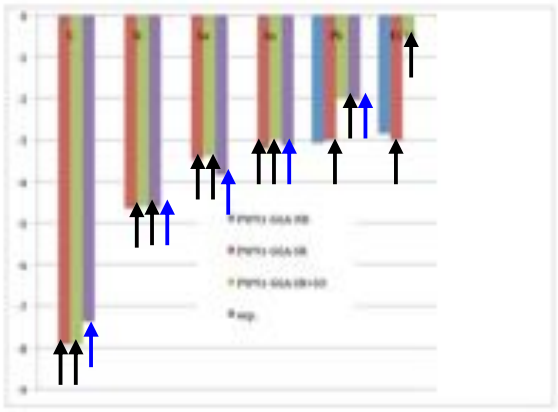

Fig. 1: Calculated (black arrows, see text) cohesive energies (in eV) and experimental (blue arrows) sublimation enthalpies of elements of group 14 (from [5]).

The calculated cohesive energy for element 114 of 0.5 eV [5] is in reasonable agreement with the experimental value of $0.23^{+0.22}_{-0.08}$ eV (1σ error bars) [1].

ACKNOWLEDGEMENT

H.G. greatly acknowledges the hospitality at Massey University.

REFERENCES

[1] R. Eichler et al., Radiochim. Acta, **98**, 133 (2010).
[2] K.S. Pitzer, J. Chem. Phys. **63**, 1033 (1975).
[3] B. Eichler, Dubna Report P12-7767 (1974) (*in russian*).
[4] R. Eichler, Radiochim. Acta, **93**, 245 (2005).
[5] A. Hermann et al., Phys. Rev. B **82**, 155116 (2010).

UV/VIS RADIATION INCREASES STEADY-STATE UPTAKE OF OZONE ON SOOT

V. Zelenay (PSI), M.E. Monge, B. D'Anna, C. George (IRCELYON), S.A. Styler (UoT), T. Huthwelker (PSI/SLS), M. Ammann (PSI)

Coated wall flow experiments were used to obtain uptake coefficients of ozone on soot under irradiation. They revealed that in presence of light the uptake was substantially enhanced.

INTRODUCTION

Oxdiative aging of soot particles in the atmosphere may contribute significantly to climate and human health effects. With their large specific surface area, soot particles are an ideal substrate for heterogeneous reactions. However, these reactions are typically of limited relevance due to deactivation of their surface. Recently, several experiments revealed a significant importance of the presence of light during uptake experiments, e.g. [1]. Therefore, we studied the ozone uptake on soot surfaces by means of a coated wall flow tube technique. Uptake coefficients were measured in the dark and in presence of near-UV radiation on passivated soot. Mechanistic insights were gained using X-ray absorption spectroscopy and contact angle measurements.

EXPERIMENTAL

The soot was produced using a combustion aerosol standard soot generator (CAST). A thin layer of soot was deposited on the inside wall of a Pyrex tube by holding the tube at the exit of the soot generator. The soot mass was determined by weighing the Pyrex tube before and after coating. The soot coated tube was then inserted into a horizontal cylindrical coated wall flow tube reactor. The reactor was surrounded by 7 sunlight lamps with a continuous emission from 300-420 nm.

RESULTS

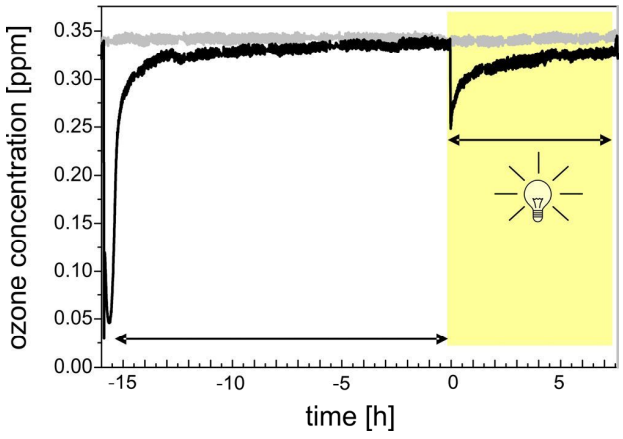

Fig. 1: Typical uptake experiments.

The black line in Figure 1 shows the evolution of the ozone concentration during a typical experiment. First, uptake is observed upon exposure of ozone to soot in the dark. The second uptake of ozone is observed after radiation was turned on, marked in yellow. The grey line shows the corresponding blank experiment. Negative times are associated with the surface passivation procedure.

We could show that the uptake under irradiation is increased by a factor of four under quasi - steady state conditions. Furthermore, we could show that the uptake increases by a factor of 15 when humidity was additionally introduced to the system.

To elucidate possible reaction mechanisms x-ray absorption spectra (XAS) were recorded and contact angle measurements were performed, see Figure 2. The XAS analysis revealed that many partially oxidized organic species are further oxidized to volatile products, leaving behind the more refractory fraction of soot. These measurements are supported by contact angle measurements that revealed a lower wettability, presumably due to the lower oxidation state of the soot upon exposure to ozone and light.

Open questions remained with respect to the role of semivolatile compounds in the photoenhanced ozone uptake in soot. Further experiments on the volatile exhaust compounds need to be conducted, so that also the reaction mechanisms could be investigated in more detail.

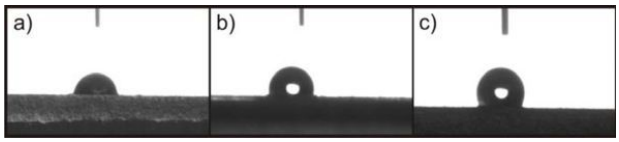

Fig. 2: Contact angle measurements of a) untreated, b) ozone treated and c) ozone with light treated soot. The water droplet shows an angle of 80, 100, and 120º, respectively.

ACKNOWLEDGEMENTS

This work was supported by the NEADS project within the Center of Excellence in Energy and Mobility (CCEM-CH). We thank M. Rossi for providing us with the CAST burner and M. Birrer for technical support. Eric Puzenat is acknowledged for helpful discussions about the contact angle analysis. Support by the Agence National de le Recherche Scientifique (ANR) is gratefully acknowledged under the grant Photoaero (N. JC08-331753).

REFERENCE

[1] Monge et al., Proceedings of the National Academy of Science of the United States of America, **107**, 6605 (2010).

NITROUS ACID FORMATION ON UVA/VIS IRRADIATED POLYPHENOLIC FILMS UPON NO_2 UPTAKE AND PHOTOLYSIS OF NITRO AROMATIC PRODUCTS

Y. Sosedova (Univ. Bern & PSI), A. Rouvière, M. Ammann (PSI)

The coated wall flow technique was used in combination with in situ gas-phase HONO detection to investigate photoenhancement of NO_2 to HONO conversion on polyphenolic films under UV or visible irradiation. Photolysis of products of dark NO_2 chemistry might be an additional precursor of HONO in the gas phase under UV irradiation.

INTRODUCTION

Elevated diurnal levels of nitrous acid (HONO) were recently measured both in rural and urban areas, suggesting that HONO was a significant OH source in the troposphere not only in the morning hours but also during the day. The exact mechanism of HONO formation is still under discussion. Light activation of chromophors within humic acids followed by electron-transfer reaction with absorbed NO_2 has been previously demonstrated to lead to HONO formation [1]. To extend our knowledge about the mechanism of the photoenhanced HONO formation, we used tannic (TA) and gentisic (GA) acids as proxies for atmospheric polyphenolic compounds and methylene blue (3,7-bis(dimethylamino)phenazathionium chloride) as a model photosensitizer absorbing in the visible part of the solar spectrum to represent a chromophoric material naturally occurring in the environment (Fig. 1).

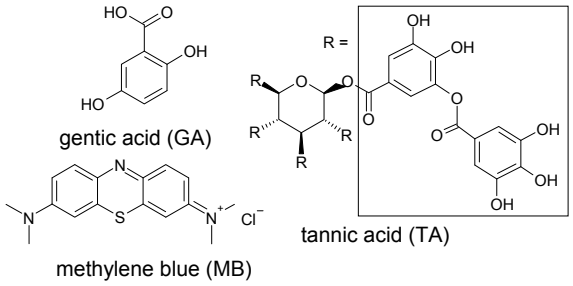

Fig. 1: Substances used for coatings preparation.

EXPERIMENTAL

Experiments were performed in a horizontal coated wall flow tube (40 cm × 0.8 cm i.d.), circularly surrounded by 7 fluorescence lamps radiating in the UV-A (Philips Cleo Effect 70W: 300-420 nm) or in the visible range of the tropospheric solar spectrum (Osram Lumilux Deluxe 954, 58W: 400-750 nm) in an air-cooled lamp housing. Coatings were prepared by applying 1 ml of either 0.01 M TA or 0.1 M GA in 0.01 M citric acid aqueous solution to the inner surface of the sand-blasted tube and gently evaporating excess water under a flow of N_2. In experiments on the influence of a photosensitizer, 1 wt% of methylene blue (MB) was added to the coating solution. Resulting coatings typically contained 160 - 200 µg cm^{-2} of either GA or TA and were operated under a relative humidity of 45% and a temperature of 23°C. For the blank experiments tubes were coated with 1 ml of 0.01 M citric acid solution.

NO_Y (NO, NO_2, and HONO) were measured by a chemi-luminescence detector (CLD), and gas-phase HONO by the LOPAP (LOng Path Absorption Photometer) instrument.

RESULTS AND CONCLUSIONS

Interaction of films containing GA and TA with gaseous NO_2 was investigated in the dark and under UV or visible (Vis) light. NO_2 uptake as well as the HONO formation rate in the dark decreased with increasing gas-phase NO_2 concentration [2]. This behavior could be explained by adsorption saturation preceding a slow surface reaction. Using the CLD, a substantial net loss of NO_Y on coatings was recorded during the first 15 min of the NO_2 exposure. Since the balance of the gas-phase products was not kept, we proposed accumulation of non-volatile products (likely nitrophenols, $ArNO_2$).

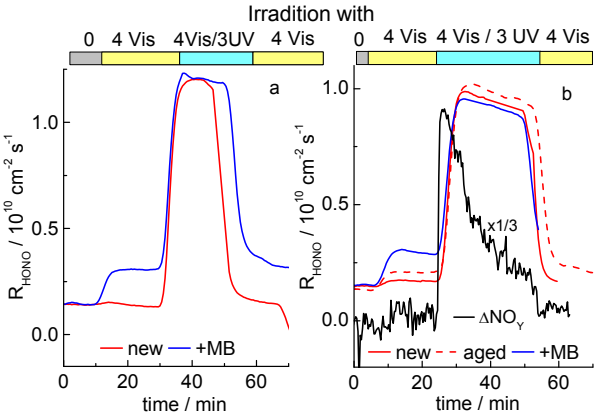

Fig. 2: Photoenhanced HONO formation rate on GA (a) and TA (b) coatings: fresh, aged and with 1% MB addition, accompanied by NO_Y emission, at $[NO_2]_0$ = 76.5 ppb.

Photoenhanced HONO formation rates R_{HONO} (molecules cm^{-1} s^{-1}) on GA and TA films are shown in Fig. 2. The uptake of NO_2 was 15% and 30% higher under Vis light than in the dark on a fresh and aged TA coating, respectively. TA degradation products that absorb light in the Vis range might explain this photosensitizing effect. As GA does not absorb light at $\lambda > 400$ nm, no enhancement in HONO formation was monitored under Vis irradiation of GA coatings. In presence of 1% MB in both coatings, NO_2 uptake was 75 % higher than in the dark. HONO formation under UV light was presumably a result of both photoenhanced NO_2 conversion and photolysis of $ArNO_2$. A difference between the CLD signal in the dark and under UV irradiation confirmed NO_Y emission (Fig. 2b).

REFERENCES

[1] K. Stemmler et al., Atm. Chem. Phys., **7**, 4237 (2007).
[2] Y. Sosedova et al., Ann. Rep. Lab. of Radio- & Environ. Chemistry, Univ. Bern & PSI (2009), p. 13.

GAS UPTAKE AND CHEMICAL AGING OF AMORPHOUS SEMI-SOLID PARTICLES

M. Shiraiwa, U. Pöschl (MPI-CH), M. Ammann (PSI)

The kinetics of ozone uptake by an amorphous protein was measured using the coated wall flow tube technique. The results show that the properties of semi-solid phases influence gas uptake and chemical aging of aerosol particles.

INTRODUCTION

Organic substances can adopt an amorphous semi-solid state [1-2], influencing the rate of heterogeneous reactions and multiphase processes in atmospheric aerosols. Here, we demonstrate how molecular diffusion in the condensed phase affects the gas uptake and chemical transformation of semi-solid particles. Flow tube experiments show that the ozone uptake and oxidative aging of an amorphous protein is kinetically limited by bulk diffusion. The reaction rate depends on the diffusion coefficients of both the gaseous and the condensed phase reactants, which can be described by a kinetic multi-layer flux model but not by the traditional resistor model approach of multiphase chemistry. Based on numerical simulations, we present first spatial and temporal profiles of the concentration and reaction rate of ozone and reactive amino acid residues in an amorphous protein matrix. The chemical lifetime of reactive compounds in atmospheric particles can increase from seconds to days and more as the diffusion coefficients decrease over ten orders of magnitude from the liquid to the solid state.

EXPERIMENTS

Figure 1 shows the uptake of ozone by Bovine serum albumin (BSA) in flow tube experiments with an initial ozone concentration of ~110 ppb. At the beginning of each experiment, the coated-wall flow tube was bypassed to obtain a stable ozone signal ($t < 0$). When the flow tube was switched in ($t=0$), the gas phase ozone concentration dropped rapidly to ~60 ppb, which corresponds to an ozone uptake coefficient of $\gamma_{O3} \approx 10^{-5}$ during the first few seconds of reaction time ($t \approx 10$ s). Then the ozone concentration started to recover asymptotically towards the initial value, and the uptake coefficient exhibited an exponential decrease that continued over many hours. When the flow tube was bypassed again, the gas phase ozone concentration quickly returned to the initial value, confirming that the experimental conditions were stable and that the observed ozone loss was due to continuing uptake by the protein film in the flow tube.

The magnitude and temporal evolution of γ_{O3} did not change when the thickness of the protein film on the flow tube walls was varied between 133 – 346 nm. This finding indicates that the ozone uptake was kinetically limited by processes at or near the surface of the protein film. If the uptake kinetics had been affected by processes involving the entire volume of the protein film, the film thickness should have influenced the results, i.e., thicker films should have exhibited higher values or slower decrease of γ_{O3}. The most plausible explanation for the observed behavior is that the uptake of ozone was limited by diffusion and reaction near the surface of the protein film.

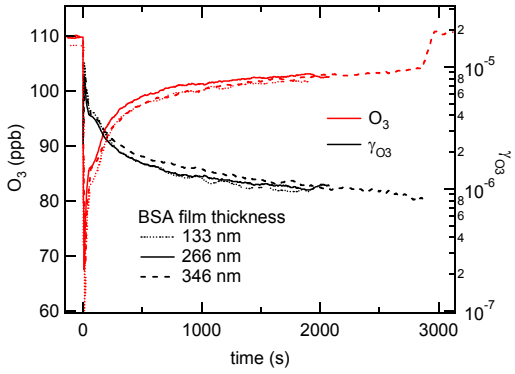

Fig. 1: Ozone uptake by BSA at 109 ppb O_3. The red line is the gas phase ozone concentration and the black line is the corresponding uptake coefficients of ozone (γ_{O3}). The BSA film thicknesses were 133 nm (dotted line), 266 nm (solid line), and 346 nm (dashed line).

KINETIC MODELING

We applied a kinetic multi-layer flux model (KM-SUB)[1] to analyze the experimental results of ozone uptake by the amorphous BSA film. KM-SUB can reproduce the observed γ_{O3} very well, showing the steep concentration gradient of ozone and the BSA turnover rate in the bulk, which confirms the bulk diffusion limited uptake kinetics. The modeling results show that mass transport can have strong non-linear effects on the chemical aging of atmospheric aerosols, and that the amorphous solid state with high viscosity and low diffusion coefficients can effectively shield reactive organic compounds from degradation by atmospheric oxidants, such as O_3, OH, NO_3, N_2O_5, or and halogen radicals.

ACKNOWLEDGEMENT

This work was funded by the Max Planck Society (MPG), Swiss National Foundation, and the European integrated project on cloud climate and air quality interactions (EUCAARI). We thank M. Birrer, Y. Sosedova, and A. Rouviere for their help in the kinetic experiments.

REFERENCES

[1] A. Virtanen, et al., Nature, **467**: 824, 2010.
[2] E. Mikhailov et al., Atmos. Chem. Phys., **9,** 9491 (2009).
[3] M. Shiraiwa et al., Atmos. Chem. Phys., **10**, 3673 (2010).

X-RAY MICROSCOPY STUDY OF TANNIC ACID PARTICLES: EFFECT OF OZONE AND UV-LIGHT

M. Lampimäki, V. Zelenay, A. Křepelová, M. Birrer (PSI), T. Huthwelker, B. Watts, J. Raabe (PSI/SLS), M. Ammann (PSI)

Tannic acid particles were characterized after exposure to O_3 and UV- light under dry and humid conditions by scanning transmission X-ray microscopy.

INTRODUCTION

Organic particles contribute significantly to the atmospheric aerosol burden and thus their climate impact [1,2]. Tannic acid, a proxy of complex organic material present in atmospheric aerosols, was used to study oxidation in terms of chemical composition and hygroscopicity in individual submicron organic particles [3]. Here, we have employed scanning transmission X-ray Microscopy (STXM) and Near edge X-ray absorption fine structure (NEXAFS) techniques to study changes in morphology and functional groups of tannic acid after exposure to ozone and UV-light.

EXPERIMENTAL

A home built ultrasonic aerosol nebulizer was employed to generate aerosol particles from tannic acid (Sigma Aldrich) dissolved in deionized water (MilliQ, 5 g/l). Particles were dried by passing them through a silica gel dryer, charged by a corona charger and deposited electrostatically on the silicon nitride window. The humid conditions were facilitated in the environmental micro reactor described in ref [4]. A separate flow tube was employed to expose samples to ozone and UV-light offline. The STXM and NEXAFS measurements were conducted at the Pollux beamline at SLS.

RESULTS

The changes in oxidized tannic acid particle morphology due to an increase in relative humidity (RH) from 0% to 70% are shown in Fig. 1 for three different photon energies clearly demonstrating changes in particle size and in absorption properties.

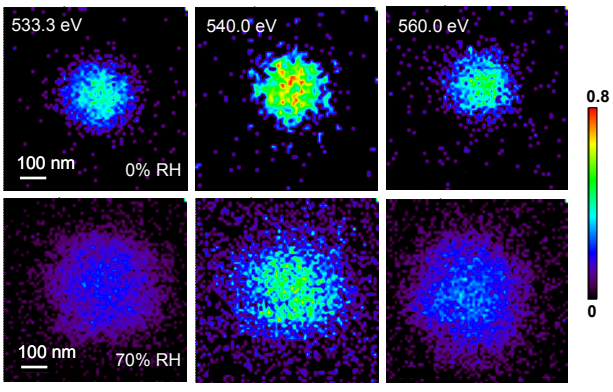

Fig. 1: Absorption images of an individual O_3 pre-treated tannic acid particle measured at 0% RH, (top row) and at 70% RH (bottom row).

At 70% RH the highest absorption intensity appears at 540.0 eV, which corresponds to water associated with the particles. Fig, 2 (a) illustrates typical oxygen k-edge spectra obtained from single unoxidized, ozone- and UV-light exposed tannic acid particles. Spectra were linearly background subtracted and normalized to 560 eV. Peaks at 533.0 eV can be assigned to π* transitions of carboxyl groups whereas the shoulder at ~536.5 corresponds to the σ* transitions of C-O and O-H bonds [5].

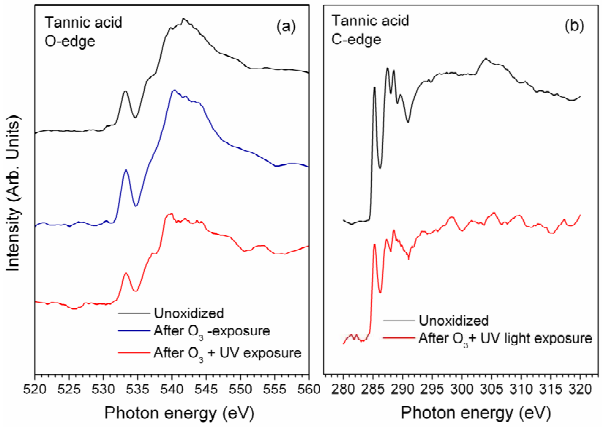

Fig. 2: (a) Oxygen NEXAFS spectra of unoxidized, ozone- and UV-light exposed tannic acid particles. (b) tannic acid carbon edge spectra.

Fig. 2 (b) Shows tannic acid carbon edge spectra for unoxidized and ozone + UV-light exposed tannic acid particles. Small changes in the spectra are distinguishable after the exposure to UV light and ozone indicating shifts in the functional group composition.

ACKNOWLEDGEMENT

This work was supported by the Swiss National Science Foundation (grant no. 130175).

REFERENCES

[1] M. Jang et al., Science **298,** 814 (2002).
[2] M. Hallquist et al., Phys. Chem. Chem. Phys. **5,** 3453 (2003).
[3] V. Zelenay et al., J. Aerosol Sci. **42** (2011) 38.
[4] T. Huthwelker et al., Rev. Sci. Instrum. **81,** 113706 (2010).
[5] Hu et al., Geochim. Cosmochim. Acta, **72** 1959 (2008).

OZONE DECOMPOSITION ON IRON OXIDES STUDIED BY XPS

M. Lampimäki, A. Křepelová, M. Ammann (PSI), H. Bluhm, M.E. Grass, Z. Liu (LBNL)

Iron oxides were investigated in presence of water vapor and ozone by ambient pressure X-ray photoelectron spectroscopy (XPS) at beamline 9.3.2 at the Advanced Light Source.

INTRODUCTION

Mineral dust particles have a significant environmental impact on atmospheric chemical processes due to their optical and chemical properties. Metal oxides as a common part of the mineral dust have an important role in the heterogeneous reactions on dust particle surfaces in the presence of ozone. However, the mechanism behind these processes is yet not well understood [1]. In the present study we have investigated the surface of Fe_3O_4 –particles and a Fe_3O_4 (111) single crystal during exposure to water vapor and ozone. Iron, oxygen, and carbon core-level XPS- and Auger transitions were measured *in situ* at elevated pressures of O_2, H_2O, and O_3.

EXPERIMENTAL

The Fe_3O_4(111) single crystal was cleaned by 1 kV Ar^+-ion sputtering in a 1×10^{-5} Torr background pressure of O_2 and annealed at ~830 K for 30 min. A layer of Fe_3O_4-powder (≥ 98% trace metal basis, Sigma Aldrich) was pressed into a one mm thick In-foil. Reagent grade de-ionized water was purified by multiple freeze-pump-thaw cycles before introducing it via a leak valve into the analysis chamber. Ozone was produced using a corona discharge device (Yanko Industries Ltd MKS Type 247). The photoelectron spectroscopic measurements were performed by employing the spectrometer described in ref. [2].

RESULTS

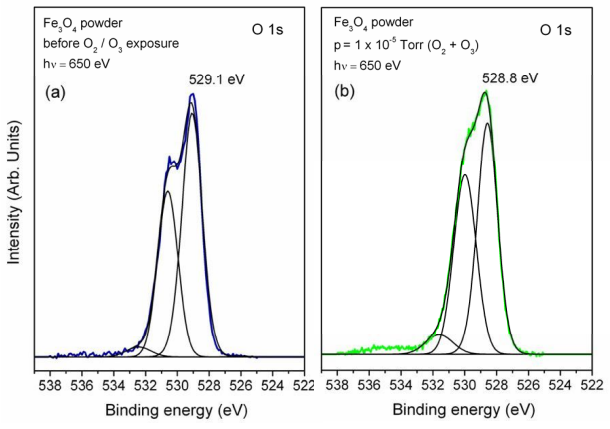

Fig. 1: O 1s photoelectron spectra of Fe_3O_4 powder obtained (a) before and (b) during exposure O_2 and O_3.

Fig. 1 (a) and (b) show intensity normalized O 1s spectra of the Fe_3O_4 powder sample measured before and during the exposure to O_2 and O_3, respectively. The peak positions related to iron oxide were at ~529 eV, which corresponds to the BE value of Fe_3O_4. The peak shoulder observed at 530.5 eV can be assigned to hydroxyl (OH-groups) and possibly in part to oxidized adventitious carbon species (component at ~532 eV). After H_2O and O_3 exposure, an increase in the shoulder of the oxide peak assigned to OH- and C-O-groups can be observed. In addition, a small change at ~535 eV is detected after exposure to O_2 and O_3.

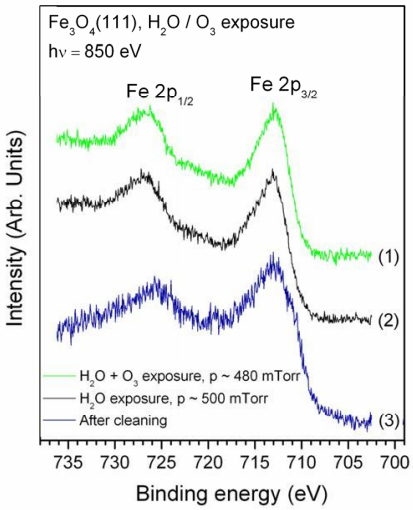

Fig. 2: Fe 2p spectra of Fe_3O_4(111) surface after cleaning (spectrum 1) and during H_2O and H_2O + O_3 exposure (spectra 2 and 3).

Changes in the Fe 2p region during H_2O and O_3 high pressure exposure are shown in Fig. 2. After cleaning, both Fe(II) cations at 711 eV and Fe(III) cations at 712.5 eV appear to be present according to Fe $2p_{3/2}$ binding energies. No reduction of iron (Fe(0) ~707 eV) due to Ar^+-sputtering or annealing of the sample was observed during the measurements. After exposure to H_2O and O_3 the shoulder at 711 eV as well as feature at 719.5 eV, characteristic to Fe(II) 2p satellite, decreases. This might indicate further oxidation of the sample surface.

ACKNOWLEDGEMENT

This work was supported by Swiss National Science Foundation (grant no. 130175). Tom Kendelewicz (Stanford) is gratefully acknowledged for providing the Fe_3O_4(111) sample.

REFERENCES

[1] C. R. Usher et al., Chem. Rev. **103**, 4883 (2003).
[2] M. E. Grass et al., Rev. Sci. Instrum. **81**, 053106 (2010).

XPS STUDY OF ACETIC ACID ADSORPTION ON ICE

A. Křepelová (PSI), H.Bluhm (LBNL), M. Ammann (PSI)

X-ray photoelectron spectroscopy (XPS) and electron yield near edge X-ray absorption spectroscopy (NEXAFS) measurements were performed to study the adsorption of acetic acid on ice.

INTRODUCTION

In this report, we continue our studies on the interaction of different types of acids with ice surfaces [1,2]. We use XPS to probe the surface of ice exposed to gas phase acetic acid (AA). Surface sensitive Auger electron yield NEXAFS spectra were taken to probe the molecular state of the adsorbed species (C-edge) and to assess the hydrogen bonding environment at the interface (O-edge).

EXPERIMENTAL

A stable ice film was grown on a Peltier cooled Cu substrate from water vapor and equilibrated at -39°C or -34°C. A known amount of AA was delivered to 4 mL/min of pure N_2 as carrier gas using a permeation device kept at 60°C. The gas mixture was dosed into the chamber by means of a calibrated leak valve so that total pressures in the XPS chamber ranged from 0.133 to 1.333 mbar. The amount of N_2 in the chamber was monitored by a quadrupole mass spectrometer at m/z 28. O1s and C1s XPS and O and C K-edge NEXAFS spectra were recorded at constant temperature.

RESULTS

Fig 1 represents typical O1s and C1s XPS spectra of ice after AA admission to the chamber recorded at a kinetic energy of 200 eV. The O1s XPS spectrum shows the characteristic broad peak at BE of 534.9 eV and FWHM of 1.96 eV, which can be assigned to the oxygen atoms of AA and ice. O1s chemical shifts are not large, and it is not possible to differentiate between the contributions of oxygen atoms of ice and the two oxygen atoms of AA.

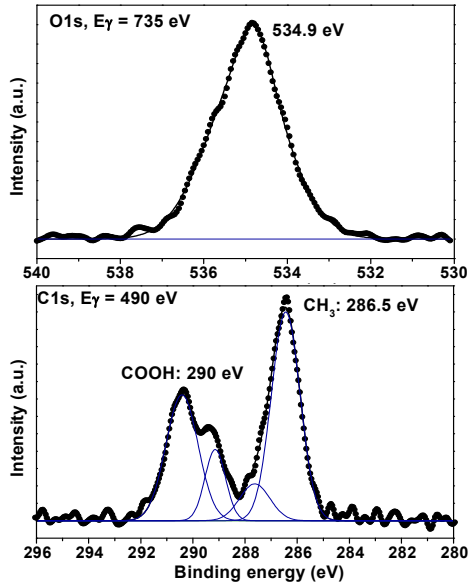

Fig. 1: O1s and C1s XPS spectra of ice with AA.

The C1s XPS has two main features at BEs of 286.5 and 290 eV with a relative shift of 3.5 eV. The peak at higher BE can be assign to carbon of the carbonyl group of AA, while the peak at lower BE belongs to carbon of the methyl group of AA. Moreover, there is a distinct shoulder at around 289 eV. It could indicate the existence of another species, probably the product of acetic acid dissociation or dimerisation. It is also possible that beam damage occurred that influenced mainly the COOH peak.

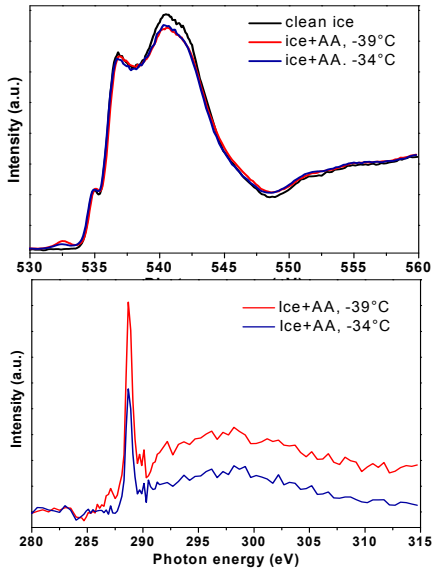

Fig. 2: O- and C-K-edge Auger electron yield NEXAFS spectra of ice in presence of adsorbed AA.

Fig. 2 shows NEXAFS spectra at the O- and C- K-edge for the ice with AA measured at two temperatures. O-K-edge NEXAFS spectra indicate the presence of AA as a peak at 532 eV from carboxyl oxygen of adsorbed AA, with only sparingly small changes in the other regions. C-K-edge NEXAFS spectra exhibit the same shape with one sharp resonance at 288.6 eV assigned to the C1s to π^* transition in C=O, followed by a broader spectral feature in the region between 292 and 303 eV reflecting the 1s $\rightarrow$ σ^* transition. The spectra are comparable to those in the literature for AA adsorption on other inert substrates. Therefore, an only weak interaction with the ice substrate is inferred.

ACKNOWLEDGEMENT

This work is part of our contribution to the EU FP6 project SCOUT-O3.

REFERENCES

[1] A. Křepelová et al., Phys. Chem. Chem. Phys., **12**, 8870 (2010).

[2] A. Křepelová et al., Ann. Rep. Lab. of Radio- & Environ. Chemistry, Uni Bern & PSI (2009), p. 21.

HONO ADSORPTION ONTO ICE

S. Schreiber (ETHZ & PSI), M. Birrer, M. Ammann (PSI)

Adsorption properties for nitrous acid on ice surfaces were measured at low surface coverage using a Knudsen cell combined with radioactively labeled tracer molecules.

INTRODUCTION

Interactions of trace gases with ice surfaces such as snow on the ground or cirrus clouds can significantly affect atmospheric chemistry processes. One example for this is the photochemistry taking place in snow, resulting in emissions of nitrogen oxides and various other species [1]. The involved chemistry is not understood in detail yet, which is partly due to insufficient data on basic physical properties such as photolysis rates and adsorption equilibrium constants.

EXPERIMENTAL

Adsorption properties of HONO were investigated using a Knudsen cell reactor that was combined with tracer molecules containing ^{13}N atoms, a short lived positron emitter [2]. Tracer molecules are provided by the PROTRAC facility at PSI. With this approach, it is possible to work at partial pressures of 10^{-8} to 10^{-10} mbar. Thus, experiments can be run under atmospherically relevant conditions. The linear partitioning coefficient $K_{lin,C}$, which describes the adsorption in case of low surface coverage well below a monolayer, given by

$$K_{lin,C} = \frac{[X]_s}{[X]_g},$$

can then be measured directly without the need to fit the data to adsorption isotherms.
The decay of the tracer molecules is detected by two gamma detectors in coincident counting geometry. The system is operated at 130 K as a cold trap in order to determine the flow of labeled molecules into the cell, which is used to calculate the tracer molecule partial pressure.

The surface coverage for the accessible temperature range of 190 to 220K is obtained from the coincident count rate due to radioactive decay of adsorbed molecules. A typical experiment is given in figure 1. The ice is exposed to the gas flow at t=0 min. After a few minutes, the adsorption equilibrium is reached. All experiments so far have been conducted on vapour deposited ice.

RESULTS

A plot for the adsorption of HONO on ice is given in figure 2. Results of these experiments are given together with datasets obtained by a flow tube study coupled to a mass spectrometer [3] and packed bed experiments with tracer molecules [4]. Our Knudsen cell results are in good agreement with the other two datasets. Next steps will be to study stronger adsorbing species such as HNO_3. So far, laboratory studies on HNO_3 were mostly performed at higher partial pressures and therefore high surface coverage.

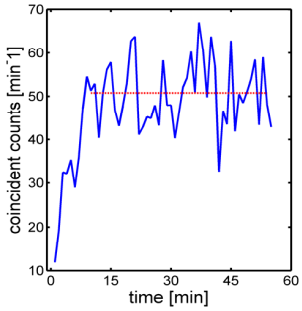

Fig. 1: Coincident counts for HONO adsorption on ice at T=205K. After a few minutes, adsorption equilibrium is established and the signal is constant except for statistical fluctuations. Surface coverage is obtained by averaging the signal (red dotted line).

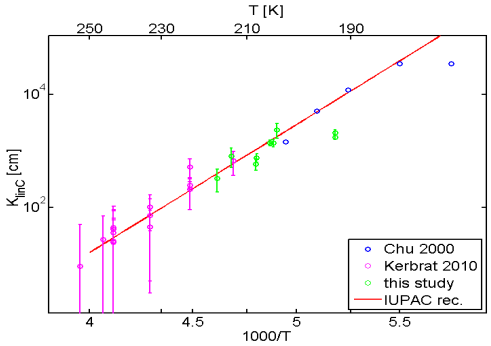

Fig. 2: Van't Hoff plot of the data obtained by Chu et al. [3] (blue), Kerbrat et al. [4] (pink) and in this study (green). The current IUPAC recommendation, based on the first two datasets, is given as red line.

ACKNOWLEDGEMENT

This work is supported by the Swiss National Science Foundation, project number 125179, and is part of a collaboration with the Snow and Avalanche Research Institute SLF/WSL in Davos.

REFERENCES

[1] A. M. Grannas et al., Atm. Chem. Phys, **7**, 4329 (2007).
[2] M. Ammann, Radiochim. Acta, **89**, 831 (2001).
[3] L. Chu et al., J. Phys. Chem. A, **104**, 3150 (2000).
[4] M. Kerbrat et al., J. of Phys. Chem. C, **114**, 2208 (2010).

A NEW CHEMICAL TRAP FOR PEROXIDES AND HONO

T. Ulrich (Univ. Bern & PSI), M. Ammann (PSI), S. Leutwyler (Univ. Bern), T. Bartels-Rausch (PSI)

In order to develop a clean synthesis for HO_2NO_2, a solution of Ti(IV) in H_2SO_4 was successfully tested to clean a gas flow containing small amounts of HO_2NO_2 from traces of HONO and H_2O_2

INTRODUCTION

Peroxynitric acid (HO_2NO_2) makes up a significant fraction of the total nitrogen oxides in cold parts of the Earth's atmosphere [1]. Nitrogen oxides, such as HO_2NO_2, influence the air quality and climate effects. To evaluate in laboratory experiments if HO_2NO_2 is removed from the atmosphere by uptake to snow or ice surfaces a clean source of HO_2NO_2 is required. Here we describe how a recently developed photochemical source of HO_2NO_2 can be cleaned from by-products for ongoing laboratory experiments.

EXPERIMENTAL

HO_2NO_2 is produced by the reaction of NO_2 with HO_2 in a photolysis cell, where water is photolysed in the presence of O_2 to yield HO_2 radicals. Typical yields of HO_2NO_2 are 25% of the initial NO. As by-products, 25% of HNO_3 and 10% of HONO were identified [2]. Additionally, up to $6.15*10^{16}$ molec/cm^3 H_2O_2 were detected. To eliminate these by-products a Ti(IV) denuder in front of a cold trap operated at 243 K was installed. The annular denuder was coated with a solution of 5% Ti(IV) in 30% H_2SO_4. The denuder system has been used earlier to quantify H_2O_2 in air samples [3]. The denuder was dried for 30 min by exposing it to a clean N_2 gas flow.

RESULTS

Figure 1 shows the evolution of nitrogen oxides and H_2O_2 signal intensities with time for the untreated gas flow and when the gas flow passed the Ti(IV) denuder, or the Ti(IV) denuder and the cold trap. A chemical ionization mass spectrometer (CIMS) with SF_6^- as ionization agent was used. The signal intensities are given in percent relative to the individual intensity measured for the untreated gas flow. Note that the intensities can not be compared quantitatively, since the CIMS has a different sensitivity for each species.

The Ti(IV) denuder leads to a significant decrease of HONO by 97% and of H_2O_2 by 99.5% (Fig. 1). About 40% of the HO_2NO_2 passes the denuder. The strong increase of NO_2 and HNO_3 of 29% and 360%, respectively, indicate that they were produced by red-ox processes in the Ti(IV) denuder system. Standard potentials indicate that HONO could be oxidized by Ti(VI) to NO_2, and HO_2NO_2 could be reduced to HNO_3 by Ti(IV), with Ti(IV) and Ti(VI) both being present in the denuder system. The observed loss or increase, respectively, is consistent with quantitative measurements by a commercial NO_x analyzer (ML 9841A). Quantification of the nitrogen oxides was done by means of the NO_x analyzer in combination with chemical traps. To quantify H_2O_2 a commercial H_2O_2 analyzer (AL1002) was used. Only for NO_2, the CIMS data and the NO_x analyzer data are not consistent, where the CIMS indicates no change while the NO_x analyzer shows an increase in NO_2 during destruction of HO_2NO_2. This discrepancy can not be explained yet.

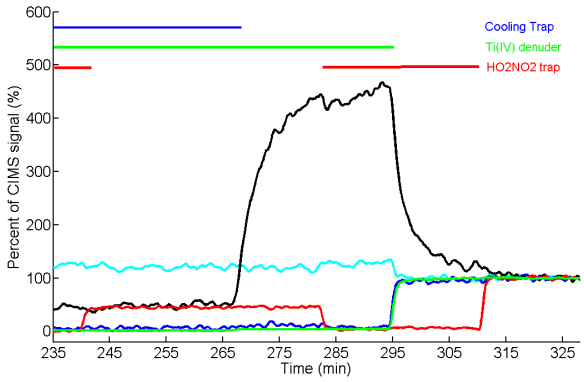

Fig. 1: Traces as measured by the CIMS with time. The signal intensities are given in percent relative to the untreated intensity. NO_2 (light blue), HONO (dark blue), HNO_3 (black), HO_2NO_2 (red) and H_2O_2 (green).

HNO_3 and remaining H_2O_2 are successfully scavenged by a cooling trap (Fig 1, 265 min). Figure 1 also shows that the specific trap for HO_2NO_2, which was used for quantification, does not remove any other species. This trap is a heating system, which decomposes HO_2NO_2 to NO_2 and HO_2.

SUMMARY

The Ti(IV) denuder reduces the H_2O_2 concentration from $6.22*10^{13}$ to $1.24*10^{11}$ molec/cm^3. The HONO concentration is reduced from $3.81*10^{11}$ to $1.74*10^{9}$ molec/cm^3. The denuder produces $3.2*10^{11}$ molec/cm^3 NO_2 and $5.2*10^{11}$ molec/cm^3 HNO_3. About 70 % of the HNO_3 in the system originates from the Ti(IV) denuder. HO_2NO_2 is reduced from $7.1*10^{11}$ to $3*10^{11}$ molec/cm^3, when both the Ti(IV) denuder and the cooling trap are active.

ACKNOWLEDGEMENT

We appreciated funding by the Swiss National Science Foundation (grant number 200021_121857).

REFERENCES

[1] D. L. Slusher et al., J. Geophys. Res., **115**, D07304 (2010).
[2] T. Bartels-Rausch et al., Radiochim. Acta, **99**, 1-8 (2011).
[3] M. Possanzini et al., Sci. Tot. Environ., **77**, 203-214 (1988).

EVOLUTION OF GRAIN BOUNDARIES IN ICE WITH TIME

F. Riche, M. Schneebeli (ETHZ & SLF), T. Ulrich (Univ. Bern & PSI), S. Schreiber (ETHZ & PSI), T. Bartels-Rausch, M. Ammann (PSI)

A new method was developed to visualize and quantify grain boundaries in complex ice or snow samples. First tests with small ice spheres, produced in the laboratory, confirm that the grain boundary content is stable over weeks.

The role of grain boundaries in the interaction of environmental pollutants with ice or snow is currently controversially debated. Ever since acidic pollutants have been found to accumulate in junctions between individual ice grains [1] it has been suggested that these junctions also act as reservoir for trace gases taken up from the atmosphere. Sound conclusions are currently hampered by the lack of a method that would allow describing the grain boundaries in ice samples that are used in experiments. Here we present a stereology method to quantify grain boundaries in ice samples that are frequently used in our laboratory. Stereology is based on the idea that properties in a 3-dimensional sample can be determined from 2-dimensional slices of the sample, without the need to reconstruct the full 3- dimensional structure.

STEREOLOGY

Figure 1 illustrates an example of such a 150 µm thick slice through a sample of packed ice spheres. The polarization microscopy image allows identifying individual ice grains, because the transmittance of polarized light, and thus the color on this image, is influenced by the crystal orientation. A few ice spheres are single crystals, for these grain boundaries exist along the contact area of the individual spheres. The majority of the spheres consist of up to a few ice grains, and for those spheres additional internal grain boundaries can be found.

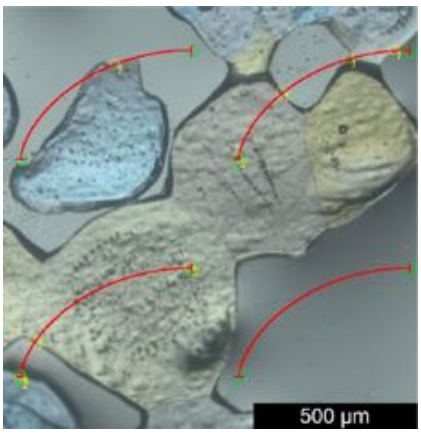

Fig. 1: Microscopic image with polarized light that allows detecting individual ice grains.

To derive the total grain boundary area, that is the total contact area of the individual grains and of the spheres in the 3-dimensional sample, intersections of specific trajectories (red lines in Fig. 1) and grain boundaries are counted in three randomly cut slices. With help of a statistic procedure the total grain boundary area can be derived. In analogy, also the total surface area can be gained. This parameter was used to test the feasibility of the stereology method for these ice samples. The results from the stereology method agree well with a surface area determination by an independent method, the X-ray computer tomography [2].

STABILITY OF GRAINS

Figure 2 shows that the grain boundary area within the individual grains adds up to about 70 % of the total surface area of these specific ice samples. The surface area of an ice sample determines, for example, the amount of trace gases that can adsorb onto the ice. Whether or not this substantial amount of grain boundary area in the sample participates in the uptake of trace gases is the focus of an ongoing project.

Grain boundaries are known to change during snow-metamorphosis such as observed in glaciers. The measurements presented here confirm that the time scales of our laboratory experiments are much too short for changes in grain boundaries.

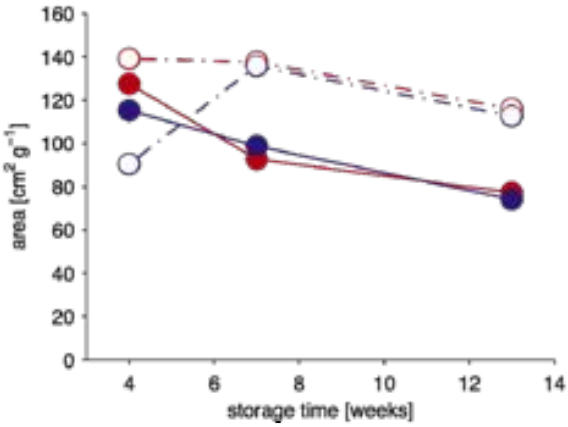

Fig. 2: Internal grain boundary area (solid lines, closed circles) and surface area (dashed line, open circles) of two snow samples over a period of 12 weeks. The snow samples have been stored at -5 °C (red) and at -20 °C (blue).

ACKNOWLEDGEMENT

This work is funded by the Swiss National Science Foundation.

REFERENCES

[1] R. Mulvaney et al., Nature, **331**, 247 (1988).
[2] M. Kerbrat, Atmos. Chem. Phys., **8**, 1261 (2008).

A SOFTWARE ENVIRONMENT FOR SOLVING CHEMICAL KINETICS

T. Bartels-Rausch, M. Ammann (PSI)

A simulation tool originally developed for chemistry models of the atmosphere was adapted and successfully tested for use in laboratory-scale reactors.

Computer simulations are used in atmospheric science to study the production and fate of pollutants and greenhouse gases. For these numerically challenging computations, with typically more than 70 species involved in 200 coupled non-linear chemical reactions, a number of software programs exist. We have used pv-wave before to solve a set of ordinary differential equations (ODE) that describe the photolysis of water in the presence of NO_2 in a laboratory-scale reactor. Here, we describe the advantages of using the kinetic preprocessor environment KPP in combination with matlab for such simulations [1].

ADVANTAGE OF PREPROCESSING

During the preprocessing step chemical equations and kinetic rate constants are parsed and put into a format required as input by matlab's ODE solver. The main two advantages are that (1) the input format is more human-readable and less prone to errors as compared to hard-coded input, as shown in the next example:

```
#PREPROCESSING EQUATIONS INPUT
{MPG P_O2} O2 + hv = O + O1D: 3.5e-19 * I_UV * 1;

# HARD-CODED INPUT
sigma_O2_Hv__O_O  = 2.2d-20; cm^2
R_O2_hv__O_O = sigma_O2_Hv__O_O * O2 * I_UV
D_O2 = D_O2 - R_O2_hv__O_O
D_O  = D_O  + R_O2_hv__O_O
```

(2) With the preprocessing method the set of ODE is also automatically generated. This allows easy changes to the chemical mechanism. In contrast, the hard-coded approach requires rewriting several parts of the hand written code. Also, the preprocessed code is optimized to allow fast simulations.

TESTING THE KPP ENVIRONMENT

In the following we have adapted and tested the kpp-matlab environment by simulating ozone production in a N_2/O_2 mixture in the gas phase during irradiation. Irradiation with light of a wavelength of 172 nm leads to cleavage of O_2 and subsequently O_3 production. Figure 1 shows that the measured ozone mixing ratio can be well reproduced by the model. The simulation was also used to estimate the effect of irradiation intensity on the ozone production. A photon flux of 3×10^{16} photons s^{-1} describes the experimental data best, which is close to the specification of 1×10^{16} photons s^{-1} as given by the manufacturer for this type of lamp.

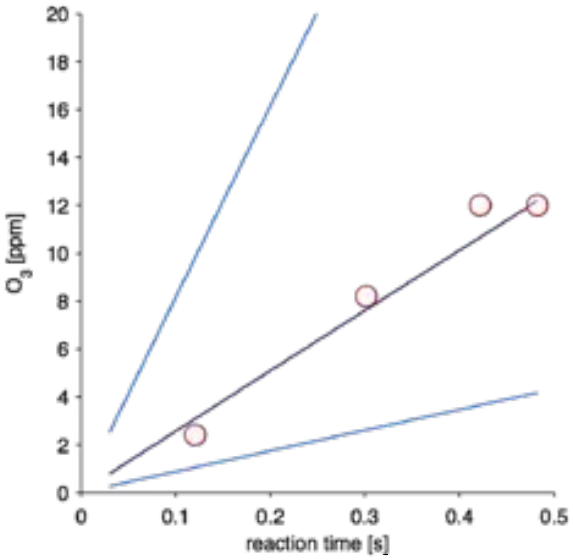

Fig. 1: Measured (open circles) and simulated (solid lines) ozone production at different irradiation times. The simulations were run with a photon flux of 3×10^{16} photons s^{-1} (dark blue), 1×10^{16} and 1×10^{17} photons s^{-1} (light blue).

SUMMARY AND OUTLOOK

We have successfully installed a convenient software environment that uses kpp to generate the kinetic code and matrixes based on chemical equations as input. The mathematical description of the experimental set-up and settings was coded in matlab, which allows easy adaptation to new reactor designs. Matlab is also used to solve the ODE and to run the simulation.

First tests in the presence of water vapour showed less good agreement between experimental measurements and simulations. It is planned to use the sensitivity tools that are integrated into KPP to identify critical rate constants and reactions and optimize their parameterization. Further this software environment will be used to set-up new synthesis routes in our research group.

REFERENCE

[1] A. Sandu et al., Atmos. Chem. Phys., **6**, 187 (2006).

AN ICE-CORE BASED CENTRAL ASIAN DUST RECORD SINCE AD 1250

A. Eichler, S. Brütsch (PSI), S. Olivier (PSI & Univ. Bern), T. Papina (IWEP), M. Schwikowski (PSI & Univ. Bern)

A pronounced dry period in the Siberian Altai around AD 1540-1600 was revealed from analyses of dust in an ice core from Belukha glacier. A potential cause for the dry conditions observed also at other sites in North-Central Asia is a persistent positive mode of the Pacific Decadal Oscillation (PDO) in the 16th century.

The arid and semi-arid regions of Central Asia are a major source area for mineral dust aerosols to the Northern Hemisphere, significantly influencing the Earth's radiative budget and albedo. Here we investigate the dust record in North-Central Asia in the period 1250-2001 using an ice core from Belukha glacier in the Siberian Altai.

Principal component analyses (PCA) was performed on the records of the nine major chemical species and temperature [1]. PC1 explains 50% of the data variance and shows high loadings of dust related ions (Ca^{2+}, Mg^{2+}, Na^{+}, Cl^{-}, SO_4^{2-}). The dominant source areas of mineral dust are the desert regions in Central Asia like the Taklimakan desert, the Kazakh loess hills, and the Aral Sea Basin.

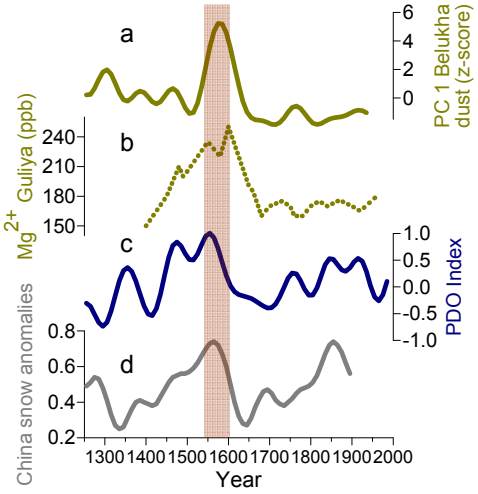

Fig. 1: Records of a) Belukha dust-proxy (PC1, olive green, bold) (AD 1250-1940), b) Guliya Mg^{2+} (olive green, dashed) (20-year averages) [2], c) PDO reconstruction (blue) [3], d) snow anomalies in China (grey, AD 1250-1900) [4], a), c), d) are 80-years lowpass filtered data.

The record of the dust proxy PC1 reveals strong short-term variations and a maximum AD 1540-1600 (Fig. 1a). This extremely dry period was not only observed in the Siberian Altai, but also at other sites in Central Asia. A pronounced Mg^{2+} maximum in the 16th century was detected in the Guliya ice core, Northwestern Tibetan plateau (Fig. 1b, [2]). There is evidence from historical documents that in the period AD 1520-1600 strong negative snow anomalies prevailed in China (Fig. 1d, [4]). These authors found a high correlation between the Index of Abnormal Snow (IAS) and the Pacific Decadal Oscillation (PDO) during the last 1000 years (Fig. 1c), although the dynamic mechanisms linking snow anomalies and the atmospheric circulation remained unclear. We investigated the spatial distribution of correlation coefficients between annual PDO values [5] and gridded annual precipitation data in the period 1948-2009 (Fig. 2a). In agreement with the study mentioned above, there is a negative correlation between PDO and precipitation near the study area. This relation is corroborated by the coherence of different PDO reconstructions with the accumulation record of the Belukha ice core in the period AD 1860-2000 (Fig. 2b). Dry (wet) periods in the Altai were found to coincide with PDO positive (negative) phases. Thus, the persistent positive mode of the PDO in the 16th century deduced from tree-ring reconstructions (Fig. 1c) is a potential cause for the extremely dry period in Central Asia at that time.

ACKNOWLEDGEMENT

This work was supported by the SNF, Marie Heim-Vögtlin program, Grant no. PMPD2-110174.

REFERENCES

[1] A. Eichler et al., Geophys. Res. Lett., **36**, doi: 10.1029/2009GL038807 (2009).
[2] M. Yang et al., J. Asian Earth Sci., **27**, 223 (2006).
[3] Mac Donald et al., Geophys. Res. Lett., **32**, L08703, doi:10.1029/2005GL022478 (2005).
[4] Chu et al., Geophys. Res. Lett., **35**, L14806, doi:10.1029/2008GL034475 (2008).
[5] Mantua et al., Bul. Am. Met. Soc., **78**, 1069 (1997).
[6] Biondi et al., J. Clim., **14**, 5 (2001).

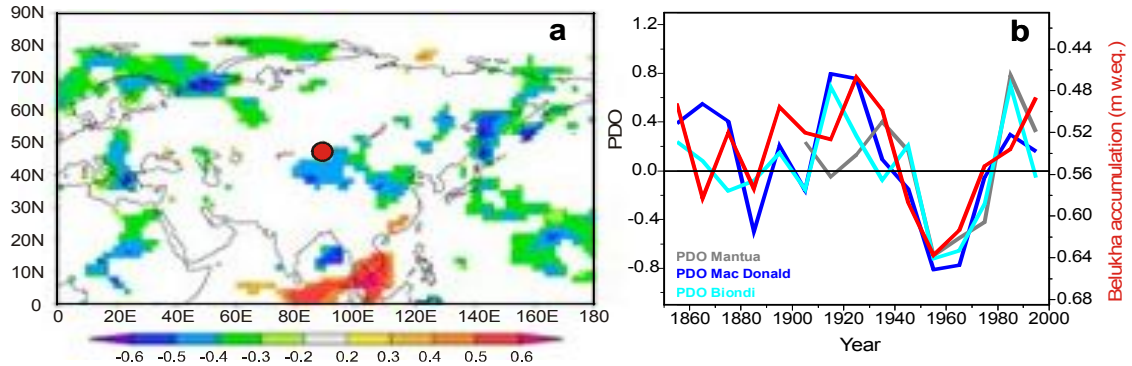

Fig. 2: a) Spatial distribution of correlation coefficients between annual PDO values [5] and gridded annual precipitation (http://climexp.knmi.nl) is shown for the period 1948-2009 (p<10%). The study site is marked (red dot). b) Compilation of different PDO reconstructions ([3]-dark blue, [5]-grey, [6]-light blue) and the accumulation from the Belukha ice core (red, note: right-hand scale is reversed). Shown are 10-year averages.

DETECTING RECENT CLIMATIC CHANGES IN THE RUSSIAN ALTAI WITH A MULTI-PROXY APPROACH

O. Sidorova, M. Saurer, R. Siegwolf (PSI/LAC), A. Eichler (PSI), M. Schwikowski (PSI & Univ. Bern)

The most reliable and detailed climate reconstructions might be obtained by combining the information from different archives, such as tree-rings, ice cores and lake sediment cores. Such multi-proxy approaches have, however, rarely been applied. The Altai region provides an ideal setting for a comparison of different archives because of the high climatic sensitivity of the region and the availability of various well dated archives. Here, we investigated tree-ring, ice core and lake sediment proxies for the assessment of past temperature and precipitation variability in the Russian Altai.

INTRODUCTION

In addition to the classical dendrochronology based on tree-ring width measurements, the stable isotope ratios $\delta^{13}C$ and $\delta^{18}O$ in wood or cellulose provide valuable information about the climate. The carbon isotope ratio in tree-rings reflects water availability and temperature. Trees respond to limited water resources during warm and dry conditions with a reduction of the stomatal conductance to prevent desiccation, which changes the isotope fractionation during CO_2 uptake. The oxygen isotope ratio in tree-rings as well as in ice-cores is dominated by the influence of the isotope ratio in precipitation, which is the source of water for both archives and is known to be influenced by temperature. A previous study on the oxygen isotope variability for the Altai Mountains from an ice core of the Belukha glacier showed strongly increasing temperatures since 1850 [1]. Complimentary information about climate changes in this region are available from sediment cores of a nearby lake (Teletskoe lake), where chemical properties of the sediment were used to characterize temperature and precipitation changes [2]. Together with stable isotope tree-ring chronologies developed here, they enable the application of a multi-proxy approach to reveal similarities in the climate response for the period 1779-2007 [3].

Fig. 1: Photo of the tree-ring sampling site at 2300 m a.s.l. in the Russian Altai (Photo by V.S. Myglan).

RESULTS

A strongly increasing trend since the 1880's was found for the tree-ring width and tree-ring $\delta^{13}C$ chronologies as well as the ice-core parameters $\delta^{18}O$ and melt layers, indicating an air temperature increase (Fig. 2). This strong increase is also clearly reflected in the lake sediment and could be explained by the rising anthropogenic CO_2 emissions in the industrial period. Additionally, similar to the temperature reconstruction from $\delta^{18}O$ in the ice core, the $\delta^{13}C$ in tree cellulose shows two pronounced minima around 1840 and 1920, possibly explained by temperature minima during periods of decreased solar activity.

The $\delta^{18}O$ in the tree-rings showed an opposite (decreasing) trend, thus not in line with the temperature course and the $\delta^{18}O$ in the ice core. This could be explained by the influence of melting permafrost at higher temperatures changing the $\delta^{18}O$ of water sources for the trees. The declining trend in $\delta^{18}O$ agrees well with the precipitation reconstruction from the lake sediment, indicating that for such site conditions $\delta^{18}O$ of tree-rings could rather be used for reconstruction of precipitation.

Long-term climate records are necessary to observe the development of the climate and track the impact of environmental changes on the high-altitude forest ecosystems and glaciers. We conclude that the combination of several independent proxies improves the reliability and quality of the temperature and precipitation reconstruction back into past.

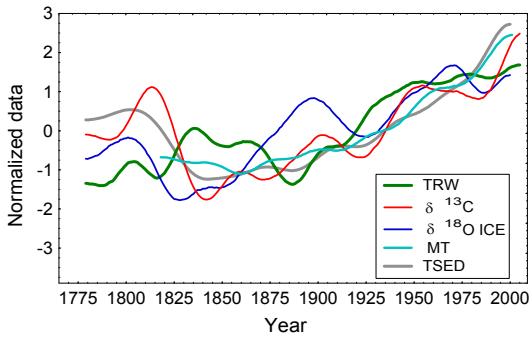

Fig. 2: Different temperature proxy records from the Altai region: Tree-ring width (TRW), carbon isotope ratio of tree-rings ($\delta^{13}C$), oxygen isotope ratio in Belukha ice core ($\delta^{18}O$ ICE), melt percent Belukha ice core (MT), and Teletskoe lake sediment parameters (TSED). Data are 41-year low-pass filtered to emphasize the long-term trends.

ACKNOWLEDGEMENTS

This project was supported by SNF 200021_121838/1, Marie Curie International Incoming Fellowship (EU-ISOTREC 235122), SCOPES Iz73z0-128035/1, RFBR no. 08-06-00253-a, RFBR no. 09-05-98015_r_sibir, AVZP Project 2.1.1/6131, Integration project SB RAS № 92, Scientific school (65610.2010.4).

REFERENCES

[1] A. Eichler et al., Geophys. Res. Lett. 36, L01808, doi:10.1029/2008GL035930 (2009).
[2] I. Kalugin et al., Quaternary Research 67, 400–410, (2007).
[3] O. Sidorova et al., Climate Dynamics, doi: 10.1007/s00382-010-0989-6 (2011).

DATING AN ICE CORE FROM THE TSAMBAGARAV, MONGOLIAN ALTAI

P.-A. Herren, A. Eichler, J. Eickenberg, L. Tobler (PSI), E. Vogel (Univ. Bern), T. Papina (IWEP), M. Schwikowski (PSI & Univ. Bern)

The upper 36 m weq of the Tsambagarav ice core were dated using three independent techniques, including identification of tritium and volcanic horizons, annual layer counting, and nuclear dating with ^{210}Pb. The results confirm the potential of this ice core for a climate reconstruction of approximately one millennium.

In summer 2009 an ice core was drilled on the Tsambagarav in the Mongolian Altai (4140 m asl, 48°39.338'N, 90°50.826'E) [1]. The feasibility to use the ice core as climate archive was demonstrated by analyzing major ion concentrations in the upper 12 m [2].

For dating the ice core three different methods were applied: Identifying horizons, annual layer counting, and nuclear dating with ^{210}Pb decay. Stratigraphic horizons are well known events, which can be detected in the core. To identify the year 1963, we used the tritium peak resulting from nuclear weapon tests. Liquid scintillation counting was applied to measure the tritium activity, first with a coarse resolution of 60 cm to identify the approximate depth, followed by fine resolution resulting in a depth of 15.3 m weq for the year 1963 (Fig. 1).

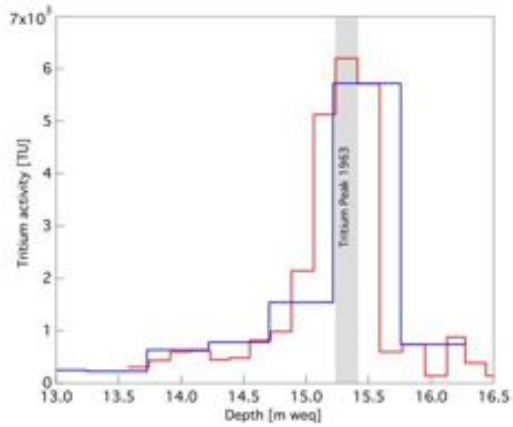

Fig. 1: Evolution of the tritium activity with depth of the Tsambagarav ice core for coarse (blue) and fine (red) resolution.

Horizons used to date the lower part of the ice core are from volcanic eruptions. The nonmineral sulfate record, referred to as excess sulfate was calculated by applying the formula: [ex-sulfate] = [sulfate] - 0.22[calcium] and used to identify volcanic horizons. Peaks in the excess sulfate record were related to the 1934 Cerro Azul, 1912 Katmai, 1854 Shiveluch and 1815 Tambora eruptions. At present state the oldest identified volcanic eruption is 1815 Tambora at a depth of 36.3 m weq. The attribution of the volcanic horizons is corroborated by similar patterns in the Tsambagarav and the Belukha records [3].

Between the horizons the three parameters ammonium, formate and δ^{18}O are used for annual layer counting. They show the most pronounced seasonality. Chemical tracers are independent of the δ^{18}O record, which increases the robustness of the dating. Within one decade of each horizon, the accuracy is estimated to be ±1 year, outside of these ranges it is ±2-3 years.

Nuclear dating with ^{210}Pb is applied as third method to confirm previous dating. Assuming a constant input of ^{210}Pb on the glacier, the decrease of activity with depth can be used to give an approximate age (Fig 2).

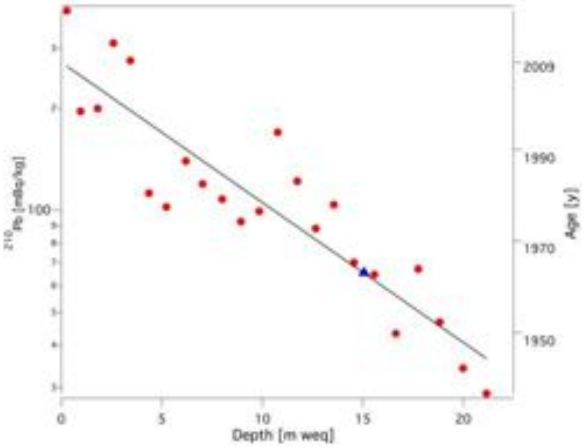

Fig. 2: ^{210}Pb activity (red dots) and linear fit (black line) with corresponding age with depth in the Tsambagarav ice core. Location of the tritium peak is indicated by a blue triangle.

The ^{210}Pb activity fluctuations can be explained by a slight divergence of the assumed constant input. The continuous decrease in activity confirms an increase of age and excludes a hiatus with depth. The layer-thinning can be neglected in the upper part of the core, enabling linear fitting. Dating with ^{210}Pb and the tritium peak coincide well, resulting in an accumulation rate of 0.33 m weq per year. Applying this accumulation rate on a simple thinning model [4] leads to an estimated age of 1000 years at the bedrock. However, the uncertainty of the attributed age increases exponentially with depth.

The remaining lower part of the ice core will be analyzed and dated identical to the upper part. Additionally, a ^{14}C dating method will be applied to date the ice close to bedrock [5]. The records of Tsambagarav and Belukha will be compared for a complete regional climate reconstruction.

ACKNOWLEDGEMENT

This work is supported by the Swiss National Science Foundation (200021_119743).

REFERENCES

[1] M. Schwikowski et al., Ann. Rep. Lab. of Radio- & Environ. Chemistry, Uni Bern & PSI (2009), p. 31.
[2] P-A Herren et al., Ann. Rep. Lab. of Radio- & Environ. Chemistry, Uni Bern & PSI (2009), p. 32.
[3] A. Eichler et al., Geophys. Res. Lett. **36** doi: doi:10.1029/2008GL035930 (2009).
[4] J. F. Nye, J. Glaciol. **4**, 36 (1963).
[5] A. Zapf et al., this report, p. 31.

ACCUMULATION RATES DERIVED FROM PÍO XI ICE CORE, SOUTHERN PATAGONIA ICEFIELD

M. Schläppi (Univ. Bern & PSI), P. Santibañez, G. Casassa, A. Rivera (CECS), M. Schwikowski (PSI & Univ. Bern)

The 50 m ice core from the Pío XI glacier is the first core from the Southern Patagonia Icefield showing a well preserved stable isotope record ($\delta^{18}O$, δD). Annual net accumulation derived from annual layers identified in the stable isotope profile ranged from 3.4 to 7.1 m water equivalent. This is comparable to precipitation amounts at the Chilean coast, but not as high as expected for the Icefield. A good correlation with upper air temperatures from Punta Arenas indicates that the Pío XI stable isotope composition is mainly controlled by temperature.

INTRODUCTION

Pío XI, the largest glacier of the Southern Patagonia Icefield, reached its neoglacial maximum extent in 1994 and is one of the few glaciers in that area which is not retreating. In view of the recent warming it is important to understand glacier responses to climate changes. Due to its remoteness and the harsh conditions in Patagonia, no systematic mass balance studies have been performed. In this study we derived net accumulation rates from a 50 m ice core collected in the accumulation area of Pío XI (2600 m a.s.l., 49°16'40''S, 73°21'14''W) [1].

RESULTS AND DISCUSSION

The annual accumulation rates were determined by identifying annual layers in the ice core stable isotope record ($\delta^{18}O$). The proposed dating results in high annual net accumulation rates of 3.4 to 7.1 m weq, with an average of 5.8 m weq (Fig. 1), comparable to precipitation amounts at the Chilean coast, but not as high as expected for the Icefield. A strong support for this dating is the fact that the Pío XI core overlaps with a shallow firn core collected from Gorra Blanca Norte (GBN) in September 2001 [2] (Fig. 1). GBN is located 26 km to the Northeast of Pío XI, with an elevation at the core site of 2300 m a.s.l. This firn core was dated by attributing two distinct minima in the $\delta^{18}O$ to July 2001 and July 2000, respectively. In order to overlap the two minima in the GBN record with the Pío XI record, the depth scale of GBN was stretched by a factor of 2.8.

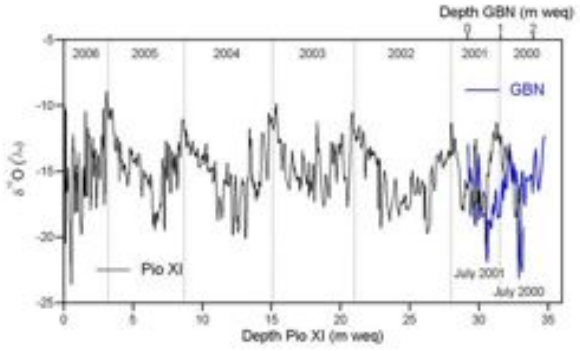

Fig. 1: $\delta^{18}O$ records from Pío XI and Gorra Blanca Norte (GBN) [1].

In order to check the potential of $\delta^{18}O$ as temperature proxy, the record was compared to temperatures at 700 hPa (approximately 2850 m a.s.l.) from upper air radiosonde data collected at Punta Arenas. The depth scale of the ice core was transformed into a time scale starting on 12th Dec. 2000 and ending on 1st Sept. 2006. The $\delta^{18}O$ data series agrees reasonably well with the air temperatures, yielding a Pearson correlation coefficient of $r = 0.63$. This indicates that the Pío XI stable isotope composition is mainly controlled by temperature (Fig. 2).

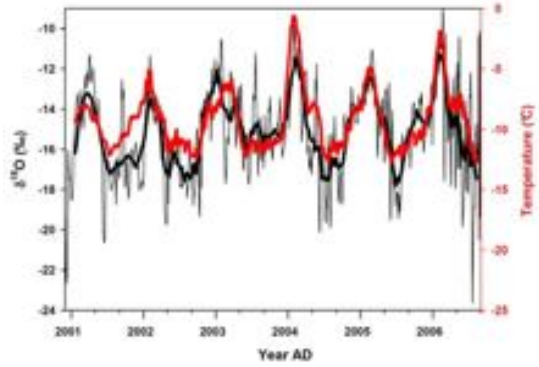

Fig. 2: Pío XI $\delta^{18}O$ record (thin black line: raw data, thick black line: 29 pt. mov. average) compared to 700 hPa temperatures from Punta Arenas (red line).

With a simple glacier flow model [3] the age near bedrock was estimated, using minimum and maximum accumulation rates of 4.4 and 7.1 m weq, respectively, and a glacier thickness of 140 m weq (Fig. 3). Assuming a well-preserved record in the deeper part, the Pío XI glacier may contain 100 to 200 years of past climate history.

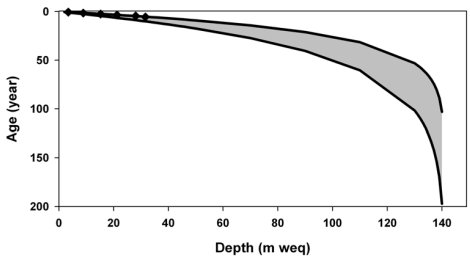

Fig. 3: Age-depth relation developed for Pío XI glacier, using a Nye type glacier flow model and ice core-derived accumulation (diamonds).

REFERENCES

[1] M. Schläppi, PhD thesis, University of Bern (2010).
[2] M. Schwikowski et al., Ann. of Glac., **43**, 8 (2006).
[3] J.F. Nye, J. Glaciology, **4**, 785 (1963).

HIGH-RESOLUTION BLACK CARBON RECORD FROM PÍO XI GLACIER, SOUTHERN PATAGONIA ICEFIELD

M. Schläppi (Univ. Bern & PSI), G. Casassa, A. Rivera (CECS), M. Laborde, M. Gysel (PSI/LAC), S. Kaspari (CWU), A. Eichler (PSI), M. Schwikowski (PSI & Univ. Bern)

First black carbon (BC) concentrations in snow and ice from the Southern Hemisphere outside Antarctica are presented, showing a very low concentration level ranging from 0.001 to 1.4 μg l^{-1}. BC seasonal maxima occur in September which is mainly determined by the forest fire activity in the Amazon Basin.

INTRODUCTION

Black Carbon (BC) is a byproduct of incomplete combustion of biomass and fossil fuels and contributes directly to global warming due to absorption of sunlight and indirectly due to its impact on snow albedo [1]. Despite its importance concerning climate forcing little is known about global concentration distribution and emission histories especially from the Southern Hemisphere. Here we present a first BC concentration record from Pío XI ice core, retrieved from the Southern Patagonia Icefield (49°S, 73°W, 2600 m a.s.l.). For details of this ice core see [2].

METHOD

BC concentrations were determined with a single particle soot photometer (SP2, Droplet Measurement Technologies©, DMT, Boulder, USA) [3]. The central component in the SP2 is a continuous Nd:YAG laser (1064 nm wavelength) which hits a dry aerosol flow. The resulting laser induced incandescence allows determination of single BC particles with 100% efficiency in the size range measured by the SP2. The mass of BC is proportional to the thermal radiation, and the method is not susceptible to interferences from organic matter or inorganic salts [4]. Ice core samples were acidified with HNO_3 to 0.5M. After sonification for 15 minutes samples were nebulized (CETAC, U5000AT$^+$). The produced dry aerosol was transferred with a particle free carrier gas to the SP2 [2].

RESULTS

BC concentrations in Pío XI ice core are characterized by high year-to-year and seasonal variability and range from 0.001 to 1.4 μg l^{-1} with an average of 0.08 μg l^{-1} in the time period from 2003 to 2006 (Fig. 1). These values are extremely low even when compared to Antarctic BC levels. However, the results are not directly comparable due to different methods used and different method sensitivity for analyzing BC concentrations. Differences of an order of magnitude in concentration were reported for BC analyzed in ice samples with SP2 compared to a thermo-optical technique (Sunset RT 3080) [5]. This is assumed to be due to the fact that the SP2 is highly specific to refractory BC, whereas thermo-optical methods are assigning a larger portion of the OC-BC spectrum to BC.

Generally, maxima are observed in September each year, and two additional peaks occurred in Mai 2003 and March/April 2005, respectively. The maxima in September coincide with the period of highest monthly total number of forest fires in Brazil [6] (Fig. 1). Forest fires emit large amounts of BC due to the low burning temperature and therefore incomplete combustion [7]. The BC maxima in September in the Pío XI core are in good agreement with the seasonality of ambient BC concentrations at Ferraz Station, situated in the northwest of the Antarctic Peninsula [8]. Similar observations were made at Halley station on Brund Ice Shelf. Maximum BC concentrations in October were associated with biomass burning in tropical regions [9]. We therefore assume that BC concentrations at Pío XI are mainly determined by long range transport of BC from forest fire activity in the Amazon Basin.

One interesting coincidence is the peak in the period from Feb. to Mar. 2005 with forest fires taking place at the end of Feb. 2005 in Torres del Paine National Park, 200 km south of Pío XI [10]. We assume that these fires are the main source for BC in the Pío XI ice core in this period.

.

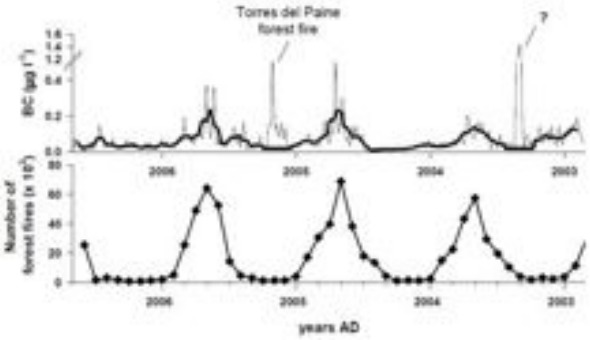

Fig. 1: BC concentrations from Nov. 2002 to Aug. 2006 (thin black line) and 9 pt. moving average (thick black line) and monthly total number of forest fires in Brazil [5].

REFERENCES

[1] J. R. McConnell et al., Science, 317, 1381 (2007).
[2] M. Schläppi, PhD thesis, University of Bern (2010).
[3] J. P. Schwarz et al., J. Geophys. Res., 111, doi:10.1029/2006JD007076 (2006).
[4] N. Moteki & Y. Kondo, Aerosol Sci. Technol., 41, 398 (2007).
[5] S. Kaspari et al., submitted to Geophys. Res. Lett. (2010).
[6] http://sigma.cptec.inpe.br/queimadas/.
[7] A. Pettus, A special CATF report, Boston (2009).
[8] E.B. Pereira et al., J. Geophys. Res., 111, doi:10.1029/2005JD005881 (2006).
[9] E.W. Wolff & H. Cachier, J. Geophys. Res., 103, 11033 (1998).
[10] R.M.N. Cerrillo et al., Rev. Chil. de Hist. Nat., 81, 95 (2008).

CONCENTRATIONS OF SEA SALT TRACERS AS WIND SPEED PROXY IN THE PÍO XI ICE CORE, SOUTHERN PATAGONIA ICEFIELD

M. Schläppi (Univ. Bern & PSI), A. Eichler, L. Tobler (PSI), A. Rivera, G. Casassa (CECS)
M. Schwikowski (PSI & Univ. Bern)

Concentration records of major ions and trace elements in the Pío XI ice core show a dominance of sea salt species, which are significantly correlated with wind speed and can thus be used as wind speed proxy.

The analysis of chemical trace species in ice cores allows investigation of changes and trends in naturally occurring and anthropogenic aerosols, natural biogeochemical cycles, but also atmospheric transport pathways and source regions even in the most remote regions. Here we present concentrations of major ions and trace elements determined in a 50 m long ice core from the accumulation area of Pío XI glacier (49°16'S, 73°21'W, 2600 m a.s.l.). The Pío XI ice core was dated using seasonal variations of the stable isotope records, which are mainly controlled by changes in air temperature. Due to the high accumulation the core covers six years only (December 2000 to September 2006) [1]. Trace element concentrations were determined by continuous ice melting inductively coupled plasma sector field mass spectrometry (CIM-ICP-SFMS) with an Element 1 (Thermo Finnigan) [2, 3] and major ion concentrations with ion chromatography.

Trace element and ion concentrations in the Pío XI core are extremely low and comparable to conditions in Antarctica [4]. This is due to the remoteness of Pío XI from emission sources and due to dilution because of high precipitation rates. The prevailing source of impurities is the ocean. Accordingly, concentrations of sea salt tracers Na^+, Cl^-, Mg^{2+}, Ca^{2+}, and Sr^{2+} are the dominant species and are highly correlated among each other (with correlation coefficients r between 0.69 and 0.95, n = 2158).

In order to investigate seasonal variations of trace species in the Pío XI ice core, data were smoothed with a low pass filter using a 1/100 year sampling frequency corresponding to approximately 3.5 day averages and a cut-off frequency of 0.25 year. Daily average wind speed from gridded NCEP/NCAR reanalysis data for coastal region between 47 and 60°S shows a high positive correlation with the variations in sea salt species for the years 2003 to 2006, which is shown for Na^+ (Fig. 1).

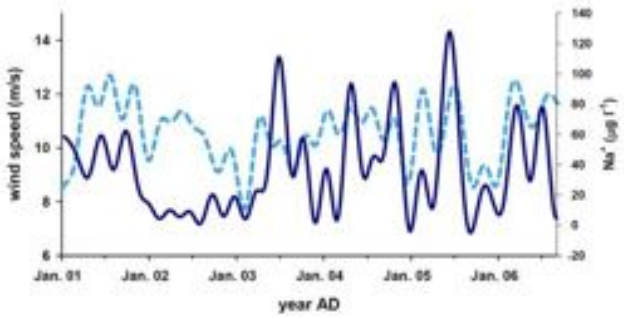

Fig. 1: Record of smoothed Na^+ concentrations (dark blue) and smoothed daily average wind speeds (light blue) from January 2001 to July 2006.

The highest correlation was found for the nearest grid at 55°S, 76°W (r = 0.54, n = 573, logarithmic Na^+ concentrations). We therefore assume that wind speed is one of the main drivers of the sea salt tracer concentrations at Pío XI. Although data sets correlate, the amplitude of the Na^+ concentration is higher. This may be a result of the nonlinear dependence of sea salt production on wind speed which is described with an exponential function [5]. Estimates based on gridded mean wind speed are biased towards lower values because the sea salt production of gusting winds is underestimated. For the years 2002 and 2001 the Na^+ signature is affected by melting.

Na^+ data, which were low pass filtered with a 1/100 year sampling frequency and a cut off frequency of one year, show again a clear positive correlation to wind speed with a maximum in austral winter (r = 0.44, n = 573), whereas the temperature proxy $\delta^{18}O$ shows a maximum in austral summer (Fig. 2). Typically, at mountain sites enhanced convection due to higher temperatures in summer leads to a more efficient transport of aerosols, resulting in a strong seasonality with maxima in this time of the year [6]. This is not observed at Pío XI, suggesting that wind speed is the dominant controlling factor for sea salt tracers in precipitation at this lower-elevation site.

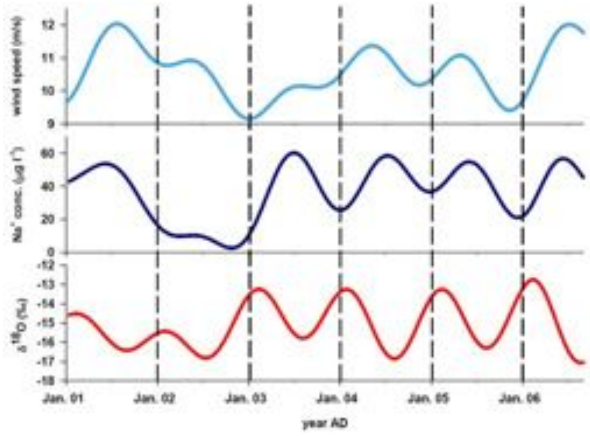

Fig. 2: Low pass filtered records of wind speed (light blue), Na^+ concentration (dark blue) and $\delta^{18}O$ values from January 2001 to August 2006 [1].

REFERENCES

[1] M. Schläppi, PhD thesis, University of Bern (2010).
[2] S. Knüsel et al., Environ. Sci. Technol. **37**, 2267 (2003).
[3] T. Kellerhals et al., Environ. Sci. Technol. **44**, 888 (2010).
[4] P. Vallelonga et al., Annals Glac. **39**, 169 (2004).
[5] D.J. Erickson et al., J. Geophys. Res., **91**, 1067 (1986).
[6] A. Döscher et al., Geophys. Res. Lett. **23**, 2741 (1996).

PLUTONIUM FROM NUCLEAR WEAPONS TESTS RECORDED IN THE COLLE GNIFETTI ICE CORE

J. Gabrieli, G. Cozzi, C. Barbante (Univ. Venice & IDPA-CNR Venice), M. Sigl, H.W. Gäggeler, M. Schwikowski (PSI & Univ. Bern), J. Eickenberg (PSI), L. Wacker (ETHZ), C. Boutron (LGGE Grenoble)

A high resolution ^{239}Pu record was obtained by analyzing 52 discrete samples of an Alpine firn/ice core from Colle Gnifetti (Monte Rosa, 4450 m a.s.l.), dating from 1945 to 1990. The ^{239}Pu activity concentration was determined directly, without preconcentration or purification steps, using an ICP-SFMS equipped with a desolvation system.

INTRODUCTION

Plutonium is present in the environment as a consequence of the atmospheric nuclear tests carried out since the 1950s as well as the production of nuclear weapons and industrial releases over the past 60 years. Pu fallout has been studied in various environmental archives and also in mid-latitude ice cores, from Mont Blanc in the Western Alps [1] and Belukha Glacier in the Siberian Altai mountains [2]. Pu was typically analyzed by Accelerator Mass Spectrometry (AMS) using an optimized sample preparation procedure. As high levels of uranium can interfere with the mass spectrometric measurement of ^{239}Pu, a purification step was required. Analyses were carried out using a 14 MV tandem accelerator to determine the concentrations of ^{239}Pu and ^{240}Pu. This method gives very accurate results but is time-consuming and requires expensive instrumentation and demanding procedures for sample preparation. Moreover, the large sample quantity required for pre-concentration (2-3 kg) precludes this procedure for high resolution analysis of ice-cores.

METHOD

A new continuous melting device for on-line decontamination and analysis of firn/ice cores was used for the Colle Gnifetti firn/ice sections. Melt water from the inner part of ice core sections was pumped to an ICP-QMS and a conductivity micro-cell for determination of trace elements and continuous conductivity measurements, respectively. Discontinuous samples were also collected with a spatial resolution ranging from 15 to 40 cm (0.5-1.5 yr). ^{239}Pu was determined in 52 discrete samples dated from 1945 to 1990 AD by direct analysis, using an Element2 ICP-SFMS (Thermo Scientific, Germany) in low resolution mode and coupled to an Apex Q high efficiency sample introduction system (Elemental Scientific, USA) to achieve the maximum instrumental sensitivity. The single data (12 for each sample) affected by signal spikes due to $^{238}UH^{+}$, the main interference for ^{239}Pu, were manually eliminated and the remaining mean values were averaged, obtaining the final result. An indirect calibration of ^{239}Pu with ^{238}U was applied using an external calibration curve ranging from 0.2 to 5.0 ppt. This approach is valid as a first approximation because the sensitivity of heavy elements in ICP-SFMS is strongly correlated to their masses.

RESULTS

The ^{239}Pu profile, as shown in the following figure, reflects the three main periods of atmospheric nuclear weapons testing: the earliest peak lasted from 1954/55 to 1958 and was caused by the first testing period reaching a maximum in 1958 [3]. Despite a temporary halt of testing in 1959/60, the Pu concentration decreased only by half with respect to the 1958 peak due to long atmospheric residence times. In 1961/62 Pu concentrations rapidly increased reaching a maximum in 1963, which was about 40% more intense than the 1958 peak. After the signing of the "Limited Test Ban Treaty" between USA and USSR in 1964, Pu deposition decreased very sharply reaching a minimum in 1967. The third period (1967-1975) is characterized by irregular Pu concentrations with smaller peaks (about 20-30% of the 1964 peak) which might be related to the deposition of Saharan dust contaminated by the French nuclear tests of the 1960s.

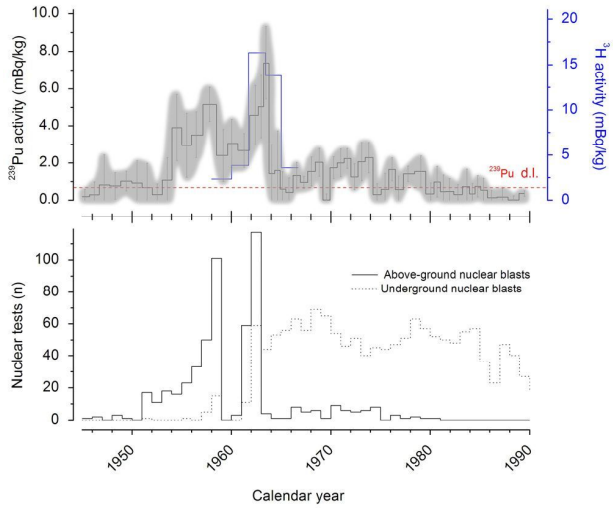

Fig. 1: ^{239}Pu activities, with the associated RSD (grey shading), in the upper 31 m of firn and ice from Colle Gnifetti and five ^{3}H measurements (blue line), corresponding approximately to the time period 1945-1990, compared with the number of worldwide nuclear tests (solid line: atmospheric tests; dotted line: underground tests).

The data presented are in very good agreement with Pu profiles previously obtained from the Col du Dome ice core (by multi-collector ICP-MS) and Belukha ice core (by AMS).

REFERENCES

[1] T. Warneke et al., Earth Planet. Sci. Lett, 203, 1047 (2002).
[2] S. Olivier et al., Environ. Sci. Technol., 38, 6507 (2004).
[3] J. Gabrieli et al., Atmos. Environ., in press (2010).

A COMPARISON OF ATMOSPHERIC CIRCULATION PROXIES FROM TWO ALPINE ICE CORES

I. Mariani, M. Sigl (Univ. Bern & PSI), T. Jenk (CIC), A. Eichler (PSI), M. Schwikowski (PSI & Univ. Bern)

The Northern and the Southern Alps are supposed to be affected by different sources of precipitation, due to the orographic barrier. Here a new study of two ice cores coming from both the sides of the Alps is presented. $\delta^{18}O$ and deuterium excess as well as the precipitation amount are investigated.

INTRODUCTION

The atmospheric circulation over the Alps is characterized by the interaction between the air masses and the orographic barrier, leading to different effects. The Northern Alps receive in general less precipitation, because their moisture sources are the colder and drier continental air masses originating from the Atlantic. In contrast, the Southern Alps are affected by the warmer and more humid air coming from the Mediterranean, with peaks of precipitation in spring and autumn [1, 2]. Convective systems in summer are important at both sides.

In order to better understand the atmospheric circulation over the Alps, we investigate in this study records from two different ice cores, obtained at the Fiescherhorn glacier, Northern Alps [3], and the Grenzgletscher glacier, Monte Rosa massif, Southern Alps [2]. Investigated proxies for temperature, humidity, and precipitation are the $\delta^{18}O$, the d excess, and the reconstructed accumulation, respectively.

RESULTS

The analysis of $\delta^{18}O$ from both ice cores shows that it reflects the seasonal cycle of temperature, with higher values in summer and lower ones in winter. More differences and fluctuations are present in the d excess series, probably indicating the effect of different air masses (Fig.1). A transformation of these ice core values in monthly series, by weighting the annual layers with the amount of precipitation, could be helpful in comparing them with, for example, temperature fields.

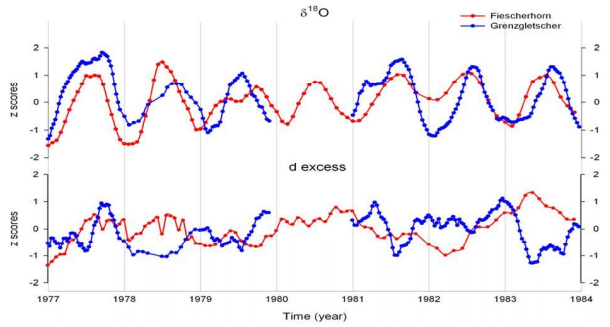

Fig. 1: $\delta^{18}O$, d excess obtained for the period 1977-1984. The gap between 1980 and 1981 in the Grenzgletscher record is due to bad core quality in this part. Different smoothing was applied because of a higher accumulation and variability in the Grenzgletscher record.

In order to test whether the accumulation can be split in monthly values, a correlation analysis with high resolution (~2.2 x 2.2 km) gridded precipitation data, provided by Meteoschweiz, was conducted. The periods were 1962-2002 for Fiescherhorn and 1962-1993 for Grenzgletscher. First results indicate that whereas Grenzgletscher shows a significant correlation with the local precipitation, this is not the case for the Fiescherhorn site. The reasons for the different behaviour are not yet understood and could be in part due to an error in the dating. Another source of uncertainty is the applied correction for glacier flow which induces thinning of annual layers. We tested different models for thinning correction ([3,4], this study), but none was suitable to fit both the upper and lower part satisfactorily (see e.g. Fig. 2). Thus the behaviour of Fiescherhorn glacier cannot be explained with a simple flow model and future effort is needed to explain annual layer thinning with depth.

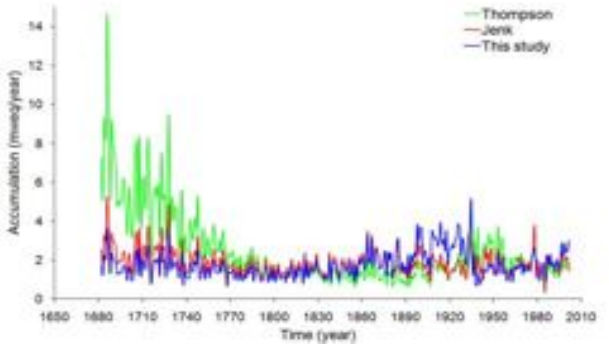

Fig. 2: Accumulation reconstructions for the Fiescherhorn ice core. Here different models are used for correction of layer thinning [3, 4].

ACKNOWLEDGEMENTS

This work is supported by the NCCR Climate program of the SNF (PALVAREX project). Meteoschweiz is acknowledged for the data provided.

REFERENCES

[1] H. Sodemann et al., Int. J. Climatol. **30**, 947 (2009).
[2] A. Eichler, PhD thesis, University of Bern (2000).
[3] T. Jenk, PhD thesis, University of Bern (2006).
[4] L.G. Thompson et al., Annals Glaciol. **14**, 288 (1990).

RECONNAISSANCE STUDY OF LA MESA GLACIER, ARGENTINEAN ANDES

M. Schwikowski, P.-A. Herren, B. Rufibach, M. Sigl (PSI & Univ. Bern)

In order to find a glacier suitable for ENSO reconstruction beyond the instrumental period a reconnaissance expedition to La Mesa glacier in the Central Argentinean Andes was conducted. This expedition revealed that the accumulation area of La Mesa is much steeper and more crevassed than expected. In addition, the final part of the access route is too steep to allow transport of equipment by mules. Thus, La Mesa glacier is not suitable for ice coring with currently available methods.

The El Niño-Southern Oscillation (ENSO) is a quasi-periodic climate pattern that occurs across the tropical Pacific Ocean with on average five year intervals. ENSO causes extreme weather such as floods and droughts. The present strong La Niña was responsible for the disastrous flooding in Pakistan in 2010 and the current inundations in Australia. The characteristics of ENSO are potentially subject to dramatic changes as a result of global warming. In order to place the recent strong ENSO events into the longer term perspective, ENSO reconstructions from natural archives are needed. Potential ENSO archives may include glacier ice cores from subtropical South America, between 28 and 35°S, a region were El Niño events are associated with increased precipitation [1]. Their suitability was indeed demonstrated with the ice core from Glaciar La Ollada, Cerro Mercedario (31°58'S, 70°07'W, 6100 m a.s.l.), showing positive accumulation anomalies and increased ion concentrations in El Niño years [2]. However, the 104 m Mercedario ice core covers only 92 years (1913-2004) and does not allow ENSO reconstruction beyond the instrumental period. This is due to unexpected high annual accumulation rates (0.91 m weq.) and to the fact that bedrock at 145±15m was not reached because of the presence of an impenetrable stone layer at 104 m.

The aim of the present study was therefore to find another glacier in the same area, potentially allowing a reconstruction going further back in time.

From areal photos, the glacier La Mesa in the Cordillera de la Ramada (Fig. 1), about 11 km south of Glaciar La Ollada, was selected for a reconnaissance study. La Mesa is one of the largest glaciers in this area. Based on the rather limited information available La Mesa seemed to fulfill all prerequisites for paleo-climate reconstruction (extended glacier plateau with smooth surface, sufficient elevation to ensure cold ice temperatures, sufficient glacier thickness to obtain long record).

The reconnaissance expedition was conducted from 15 February to 4 March 2010. The approach started from Casa Amarilla (1950 m a.s.l.) at the confluence of Rio Colorado and Rio Blanco, the highest point reached by cars. The equipment was carried by mules which were also used for river crossing of the Rio Colorado. Three intermediate camps were established at 2800 m, 3600 m, and 4600 m, respectively, in order to establish after five days the high camp at 5300m a.s.l. This was the highest point the mules could reach. From the high camp it took a three to four hours climb to the pass at 5800 m a.s.l. between La Mesa and Alma Negra summits, from where we had the first view of La Mesa glacier (Fig. 2). This showed that the accumulation area of La Mesa is much steeper than expected, that it is crevassed and that the smooth parts are below the Equilibrium Line Altitude (ELA), and therefore not suitable for ice coring. Furthermore the final parts of the access route are too steep for transport of equipment by mules. Thus, we conclude that La Mesa glacier is not suitable for ice coring and no further expedition will be conducted to extract a deeper core from that glacier.

Fig. 1: View from south to La Mesa glacier with Alma Negra, the highest mountain on the right (photo Raphaël Joliat). The Pass reached at 5800 m is the lowest part on the northern crest. From there the photo from fig. 2 was taken.

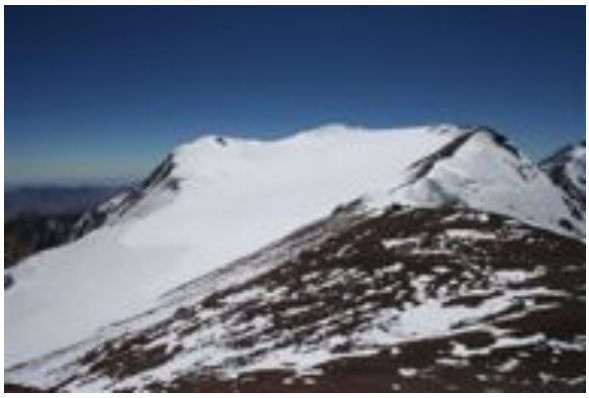

Fig. 2: View from east of the accumulation area of La Mesa glacier from the pass (5800 m a.s.l.) between La Mesa and Alma Negra summits (photo Beat Rufibach). The ELA is the s-shaped line, separating the upper snow-covered, white accumulation area from the lower ice-covered, grey ablation area.

ACKNOWLEDGEMENT

We thank Raphaël Joliat for the fantastic work in organizing the logistics.

REFERENCES

[1] P. Aceituno, Mon. Wea. Rev., **116**, 505 (1988).
[2] A. Ciric, PhD thesis, University of Bern (2009).

EFFECTS OF SOOT, ALGAE AND MINERAL DUST ON THE ALBEDO OF THE PLAINE MORTE GLACIER, SWITZERLAND

E. Buehlmann, P.A. Herren (Univ. Bern & PSI), M. Hoelzle (Univ. Fribourg), I. Lehner (ETHZ), M. Schwikowski (PSI & Univ. Bern)

During the melting season, particulate matter enriches on the surface of glaciers, causing a surface darkening and consequently reducing the glacier albedo. Here, first results of albedo measurements on the Plaine Morte glacier throughout summer 2010 are presented.

INTRODUCTION

Accumulation of particles on glaciers occurs by wet and dry deposition during all seasons. The concentration at the surface, however, is most significantly enhanced during summer, when the particle containing snow cover melts and the particles remain at the glacier surface. The resultant albedo reduction is principally determined by the chemical composition of the accumulating debris. Black carbon (BC) is formed by incomplete combustion and has been found to contribute strongly to the overall absorption of solar radiation [1]. Deposited to a snow or ice surface, its radiative forcing potential has been estimated to outweigh the temperature increase of an equivalent CO_2 radiative forcing by a factor of 1.7 [2]. However, the composite effect of other debris components like mineral dust [3] or algae [4, 5] on glacier albedo has not been studied in detail. Therefore, the purpose of this study is to follow albedo changes during the melt season and relate the findings to the chemical composition of the accumulated debris.

STUDY SITE

The Plaine Morte glacier is situated at an altitude of ~2750 m a.s.l. and extends over an area of roughly 9 km^2, showing no distinct tongue and little gradient. In recent years, melting processes dominated the entire glacier surface, which illustrates that the Plaine Morte glacier is in a state of retreat. The glacier is accessible with a cable car throughout the year. During winter time, a ski lift connects several slopes on the glacier surface to the main skiing area on the southern slopes of the Crans-Montana region. Thus the Plaine Morte glacier is strongly influenced by human activities, which implies a local soot source.

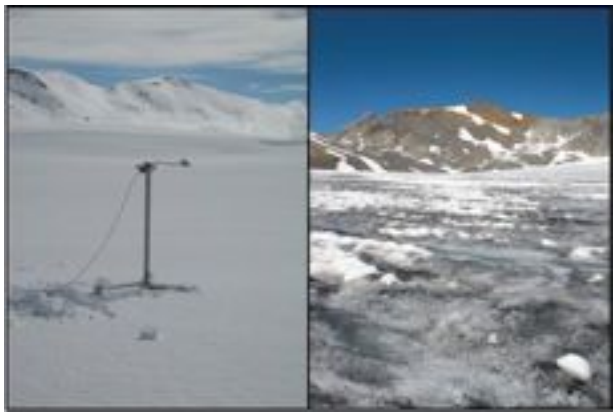

Fig. 1: Pictures of Plaine Morte glacier on 1 June 2010 (with albedometer) and 25 August 2010, illustrating the change in surface albedo.

METHODS AND RESULTS

The albedo was measured with a broadband albedometer from ETH Zurich on four dates throughout summer 2010 (1 June, 6 July, 20 July and 25 August). All four days met the condition of low cloud cover (estimated less than 10%). On the first two dates, the glacier was still snow covered (Fig. 1). On these measurement days, snowpit sampling was performed. From 20 July onward, the glacier ice was exposed, which facilitated sampling of contaminated surface ice.

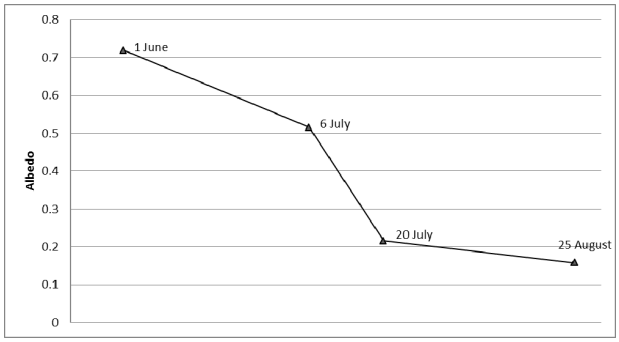

Fig. 2: Mean albedo of the Plaine Morte glacier on the four measurement days (11:30am-12:30pm).

As can be seen in Figure 2, the albedo decreased strongly, from 0.72 in early June to 0.16 in late August (mean value of data measured from 11:30 am to 12:30 pm in 10 sec intervals). The prominent albedo reduction within two weeks in July is attributed to a prolonged heat wave, causing melt of the entire snowpack. However, these values are not yet corrected for the solar angle and the albedo reduction due to snow grain metamorphosis. Marshall et al. (1994) report the relative importance of snow grain size to be larger in the early melting season, when grain-radius-increase is fastest [6], while the effect of solar angle increases towards the end of summer. Additionally to these facts, also the chemical composition of debris (analyses in process) need to be considered before the relative effect of particulate matter on the surface albedo can be estimated.

REFERENCES

[1] M.G. Flanner, J. Geophys. Res. **112,** doi:10.1029/2006JD008003 (2007).
[2] IPCC, Fourth Assessm. Report, Physical Sc. Basis, p. 185 (2007).
[3] J. Oerlemans et al., J. of Glaciol. **55**, 192 (2009).
[4] N. Takeuchi, Bulletin of Glaciol. Res. **19,** 63 (2002).
[5] H. Thomas et al., Arctic a. Alpine Res. **27**, 4 (1995).
[6] S. Marshall et al., Climate Dynamics **10,** 35 (1994).

VOLCANIC ASH FROM THE EYJAFJALLA DETECTED IN SURFACE SNOW AND AEROSOL SAMPLES FROM JUNGFRAUJOCH

L. Tobler, R. Brütsch, S. Brütsch (PSI), N. Bukowiecki (PSI/LAC), M. Schwikowski (PSI & Univ. Bern)

Volcanic ashes from the Eyjafjalla eruption in Iceland in April and May 2010 were clearly detected in surface snow and in aerosol samples from the Jungfraujoch (Switzerland).

INTRODUCTION

The eruption of the volcano Eyjafjalla in Iceland in April-May 2010 had a strong impact on the air traffic over whole Europe [1]. The aerosol plume was detected over Switzerland during two time periods (April, 17-19 and May 16-19, 2010). Different analyses of ash deposited with snow and collected on aerosol filters from the Jungfraujoch (3580 m asl.) were conducted, in order to investigate the chemical composition of the samples and to corroborate the volcanic origin.

METHODS

Snow samples were collected from two shallow snow pits at the Jungfraujoch on April 23, 2010 after the initial arrival of the volcanic aerosol plume. Sampling resolution was 5 cm to a maximal depth of 50 cm, respectively 15 cm.

Major ions were analyzed by ion chromatography (IC). Trace element analysis was done by high-resolution inductively coupled plasma mass spectrometry (ICP-SF-MS) after acidification of the samples to 0.2 mol with ultra pure concentrated nitric acid. Furthermore, snow samples were filtrated to analyze the particles on the filters by energy-dispersive X-ray spectroscopy conducted by scanning electron microscopy (SEM-EDX). The same method was applied for the aerosol filters collected at Jungfraujoch.

RESULTS

Snow samples show for all elements an increase in concentrations in the top 15 cm compared to the concentrations in the depth range between 16 and 50 cm. As examples the concentration profiles of Fe and sulphate are given in Fig. 1.

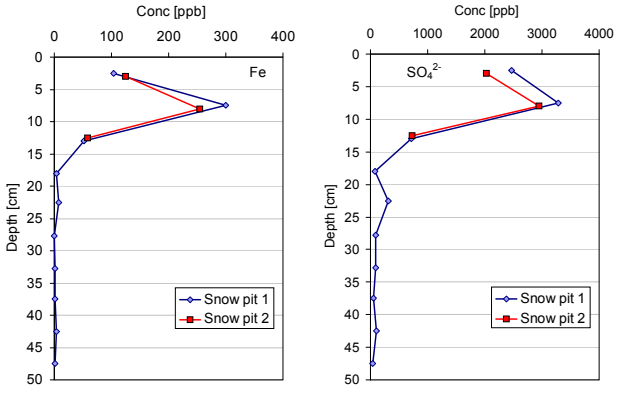

Fig. 1: Snow pit concentration depth profile for the trace element Fe and ionic species SO_4^{2-}.

Fig. 2 depicts the ratio between the mean concentrations of the top 10 cm and the baseline values (mean concentrations between 16-50 cm). The largest enrichment is found for the elements Fe, Zr, and the seven rare earth elements (REE) analyzed, followed by Al, sulphate, Mn, V, and Mo, which is a strong indication of volcanic origin.

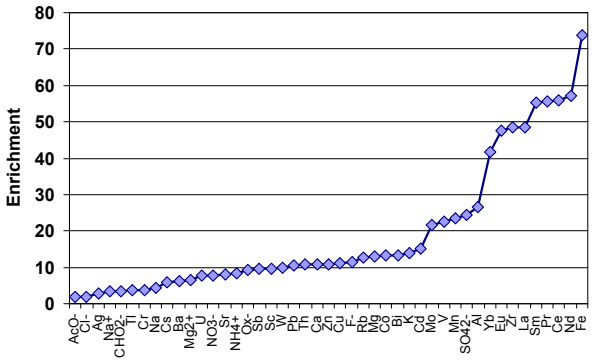

Fig. 2: Enrichment of elemental and ion concentrations in snow samples containing volcanic ash.

SEM-EDX results of particles filtrated from snow samples of the top 10 cm as well as from aerosol filters further corroborate the existence of volcanic ash particles. This can be seen in fig. 3, where the chemical composition of the snow filtrates and of an aerosol filter are compared to the concentrations of rocks collected at Eyjafjalla in April 2010 [2]. The major compounds lie very close to the 1:1 line, whereas mid ocean ridge basalt (MORB) deviates strongly.

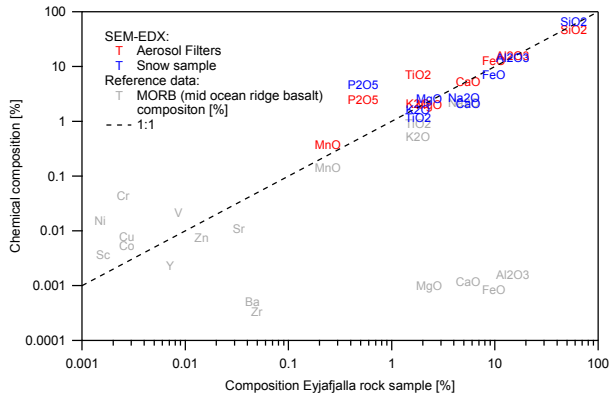

Fig. 3: Comparison of the composition of snow and aerosol samples from Jungfraujoch with the composition of a rock sample from Eyjafjalla [2].

REFERENCES

[1] Federal administration, Switzerland, http://www.news.admin.ch/message/?lang=de&msg-id=32655.

[2] F. Sigmundsson et al., Nature, **468**, 426, (2010).

RESULTS FROM A SNOW PIT STUDY ON BLACK CARBON AND SEA SALT CONCENTRATIONS IN SVALBARD, NORWAY

I. Schuck (PSI & Univ. Bern), C. Vega Riquelme (UU), J. Zarsky (Univ. Innsbruck), T. Martma (Univ. Tallinn), M. Björkman, H. Anschütz, E. Isaksson (NPI), M. Gysel, M. Laborde (PSI/LAC), M. Schwikowski (PSI & Univ. Bern)

The study of the 2009/2010 winter snow pack at three different sites on Svalbard revealed that the geographic location plays an important role for the ion as well as the black carbon (BC) concentrations. The lowest values for the sea salt tracers sodium and chloride as well as for BC were found at Lomonosovfonna, confirming the remote location of this glacier that makes it suitable for the study of long-range transported species.

In March/April 2010 a snow pit study was conducted in Svalbard, Norway, with the aim to analyse the winter snow pack of one year for BC and major ion concentrations. On the one hand these results extend the ice core record of the Lomonosovfonna core drilled in 2009; on the other hand they give an idea of the spatial variation of the considered species in Svalbard.

Black carbon (BC) is a byproduct of incomplete combustion and has light-absorbing properties. Therefore it affects the albedo and leads to an enhanced melt when deposited on snow or ice. In Svalbard BC originates from local or long-range sources. Local sources include mining activities, coal and diesel power plants as well as vehicles. Long-range transport of BC occurs from sources in Europe and Russia.

The snow chemistry is dominated by sea salt species (mainly sodium and chloride) since the archipelago of Svalbard is surrounded by ocean.

Samples were taken at three glaciers: Foxfonna, Tellbreen and Lomonosovfonna. The first two are located in the vicinity of Longyearbyen (12-15 km), the biggest settlement on Svalbard, and close to the ocean (11-15 km). They have an altitude between 500-800 and 300-750 m asl, respectively. In contrast, Lomonosovfonna is a remote site, located far from any settlement (~75 km to Longyearbyen), situated at an altitude of ~1200 m asl and ~20 km distance from the ocean.

The major ion concentrations were determined by ion chromatography, BC concentrations with a single particle soot photometer (SP2).

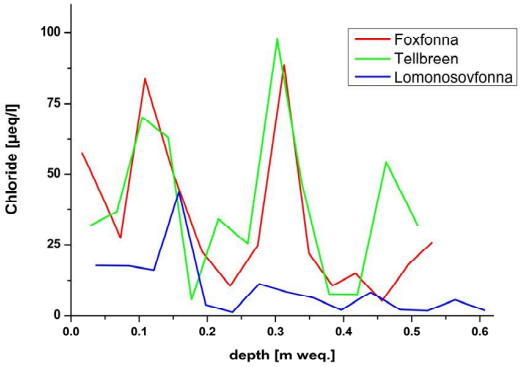

Fig. 1: Chloride concentration record at the three sampling sites.

The major ion concentrations show that the values at the Lomonosovfonna site are by a factor of two lower than those at Foxfonna and Tellbreen. This can particularly well be seen in the record of the sea salt tracers such as chloride (Fig. 1). This difference can be explained by the distance of the sites to the ocean. The altitude has an additional effect since air masses reaching Lomonosovfonna may have lost some of their coarse sea salt particulate load during the rise due to rapid sedimentation.

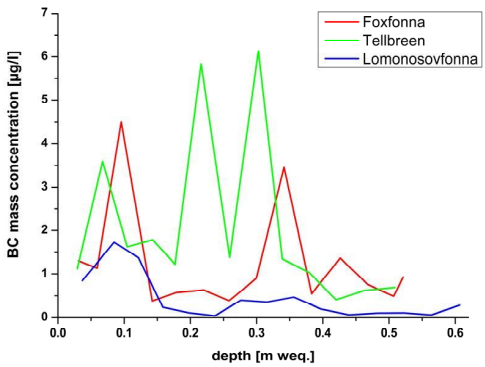

Fig. 2: BC records at the three sampling sites.

The BC concentrations show a similar effect like the ions. The values at Foxfonna and Tellbreen are more than double those at Lomonosovfonna (Fig. 2). This is a result of the distance to the local sources of BC, mainly the settlements and mines.

Tab. 1: BC concentrations from different studies.

This study 2010	
Median for all sites	0.73 ng/g
Lomonosovfonna	0.26 ng/g
Foxfonna	1.02 ng/g
Tellbreen	1.36 ng/g
Snow pit studies on Svalbard 2007 [1]	
Median	4.1 ng/g
Surface snow in the Arctic [2]	
Median for Svalbard	13 ng/g
Greenland ice [3]	
Preindustrial: annual avg.	1.7 ng/g
1851-1951 AD: annual avg.	4.0 ng/g
1952-2002 AD: annual avg.	2.3 ng/g

The BC values obtained in this study are lower than those published in previous studies from Svalbard but also from Greenland (Table 1). On the one hand this is explainable by different methods applied. On the other hand this study only represents one year of winter snow. Thus further investigation is needed.

REFERENCES

[1] Forsström et al., J. Geophys. Res., **114**, D19112, doi: 10.1029/2008JD011480 (2009).
[2] Doherty et al., Atmos. Chem. Phys. Discuss., **10**, doi: 10.5194/acpd-10-18807-2010 (2010).
[3] McConnell et al., Science, **317**, 1381, doi: 10.1126/science.1144856 (2007).

NEW RADIOCARBON DATES SUPPLEMENTING THE AGE-DEPTH RELATION OF THE NEVADO ILLIMANI ICE CORE

A. Zapf (Univ. Bern & PSI), S. Szidat (Univ. Bern), L. Wacker (ETHZ), M. Schwikowski (PSI)

The dating for the ice core from Nevado Illimani (Bolivian Andes) was supplemented by a series of radiocarbon dates. Discrete samples were analysed in the ice core section between 55 to 92 m weq.

During the last years intensive analyses on the ice core from Nevado Illimani (drilled in 1999) have been carried out in our group. Two recent publications about this core deal with new approaches to determine preindustrial volcanic eruptions and to reconstruct regional temperature respectively [1, 2]. In order to draw meaningful conclusions from such an approach a well-established age-depth relationship is indispensable.

Radiocarbon dating of carbonaceous particles embedded in the ice matrix proved to be an appropriate tool to retrieve age information for time periods not accessible with common dating techniques such as annual layer counting on seasonally varying parameters [3]. Carbonaceous particles are extracted from the ice samples via filtration and subsequently separated into organic and elemental carbon in a two-step combustion process [4]. The generated CO_2 fraction is cryogenically trapped and dated at the MICADAS AMS system [5]. As we deal with carbon amounts in the microgram range it is essential to have a rather low, stable and well-known process blank. Blank determinations for the organic carbon fraction (OC) were carried out by different persons over the last years resulting in 1.5 ± 0.6 µg C per sample hence making sure to have the method under control with respect to blank input (Fig. 1).

The present Illimani timescale was established by applying a multi-parameter approach, including annual layer counting, identification of reference horizons from nuclear weapon tests and from volcanic eruptions and radiocarbon dating of the lowermost part of the ice core. A two-parameter model (grey curve in Fig. 2) was fitted to the volcanic horizons and the two youngest ^{14}C time markers (red triangles in Fig. 2). All radiocarbon dates presented here were determined using the OC fraction of the carbonaceous particles retrieved from the ice. This was mainly due to the larger carbon amounts (44-134 ppb) compared to the elemental carbon fraction (EC, 12-56 ppb) therefore yielding lower uncertainties. Furthermore it is not yet fully understood whether the ^{14}C signal from the EC fraction represents the true age of the ice.

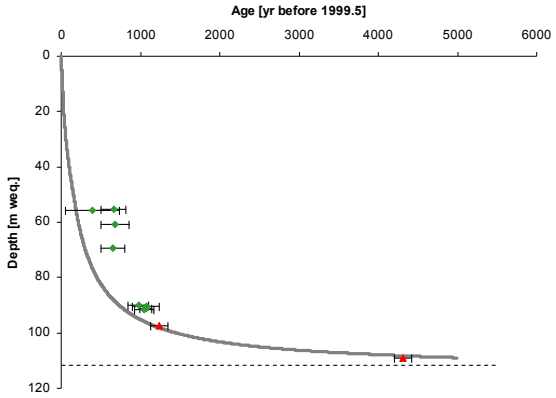

Fig. 2: Age-depth relation of the Nevado Illimani ice core. The grey curve represents the output of a two-parameter model using six volcanic reference horizons and two radiocarbon dates (red triangles) as time markers. Eight independently measured ^{14}C dates are shown as green diamonds (error bars envelop 1σ uncertainty). The dashed horizontal line indicates bedrock at 113 m weq (adapted from [6]).

Four samples were measured between 89.3 and 91.4 m weq containing and surrounding the ice-layer with the "unknown 1258" volcanic eruption. These show a very high consistency amongst each other and match the two-parameter model fairly well. ^{14}C dates from around 55 to 70 m weq show an offset of roughly 150 to 350 years compared to the fitted 2-p model.

ACKNOWLEDGEMENT

This Work is supported by the Swiss National Science Foundation (200021_126515).

REFERENCES

[1] T. Kellerhals et al., Env. Sci. Techn., **44**, 888 (2010).
[2] T. Kellerhals et al., JGR, **115**, D16123 (2010).
[3] M. Sigl et al., Journal of Glaciology, **55**, 985 (2009).
[4] T. Jenk et al., JGR, **114**, D14305 (2009).
[5] M. Ruff et al., Radiocarbon, **49**, 307 (2007).
[6] T. Kellerhals, PhD thesis, University of Bern (2008).

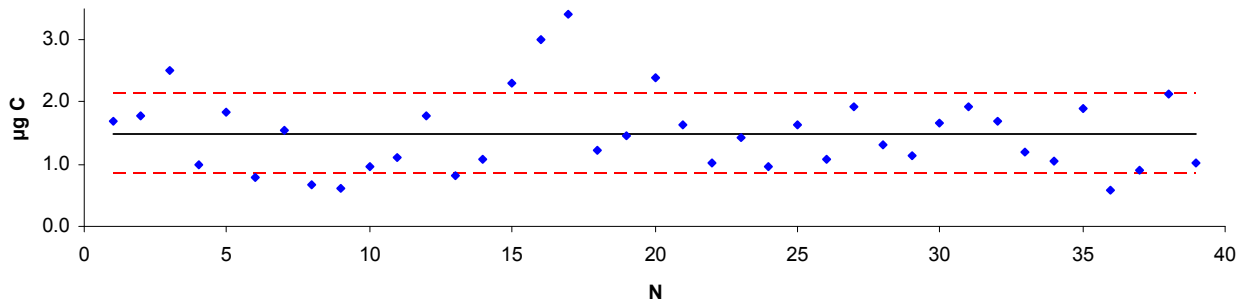

Fig. 1: Variations for N=39 OC blank determinations. The black line indicates the mean of the blank carbon amount per filter (red dotted line shows the 1σ-band of the measurements).

ACCELERATED RELEASE OF PERSISTENT ORGANIC POLLUTANTS FROM ALPINE GLACIERS

P.A. Pavlova (PSI & Univ. Bern), P. Schmid (EMPA), C. Bogdal (ETHZ), F. Anselmetti (EAWAG), M. Schwikowski (PSI & Univ. Bern)

Untypical high concentrations of POPs in recent sediments of glacial fed lakes in the Swiss Alps were observed. In order to study in details the behavior of those substances in a glacier-lake ecosystem, we analyze ice and lake sediment cores for PCBs and DDT concentrations.

INTRODUCTION

Persistent organic pollutants (POPs) represent a group of halogenated organic compounds, characterized by high bioaccumulation rates and resistance to chemical and biological degradation. Since the middle of the 20th century, these substances, such as polychlorinated biphenyls (PCBs) or dichlorodiphenyl trichloroethane (DDTs) have been widely used in agriculture, electrical industry, engineering, etc. Although their production was restricted since the 1970s and eliminated globally with the Stockholm convention, recent studies revealed that melting Alpine glaciers represent a secondary source of POPs [1]. Due to the global-warming-induced rapid melting of glaciers, the substances deposited to and incorporated into the glacier ice are now released to the environment (¨glacier hypothesis¨) [2].

In order to investigate selected anthropogenic organic chemicals regarding their deposition on, incorporation into, transport within, and release from temperate Alpine glaciers, the Silvretta glacier and lakes were selected as a study site (Fig. 1).

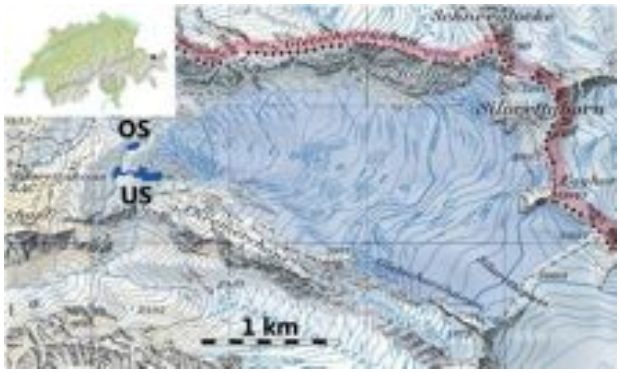

Fig. 1: The two Silvretta proglacial lakes with an overview map of Switzerland, showing the location of Silvretta Glacier (copyright of map; swisstopo).

SAMPLING SITE

Silvretta Glacier, located in the North-East part of Canton Graubünden, has a surface of more than 3 km^2 and is one of the biggest glaciers in the Silvretta massif. Since 1860 it has retreated more than 1 km, resulting in the formation of few small proglacial lakes. The glacier has been extensively explored by the Laboratory of Hydraulics, Hydrology and Glaciology (VAW) at ETH Zurich.

METHOD DEVELOPMENT

In order to test if the Silvretta lake sediments contain a signal of accelerated POPs release, six sediment cores were sampled in August 2010. They were retrieved in plastic tubes with a diameter of around 6 cm by use of a percussion-piston corer. After sampling, the sediment cores were opened in the laboratory at Eawag by splitting the cylindrical cores lengthwise into two halves. The first half is kept in a storage room for further investigation.

Subsequent to drying at room temperature and removing the surface layer, the varved structure of the cores was inspected. As a result, two master sections (one for each lake) were selected and divided into 2 cm samples. Concentrations of radioactive isotope ^{137}Cs will be used for obtaining age to depth relationship. The analysis of POPs in freeze dried, pulverized lake sediments is accomplished through Soxhlet-extraction with *n*-hexane/dichloromethane (1/1) mixture. The extracts are then subject to chromatographic separation through self-packed chromatographic columns, containing silica gel and anhydrous sodium sulfate. In the obtained fractions, PCBs and DDT are determined by gas chromatography coupled to mass spectrometry (GC/MS). For quantification and quality assurance isotope labeled internal standards are used. These challenging analyses require not only highly sensitive measurements, but also minimization of the blank values. Therefore, all the glassware is preheated and rinsed with acetone and dichloromethane immediately before use. The development of the analytical method included preparation of blank samples from different stages of the cleanup procedure as well as analysis of archived samples from already published studies [2, 3].

OUTLINE

Next steps include method development for determination of POPs in ice samples and analysis of the ice core from Ewigschneefeld [4].

ACKNOWLEDGMENT

This project is partly funded by the Swiss National Science Foundation (grant number #20021_130083).

REFERENCES

[1] P. Schmid et al., Environ. Sci. Technol, **45**, 203 (2011).
[2] C. Bogdal et al., Environ. Sci. Technol, **43**, 8173 (2009).
[3] N. Blüthgen, MSc Thesis, University of Zürich (2009).
[4] M. Schwikowski et al., this report, p. 33.

FIRST ICE CORE FROM TEMPERATE EWIGSCHNEEFELD

M. Schwikowski (PSI & Univ. Bern), I. Mariani, P.A. Pavlova, B. Rufibach, I. Schuck, A. Zapf (PSI), C. Bogdal (ETHZ), D. Stampfli, F. Stampfli (FS INVENTOR)

On 12 September 2010 our team finished ice core drilling at 57 m depth on Ewigschneefeld in the Swiss Alps. Ewigschneefeld is a temperate glacier, containing a water table. The ice core will be analyzed in order to investigate the transport of persistent organic pollutants in temperate ice and quantify their release by melting.

Persistent Organic Pollutants (POPs) are regulated by international conventions due to their particularly hazardous properties to persist in the environment, accumulate along food chains, and exhibit serious toxic effects. Recent studies indicated that melting Alpine glaciers represent a secondary source of legacy POPs, which were previously deposited to and incorporated into glaciers and are now released to the environment due to the rapid melting induced by climate warming [1, 2]. In order to assess the relevance of this secondary source for the alpine environment a better understanding of the behavior of POPs in cold and temperate glaciers is needed. In cold glaciers most of the ice has a temperature below the pressure melting point. In temperate glaciers, liquid water is present within the ice matrix in lenses between ice grains, in veins at triple grain intersections, and in nodes where veins intersect. Bulk water content of temperate ice ranges from 0% to 9%. The majority of Alpine glaciers is temperate.

In the frame of a new SNF project „Accelerated release of persistent organic pollutants (POPs) from Alpine glaciers“, a collaborative effort, involving scientists from PSI, University of Bern, ETH Zurich, EAWAG, and EMPA, the distribution and transport of POPs through temperate glaciers is examined.

The strategy of our contribution is determining inventories of POPs in three ice cores from different types of glaciers: i) to establish the undisturbed input function of POPs from a cold Alpine glacier, ii) to investigate the transport of POPs in a temperate glacier having an intact water-saturated firn layer, and iii) to determine the remaining signal of POPs in a temperate ablation area. For the first purpose the well-dated Fiescherhorn ice core is available, obtained in 2001 [3]. For the second goal we selected the Ewigschneefeld in the Bernese Alps (46°33'N, 08°01'E) for ice core drilling. Ewigschneefeld is a temperate glacier, containing a water table in depths between 14 and 32 m below surface [4]. For the third purpose Silvretta glacier was chosen, a glacier in the Grisons, with temperate ablation area connected to proglacial lakes [5].

Ice coring in temperate ice is a special challenge. Commonly used electromechanical drills have problems with freezing and transport of drilling chips due to the presence of liquid water. Instead we used our new combined electromechanical and thermal drill (TD) [6], which has a modified control unit and power supply, since thermal drilling consumes more power. The TD itself consists of two barrels. The upper barrel contains two pumps and two containers, for ethanol and for the ethanol/meltwater mix, respectively. The lower one is the core barrel bearing the melting ring and the core catchers. In September 2010 we obtained a 57 m ice core from 3462 m a.s.l. on Ewigschneefeld (Fig. 1). The upper 31 m were drilled electromechanically and for the deeper part the TD was used. At about 21 m depth the water table was reached. The new drill produced ice cores of excellent quality even in the water-filled borehole.

The next steps include method development for determination of POPs in ice samples, analysis of POPs in the ice cores from Fiescherhorn glacier and Ewigschneefeld, and ice core drilling on Silvretta glacier.

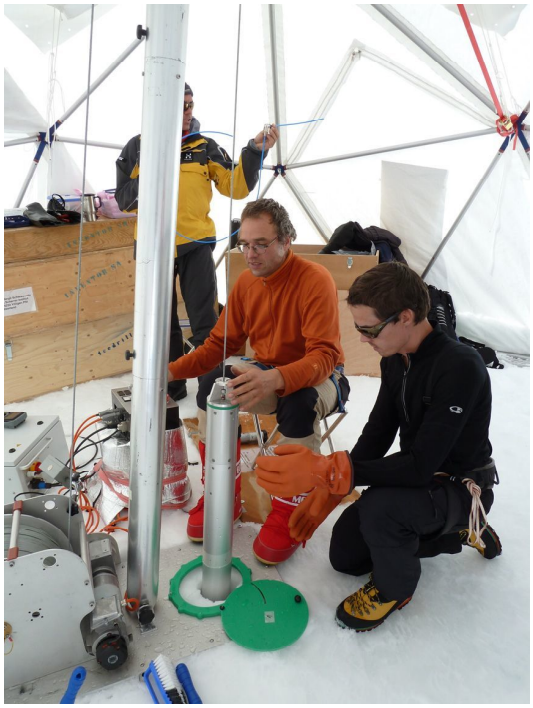

Fig. 1: Ice coring with the thermal drill at Ewigschneefeld.

ACKNOWLEDGEMENTS

This project is supported by the Swiss National Science Foundation (# 200021_130083). The development of the thermal drill was funded by the PSI FoKo.

REFERENCES

[1] P. Schmid et al., Environ. Sci. Technol. **45**, 203 (2011).
[2] C. Bogdal et al., Environ. Sci. Technol, **43**, 8173-8177 (2009).
[3] T.M. Jenk et al., Atmos. Chem. Phys., **6**, 5381 (2006).
[4] H. Lang et al., Z. Gletscherk. und Glazialgeologie XII, 109 (1977).
[5] P.A. Pavlova et al., this report, p. 32.
[6] M. Schwikowski et al., Ann. Rep. Lab. of Radio- & Environ. Chemistry, Uni Bern & PSI (2008), p. 33.

DISTRIBUTION OF RADIONUCLIDES IN A PROTON IRRADIATED LBE TARGET FROM ISOLDE. PART 1: SAMPLE CUTTING AND α-SPECTROMETRY

J. Neuhausen (PSI), B. Hammer (Univ. Bern & PSI), D. Schumann (PSI), L. Zanini (PSI/GFA), M. Rüthi, J. Eikenberg (PSI/LOG), E. Noah (CERN)

The distribution of nuclear reaction induced impurities in a proton irradiated lead bismuth eutectic target from the ISOLDE facility at CERN was radiochemically analyzed using α-spectrometry. The results are in reasonable agreement with predictions based on nuclear calculations.

INTRODUCTION

In support of the MEGAPIE experiment, a target containing liquid lead bismuth eutectic (LBE) was irradiated with high energy protons (1 – 1.4 GeV) at CERN to study the release of volatile nuclear reaction products from the liquid metal between 250 and 600 °C [1]. After a cooling period of several years, the target was transferred to PSI and is now radiochemically analyzed. These analyses serve three purposes: 1. to develop separation techniques applicable to the LBE samples from MEGAPIE that will be analyzed starting in 2011 target in the frame of the Post Irradiation Examination (PIE) program, 2. to obtain some basic knowledge on the distribution of radionuclides in an LBE target, and 3. to benchmark nuclear codes used for the prediction of radionuclide production. The development of the separation scheme is described in [2]. In this report we describe the sample preparation and present results on polonium content and distribution. Radioanalytical results concerning γ-emitters are presented in [3].

SAMPLE PREPARATION AND ANALYSES

A schematic drawing of the target is shown in Fig. 1. Four disks were cut at positions 2, 3, 5, and 7. From each of these disks, a bar of appr. 15 mm length and 2 x 2 mm base area was cut in such a way that the former LBE-vacuum and LBE-tantalum interfaces can be assessed. For more details on the cutting procedure see [4].

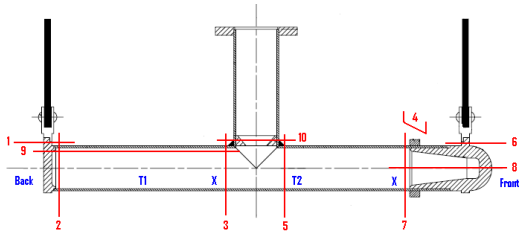

Fig. 1: Cutting scheme for the ISOLDE LBE target

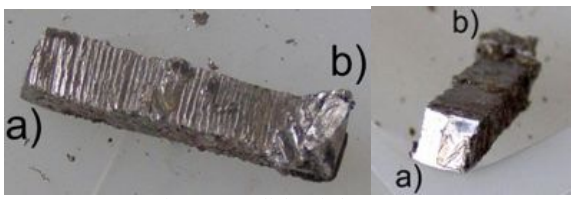

Fig. 2: Bar cut from one disk of the ISOLDE LBE target. The ends where the LBE-vacuum and LBE-tantalum interfaces were located are designated as a) and b).

To obtain an overview on the radionuclide distribution, samples of a few mg of the material with a thickness of about 100 µm were hand-cut from one of the bars using a scalpel. Various samples were taken at the LBE-vacuum interface a), appr. 100 µm below this interface, from the LBE-tantalum interface b) and from the bulk. For α-spectrometry, the samples were dissolved in HNO_3 and polonium was deposited onto a silver disk.

RESULTS

The results obtained by α-spectrometry for the samples taken from four different locations are compared to the results of nuclear calculations. The calculation results are in reasonable agreement with the measured specific activities. While the calculated activities for ^{208}Po and ^{210}Po are about 40% higher than the measured ones, the calculated activity of ^{209}Po is in very good agreement. The measured specific activities of the samples seem to show a systematic trend, indicating enrichment towards the surfaces. However, the error of 10% quoted for the α-spectrometry results precludes a definite statement about surface enrichment from the α-spectrometry data. The results are however not contradictory to the observation of an approximately 5-fold polonium enrichment observed in an appr. 5 µm thick surface layer in Po-containing LBE samples [5]. Indeed, the presence of such a surface layer in a sample of ≈100 µm thickness would perfectly account for the differences in the α-spectrometry results for bulk and surface samples. More detailed studies of polonium surface enrichment in the ISOLDE target are underway.

Tab. 1: Comparison of calculated bulk specific activity [6] and measured specific activities of polonium isotopes in samples from different positions of the target (June 2008).

	^{208}Po	^{209}Po	^{210}Po
Sample position	A_{sp} [Bq/g]	A_{sp} [Bq/g]	A_{sp} [Bq/g]
LBE-vacuum interface	8338	141	122
100 µm below LBE-vacuum interface	8107	136	111
Bulk LBE	6926	109	97
LBE-tantalum interface	7847	131	113
Calculated, bulk LBE (FLUKA)	11700	133	167

REFERENCES

[1] Y. Tall et al., Proc. Intern. Conf. Nucl. Data for Science and Technology, April 22-27, 2007, Nice, France, EDP Sciences, 2008, pp 1069- 1072.
[2] B. Hammer et al., this report, p. 36.
[3] J. Neuhausen et al., this report, p. 35.
[4] V. Boutellier, TM 43-08-14, PSI (2008).
[5] S. Heinitz et al., this report, p. 45.
[6] L. Zanini, PSI, personal communication.

DISTRIBUTION OF RADIONUCLIDES IN A PROTON IRRADIATED LBE TARGET FROM ISOLDE. PART 2: γ-SPECTROMETRY

J. Neuhausen (PSI), B. Hammer (Univ. Bern & PSI), D. Schumann (PSI), L. Zanini (PSI/GFA), M. Rüthi, J. Eikenberg (PSI/LOG), E. Noah (CERN)

The distribution of nuclear reaction induced impurities in a proton irradiated lead bismuth eutectic target from the ISOLDE facility at CERN was analyzed using γ-spectrometry. The majority of the radionuclides identified are not homogeneously distributed in the formerly liquid metal. In particular, electropositive metals are enriched at the interfaces of the liquid metal with the walls of the target container and the vacuum.

In order to study the distribution of radionuclides in the proton irradiated ISOLDE target, several samples from various locations as described in the previous report [1] were analysed using γ-spectrometry.

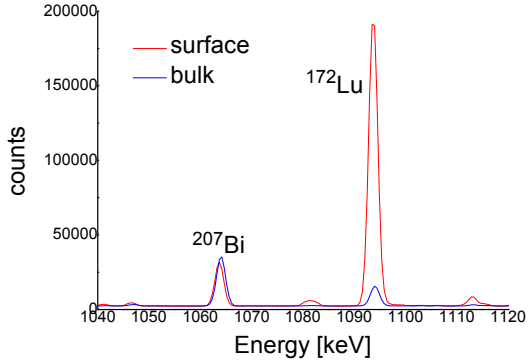

Fig. 1: Comparison of a section of the γ-spectra of a bulk LBE sample and a sample from the former LBE-vacuum interface of the ISOLDE LBE target.

The results given in Tab. 1 show that the distribution of radionuclides in the target is non-trivial. While ^{207}Bi is homogeneously distributed throughout the bulk, a depletion of this nuclide was observed in one of the samples taken appr. 100 µm below the former liquid metal-vacuum interface. Overall, the specific activity of ^{207}Bi in the bulk agrees well with predictions from nuclear calculations. As exemplified in Fig. 1, for ^{172}Hf/Lu an enrichment compared to the bulk is observed at the LBE-vacuum and LBE-tantalum interfaces. Within the bulk, the majority of the samples have – in good agreement with theoretical predictions - specific ^{172}Hf/Lu-activities around, 28 kBq/g, however, one sample shows a significant enrichment of ^{172}Hf/Lu. ^{60}Co, ^{102m}Rh, ^{133}Ba, and ^{173}Lu show a behaviour similar to ^{172}Hf/Lu, while ^{110m}Ag is not enriched at the surfaces. A possible explanation is that the more electropositive metals form insoluble oxides with the oxygen present in the liquid metal that separate from the liquid, while noble metals with a high solubility in LBE such as Ag remain dissolved.

Tab. 2 gives a comparison of specific activities of various nuclides in the 3rd and 4th sample of bulk LBE listed in Tab. 1. These samples were cut from one single LBE piece of 2 mg taken from the centre of a bar cut from the target as described in [1]. The results show that most of the detected radionuclides are strongly enriched in sample 4, compared to sample 3. Possible explanations for this observation could be either the preferred deposition of radionuclides on dispersed particles that are suspended in the liquid metal or the precipitation of insoluble compounds that partly remain suspended in the liquid. A deeper exploration of these effects and a more detailed study of the spatial distribution of various radionuclides within the ISOLDE LBE target are ongoing. The preliminary results presented here indicate that a carefully planned sampling, including a sufficient number of samples from selected locations, is essential to extract reliable and meaningful results from the radiochemical analysis of liquid metal targets. The sampling plan for the post irradiation examination of the MEGAPIE target has been devised bearing in mind the expected inhomogeneity of the target material [2].

Tab. 1: Comparison of calculated bulk specific activity [3] and measured specific activities of ^{172}Hf/Lu and ^{207}Bi in samples from different positions of the target (June 2008).

Sample position	Sample No.	Sample mass [mg]	^{172}Hf/Lu A_{sp} [kBq/g]	^{207}Bi A_{sp} [kBq/g]
LBE-vacuum interface	1 2	6.1 4.1	200 230	27 28
100 µm below LBE-vacuum interface	1 2	7.8 10.6	11 9	28 3
Bulk LBE	1 2 3 4	16.9 17.2 0.8 1.2	27 28 28 103	31 32 30 30
LBE-tantalum interface	1 2	2.64 1.88	78 66	35 32
Calculated, bulk LBE (FLUKA)			33	33

Tab. 2: Comparison of measured and calculated [3] specific activities of several nuclides in bulk LBE samples from the ISOLDE LBE target (June 2008).

Nuclide	A_{sp} [Bq/g] measured Bulk Sample 3	A_{sp} [Bq/g] measured Bulk Sample 4	A_{sp} [Bq/g] calculated
^{60}Co	565	1520	1670
^{102m}Rh	2310	3920	833
^{110m}Ag	1310	1080	-
^{133}Ba	745	2780	1670
^{172}Hf/Lu	27900	103000	33000
^{173}Lu	25400	122000	33000
^{207}Bi	29700	29500	33000

REFERENCES

[1] J. Neuhausen et al., this report, p. 34.
[2] J. Neuhausen et al., Ann. Rep. Lab. of Radio- & Environ. Chemistry, Uni. Bern & PSI (2009), p. 60.
[3] L. Zanini, PSI, personal communication.

DETERMINATION OF LONG-LIVED RADIONUCLIDES IN A LBE-TARGET FROM ISOLDE. PART I: DEVELOPMENT OF THE SEPARATION SYSTEM

B. Hammer (Univ. Bern & PSI), D. Schumann, J. Neuhausen (PSI)

A chemical separation procedure was developed allowing isolation of ^{36}Cl ($T_{1/2} = 3.01 \cdot 10^5$ y), ^{129}I ($T_{1/2} = 1.57 \cdot 10^7$ y), ^{108m}Ag ($T_{1/2} = 418$ y), ^{110m}Ag ($T_{1/2} = 249.79$ d), ^{101}Rh ($T_{1/2} = 3.3$ y), ^{102m}Rh ($T_{1/2} = 2.9$ y), ^{172}Lu ($T_{1/2} = 6.7$ d), ^{173}Lu ($T_{1/2} = 1.37$ y), and ^{207}Bi ($T_{1/2} = 31.55$ y) from the lead-bismuth target from ISOLDE. The developed chemical separation methods later will be used for the analysis of the long-lived radionuclide inventory in the MEGAPIE target.

INTRODUCTION

Liquid eutectic lead-bismuth alloy (LBE) is considered to be used as target material in future high power spallation targets for neutron production [1]. The goal of the presented work here is the development and optimization of chemical separation methods for the quantitative determination of long-lived radionuclides, such as ^{36}Cl ($T_{1/2} = 3.01 \cdot 10^5$ y), ^{129}I ($T_{1/2} = 1.57 \cdot 10^7$ y), ^{108m}Ag ($T_{1/2} = 418$ y), ^{148}Gd ($T_{1/2} = 74.6$ y), several polonium isotopes ($^{208,209,210}Po$, $T_{1/2}$ from 138.38 d to 102 y) and others, which will be produced in proton-irradiated lead-bismuth targets. A special focus is given to the lanthanide fraction, because of the long-lived α-emitter ^{148}Gd.

The separation from macro amounts of bismuth and lead is essential, because otherwise they will disturb the identification of trace elements. The developed chemical separation methods will be used later for the analysis of the long-lived radionuclide inventory in the MEGAPIE target. The knowledge of the residual nuclide production is essential for estimation and validation of target handling in future LBE-cooled nuclear facilities during and after operation, including also options for intermediate or final disposal.

EXPERIMENTAL

The proposed separation procedure is shown in Fig. 1. A LBE sample of 12 mg was dissolved in 7 M aq. HNO_3. The solvent was spiked with ^{206}Po ($T_{1/2} = 8.8$ d), a γ-emitting polonium isotope, to monitor polonium during the separation procedure. First of all, chlorine and iodine were separated from the residue by distillation in a N_2 atmosphere (step 1) (same procedure as described for the lead samples [2]). The residue from step 1 was dissolved in 7 M aq. HNO_3 and a silver separation as described for bismuth [3] was performed. The filtrate from step 2 was evaporated to dryness. The residue was dissolved in 60 µl aqua regia ($HCl:HNO_3$, 3:1) and 6 ml deionized water, forming a white precipitate of BiOCl. The solution was decanted and the BiOCl was washed. The two solutions were combined and evaporated to dryness. The BiOCl fraction was dissolved in 5 ml 7 M HNO_3 and measured by γ–spectrometry. In step 4 the residue was dissolved in 3 M HNO_3 and was loaded to the Pb-column. The sample was eluted with 10 ml 3 M HNO_3 and evaporated to dryness and stored for further analysis. Lead was eluted with 20 ml 0.1 M HNO_3 and 20 ml deionized water. The fraction of lead was evaporated to dryness, dissolved in 7 M HNO_3 and precipitated as $PbSO_4$ by adding 2 M H_2SO_4. In step 5 the residue was dissolved in 0.1 M HNO_3 and stored for further purification of the desired lanthanide fraction. Details of this separation step are described in [4].

RESULT

In Fig. 1 the developed chemical separation system is depicted. Every step was repeated several times with fresh LBE material in order to check the reproducibility.

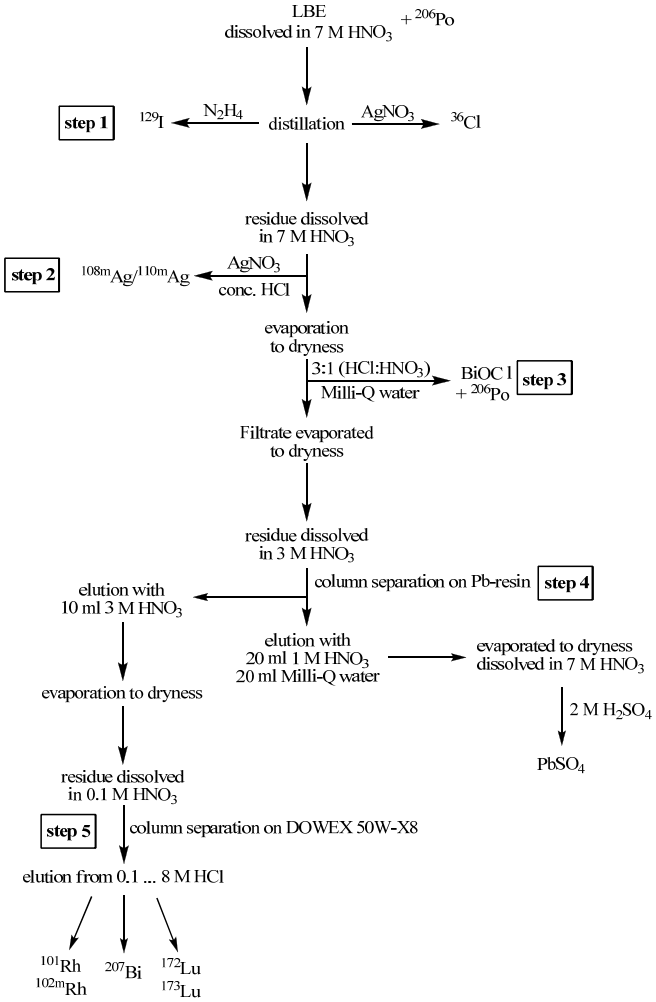

Fig. 1: Separation scheme for the separation of radionuclides from proton-irradiated LBE.

REFERENCES

[1] D. Gorse-Pomonti et al., J. of Non-Crystalline Solids, 353(32-40): 3600-3614 (2007).
[2] D. Schumann et al., NIM A 562, 1057 (2006).
[3] D. Schumann et al., Ann. Rep. Lab. of Radio- & Environ. Chemistry, Uni. Bern & PSI (2006), p. 37.
[4] B. Hammer et al., this report, p. 37.

DETERMINATION OF LONG-LIVED RADIONUCLIDES IN A LBE-TARGET FROM ISOLDE. PART II: FIRST RESULTS

B. Hammer (Univ. Bern & PSI), D. Schumann, J. Neuhausen (PSI), V. Alfimov (ETHZ)

First results on the determination of the radionuclide inventory of the ISOLDE target are presented.

INTRODUCTION

In part I of this report, the principal development of the chemical separation system applicable for further MEGAPIE samples is described [1]. First results using samples from the ISOLDE targets are represented here.

MEASUREMENTS

^{36}Cl and ^{129}I have been measured by AMS (Accelerator Mass Spectrometry) at the ETHZ. The γ-measurements were carried out using a conventional high-purity-germanium detector (ORTEC).

RESULTS AND DISCUSSION

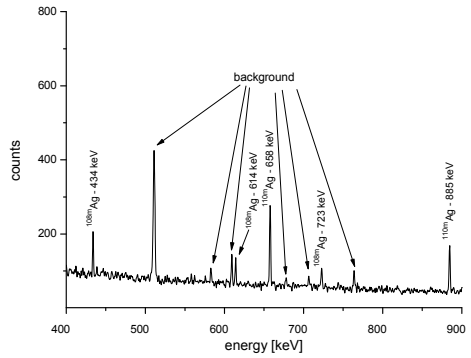

Fig. 1: γ-spectrum of the silver fraction.

In Fig. 1, the γ-spectrum of the Ag-fraction is shown. The 3 main γ-lines of ^{108m}Ag and the 2 main γ-lines of ^{110m}Ag are detected. In Tab. 1 the measured specific activities are shown. The chemical yield of the precipitation was nearly 100%.

Tab. 1: Measured specific activities of the silver-fraction.

sample	A_{sp} [Bq/g] ^{108m}Ag	A_{sp} [Bq/g] ^{110m}Ag
5	126	323
6	154	223

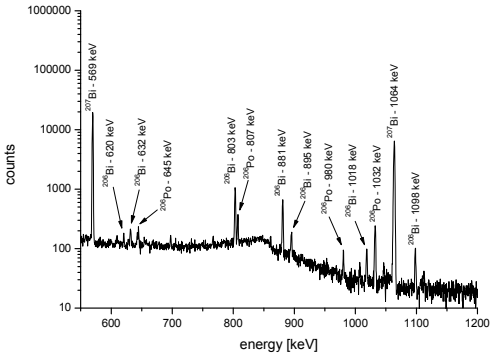

Fig. 2: γ-spectrum of the bismuth fraction.

Fig. 2 shows a section of the γ-spectrum of the BiOCl-fraction. The main γ-lines of ^{207}Bi, 569 keV and 1064 keV, are visible and the main γ-lines of ^{206}Bi and ^{206}Po are detected. The macro amount of bismuth was precipitated successfully, only 10% remain in the residue. The recovery of ^{206}Po was 90%. This fraction is stored for the determination of long-lived $^{208/209}$Po expected to be present in the ISOLDE target.

The separation of rhodium, bismuth, and lutetium has been performed by cation-exchange chromatography with hydrochloric acid using gradient elution from a Dowex 50Wx8 ion-exchange column. In Fig. 3 the elution profile is shown. The recovery of ^{101}Rh was 100% and for ^{102m}Rh 86%. 98% ^{206}Bi and 93% ^{207}Bi were eluted by 10 ml 0.3 M HCl. About 100% ^{172}Lu and 88% ^{173}Lu were eluted by 10 ml 1 M HCl. An additional 6% ^{173}Lu were eluted by 5 ml 3 M HCl. This indicated that the absorption of Lu(III) was stronger than that of other trivalent ions, such as Rh(III) and Bi(III).

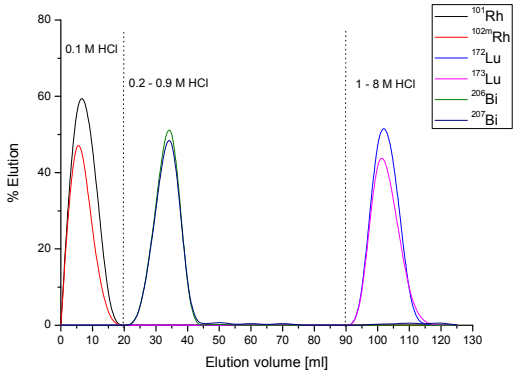

Fig. 3: Elution of ^{101}Rh, ^{102m}Rh, ^{206}Bi, ^{207}Bi, ^{172}Lu, and ^{173}Lu from Dowex 50Wx8 using gradient elution with HCl.

First preliminary results obtained for ^{36}Cl and ^{129}I are shown in Table 2.

Tab. 2: Results of ^{36}Cl and ^{129}I samples. The error of these measurements was ± 10%.

sample	m_{Cl-36} [mg]	m_{I-129} [mg]	m_{Cl-36}/m_{LBE} [mg]	m_{I-129}/m_{LBE} [mg]
1	$1.10\cdot10^{-10}$	$5.76\cdot10^{-10}$	$7.80\cdot10^{-12}$	$4.09\cdot10^{-11}$
2	$9.50\cdot10^{-12}$	$1.45\cdot10^{-10}$	$7.57\cdot10^{-13}$	$1.16\cdot10^{-11}$

REFERENCE

[1] B. Hammer et al., this report, p. 36.

EXCITATION FUNCTIONS FOR THE PRODUCTION OF ^{10}Be AND ^{26}Al IN THE REACTION ^{nat}Bi(p;xn,yp)Z

D. Schumann, J. Neuhausen, S. Lüthi, S. Köchli (PSI), R. Michel (IRS Hannover), A. Wallner (Uni. Vienna), J.-Ch. David (CEA Saclay)

The production cross sections of long-lived ^{26}Al and ^{10}Be were determined using AMS after chemical separation from proton-irradiated Bi-targets. The results are compared with theoretical predictions.

INTRODUCTION

Lead-Bi-Eutectic (LBE) counts as a possible target material for high power spallation facilities like ESS, ADS, or LBE-cooled fast reactors. The knowledge of the induced radioactivity is mandatory for their design and safe operation. Theoretical predictions rely on basic data like production cross sections, but, unfortunately, especially for long-lives radionuclides, such data are missing or incorrect. Therefore, experimental work is still necessary.

In previous works we reported on the determination of residual nuclides produced in proton-induced reactions on the target element lead [1,2] and bismuth [3,4].

EXPERIMENTAL

A description of the Bi targets, the irradiation conditions and the chemical pre-treatment, can be found in [3,4]. For the ^{26}Al and ^{10}Be determination, we used the residue after dissolution of the Bi. The following separation procedure was developed:

Pre-separation by using a 50-ml-cation-exchange column filled with DOWEX 50x8 (200-400 mesh).

To the sample solution 1mg stable Al and 0.5 mg Be were added, the solution was evaporated to dryness and the residue dissolved in 1M HNO_3. Two drops of concentrated HCl were added to form the unsoluble BiOCl. The phases were separated, the solution was evaporated to dryness and the residue dissolved in 0.1 M HNO_3. The Bi content was controlled using Inductively-Coupled-Plasma-Optical-Emission-Spectroscopy (ICP-OES). The solution was loaded onto the cation exchange column and then the column was washed with 20 ml of 0.1M HNO_3 in order to remove most of ^{10}B, the isobar of ^{10}Be, which could disturb the AMS measurement. With 50 ml of 0.4 M HCl, up to 50 mg Bi could be eluted. The following fraction, eluted with 30 ml 1.1 M HCl, contained the Be, and finally Al was separated with 30 ml 4 M HCl. For samples, where the Bi content was slightly higher, a shift of Be into the Al fraction was observed. Therefore, it was necessary to add an additional purification step.

Purification with a 2-ml-cation-exchange column filled with DOWEX 50x8 (200-400 mesh).

The Al- and Be fractions from the first separation step were unified and evaporated. The residue was dissolved in 0.1 M HNO_3 and loaded onto the column. Remaining traces of Bi were eluted with 10 ml 0.4 M HCl. The Al fraction could then be obtained in 4 ml 4 M HCl. Samples for AMS measurements were prepared as described in [1]. The measurements were performed at the VERA (Vienna Environmental Research Accelerator) laboratory in Vienna.

RESULTS AND DISCUSSION

In the Figs. 1 and 2, the measured excitation functions for the production of ^{10}Be and ^{26}Al are shown. The calculation agrees well for the high-energetic part of the ^{26}Al production. However, we do not have any explanation for the strange trend in the lower energy range. Similar trends were observed also for the production of ^{36}Cl in Pb and Bi-targets [2,3] as well as for the production of ^{26}Al in the reaction ^{40}Ar(p,x)^{26}Al [5].

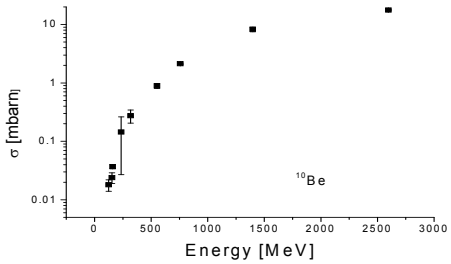

Fig. 1: Cross sections for the production of ^{10}Be determined from proton-irradiated Bi targets.

Unfortunately, no appropriate theoretical description could be obtained for the low-energetic part for ^{26}Al and for the entire ^{10}Be production: reaction models like the Intra-Nuclear Cascade Model combined with evaporation/fission features are obviously not capable of a correct description of the experimental values. Probably, multi-fragmentation or another binary splitting as a possible reaction path has to be taken into consideration.

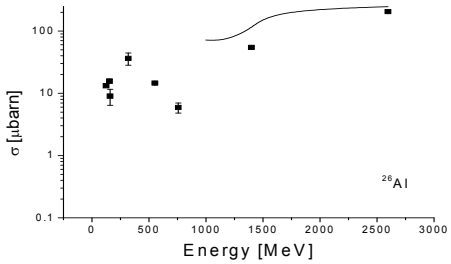

Fig. 2: Cross sections (squares) and calculated excitation function (line) for the production of ^{26}Al determined from proton-irradiated Bi-targets.

REFERENCES

[1] D. Schumann et al., NIM A 562 1057 (2006).
[2] D. Schumann et al., AIP Conf. Proc. Vol. 769. 1517. (2005).
[3] D. Schumann et al., Ann. Rep. Lab. of Radio- & Environ. Chemistry, Uni. Bern & PSI (2006), p. 37.
[4] D. Schumann et al., Ann. Rep. Lab. of Radio- & Environ. Chemistry, Uni. Bern & PSI (2007), p. 43.
[5] F. Kubo, PhD thesis, TU Munich 2001.

LEAD-GOLD EUTECTIC, AN ALTERNATIVE LIQUID TARGET MATERIAL CANDIDATE FOR HIGH POWER SPALLATION NEUTRON SOURCES

M. Medarde (PSI/NUM), R. Moormann (FZ Juelich), K. Thomsen, R. Frison, R. J. Puźniak, E. Pomjakushina, K. Conder (PS/NUM), E. Platacis (University of Latvia), Y. Dai, D. Kiselev, L. Zanini (PSI/GFA), S. Török, P. Zagyvai (KFKI), S. Heinitz (Univ. Bern & PSI), J. Neuhausen, D. Schumann (PSI)

Lead-gold eutectic (LGE), a heavy, low melting point alloy, has been recently proposed as alternative liquid target material for MW-class spallation neutron sources. Here we present novel results concerning sample preparation & characterization, neutronics simulations, decay heat & nuclide inventory calculations and some preliminary corrosion tests aimed at providing a first, broad assessment on the suitability of LGE as liquid spallation target material.

INTRODUCTION

In an effort to pave the way to the realization of the European neutron Spallation Source (ESS), the European Community's Seventh Framework Programme financed a 2 years ESS-Preparatory Phase project from March 2008 to April 2010[1]. As one of the outcomes of this work, we present here a first experimental and theoretical assessment of the suitability of a novel liquid spallation target material, a lead-gold eutectic alloy (LGE) of composition $Pb_{0.841}Au_{0.159}$. This heavy, low melting point alloy (T_m=212.8ºC) has been recently proposed as alternative to the already established materials mercury and lead-bismuth eutectic (LBE) [1]. We show here that the good neutronic performance of this material combined with its less demanding safety and environmental requirements make further research efforts worthwhile [2].

RESULTS

Several LGE samples were prepared using different procedures. The composition of the alloy between RT and the melting point was investigated using x-ray diffraction. As shown in Figs. 1a and 1b, the LGE equilibrium composition is a mixture of Pb and $AuPb_3$, although the metastable phase $AuPb_2$ may appear in fast-cooled samples. The density variations associated with these compositional fluctuations were determined from the thermal evolution of the unit cell volume of the different phases. They were found to be 10 times smaller than those reported for LBE, where density changes as large as 2% have been experimentally measured in the solid phase [3].

Particle transport Monte Carlo simulations were carried out using the program MCNPX in order to investigate the neutronic performance, decay heat, and nuclide inventory. For this purpose, a simplified 37.6 l LGE target irradiated by a 1.334 GeV proton beam during 40 years was used. We obtain a larger heat deposition than for LBE during operation but a faster decrease of decay heat than for LBE after shutdown. Also, the concentration of problematic alpha-emitting Po isotopes after 40 year operation is found to be three orders of magnitude lower than in LBE. Optimization of the target design should yield a neutronic performance virtually indistinguishable from that of LBE.

Preliminary test of the compatibility of structural steels T91 and SS 316LN with LGE were carried out on a LGE/LBE twin loop at 400ºC during 1800h. While the damage caused by LBE and LGE in T91 are similar, the deterioration of SS316LN is higher in presence of LGE. This is an important point which will need further investigation.

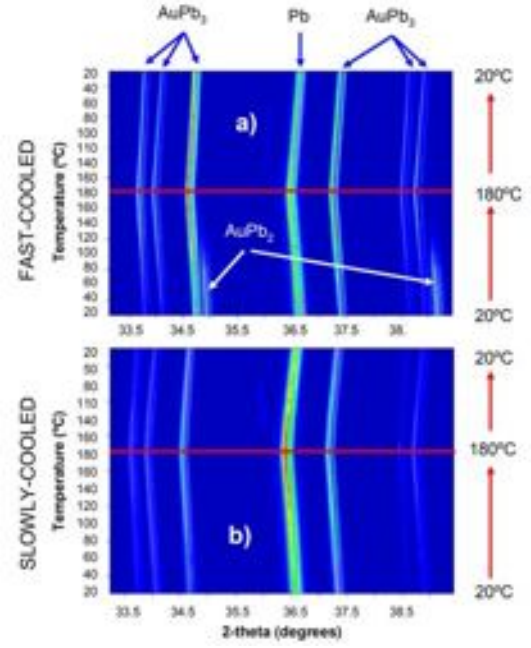

Fig. 1a-b: Temperature dependence of the composition of fast and slowly-cooled LGE samples. The contour plots show the evolution of the x-ray diffraction patterns of both kinds of samples during a 20ºC-180ºC-20ºC heating-cooling cycle.

CONCLUSIONS

The present results suggest that LGE could constitute a viable alternative to the already tested liquid spallation target materials [2]. Besides a chemical toxicity lower than mercury, this dense, low melting point alloy has the advantage of being solid at RT. Moreover, it combines a neutron production similar to mercury and LBE with smaller amounts of alpha-emitting nuclides, relieving safety and environmental requirements. Further advantages are a reduced decay heat a few weeks after stopping operation and density variations in the solid state significantly smaller than LBE. Steel corrosion appears to be more important than expected and will need further investigation in order to identify the most suitable structural material.

REFERENCES

[1] R. Moormann et al., Proc. Int. TCADS Workshop, Karlsruhe, Germany, 15-17 March 2010, in press.
[2] M. Medarde et al., J. Nucl. Mater., in press.
[3] H. Glasbrenner et al., J. Nucl. Mater., 343, 341-348 (2005).

[1] Coordinator: PSI (Switzerland). Participants: ESS-Bilbao (Spain), Univ. of Lund (Sweden), ESS-Hungary (Hungary), Univ. of Huddersfield (UK), STFC (UK), FZJ (Germany), CNR-INFM (Italy), CNISM (Italy), CEA (France) and Univ. of Latvia (Latvia)

CORROSION BEHAVIOUR OF LEAD-GOLD EUTECTIC

S. Heinitz (Univ. Bern & PSI), J. Neuhausen, S. Köchli, D. Schumann (PSI)

We have measured the concentration of steel alloying elements dissolved in lead-gold and lead-bismuth alloys used for a corrosion experiment by ICP-OES. The results are used to estimate the corrosion behavior of liquid lead-gold eutectic in order to assess its suitability as alternative to lead-bismuth eutectic.

INTRODUCTION

Liquid metals based on lead alloys are foreseen as target materials and coolants in various fields of nuclear science. Since alloys with bismuth (lead-bismuth eutectic, LBE) have the major disadvantage of polonium formation under neutron bombardment, the eutectic mixture of lead and gold (LGE, T_m = 212°C) was suggested as alternative material [1]. To test the behavior of flowing LGE towards steel structures and to compare it to LBE, two identical isothermal test loops were built and operated in Salaspils, Latvia. In each loop 0.5 L of liquid metal circulated at a speed of 1 m/s for 3100h during two test campaigns performed at two different temperatures (see [2] for further details). We have measured the concentration of corrosion products dissolved in both alloys via ICP-OES for samples obtained after various times during both test campaigns.

EXPERIMENTAL

For lead-gold eutectic, samples of 1-2 g were taken immediately (0 h), 900 h, and 1800 h after the start of the first loop experiment at 400°C. LBE samples were only obtained for 1800 h. For the second campaign at 450°C, LGE and LBE samples were obtained after 1300h.

From each sample approx. 300 mg were taken and dissolved in 5 ml of 7M HNO_3. For LGE additional dissolution was required, as gold does not dissolve in nitric acid. It remained as a brown sludge and was separated from the solution and dissolved in 2 ml of aqua regia. For each sample, a 4-fold repetition was made to decrease uncertainty. Together with blank solutions of 7M HNO_3 and aqua regia, all aqueous solutions were analyzed via a Varian Vista Pro AX ICP-OE spectrometer.

RESULTS

The concentrations of relevant trace elements dissolved in both investigated alloys are given in table 1. Only elements which are constituents of the structure material of the loop (316L stainless steel) are shown.

As indicated in table 1, the dominant species which is preferentially dissolved in LGE is nickel. Its concentration continuously increases with longer operation times of the loop at 400°C. Compared to LBE, there is clearly a larger dissolution effect of nickel - after 1800h the concentration of Ni in LGE is ten times higher than in the bismuth containing alloy. For other elements, this enhanced corrosion behavior is less pronounced, but is still clearly visible.

The concentration of corrosion products within both alloys drastically increases in the second loop experiment operating at a higher temperature (450°C). Here LGE shows heavy dissolution attack to the steel structure resulting in high concentrations of Fe, Cr, Ni, and Mn. The corrosion behavior of LBE at 450°C is far less pronounced; however, significant dissolution of nickel is observable. For both investigated alloys, this element is the dominating species. No molybdenum dissolution was found either in LGE or in LBE. These results agree well with the results of analyses of the corresponding steel surfaces obtained in a Scanning Electron Microscopy (SEM) equipped with an Energy Dispersive X-Ray analyzer (EDX) [3].

The corrosion behavior of liquid lead-gold eutectic in contact with 316L stainless steel is significantly worse than that of LBE at the same operational conditions. Substantial dissolution of nickel was observed at temperatures of 400 and 450°C. This either implies the rejection of LGE as a possible alternative to LBE or calls for detailed investigations towards steels with higher corrosion resistance toward LGE, like for instance, the more resistant T91.

Tab. 1: Concentration of corrosion relevant elements dissolved in both investigated alloys for different loop temperatures and sampling times. Values denoted by "<" were below the detection limit of the spectrometer. The overall errors were in the range of ± 15%.

loop temperature	sampling time after startup	analyzed alloy	element concentration [mass ppm]				
			Fe	**Cr**	**Ni**	**Mo**	**Mn**
400°C	**0h**	**LGE**	28	6	6	<	1
	900h		15	4	81	<	2
	1800h		10	4	144	<	3
		LBE	3	1	14	<	<
450°C	**1300 h**	**LGE**	86	134	539	<	53
		LBE	15	2	74	<	<
316L stainless steel composition [%]			65	18	13	2	2

REFERENCES

[1] R. Moormann et al., Proc. Int. TCADS Workshop, Karlsruhe, Germany, 15-17 March 2010, in press.
[2] K. Thomsen et al., Proc. IWSMT Workshop, Beijing, China, 18 – 22 October 2010, submitted.
[3] Y. Dai et al., IWSMT Workshop, Beijing, China, 18–22 October 2010, submitted.

^{206}Po EVAPORATION STUDIES FROM LIQUID LEAD AND LIQUID LEAD-GOLD

M. Rizzi (Univ. Bern & PSI), S. Lüthi, J. Neuhausen, D. Schumann (PSI)

The evaporation of ^{206}Po from liquid lead and liquid lead-gold eutectic within a temperature range from 875-1273K was investigated. The relative release of Polonium was measured and compared with former evaporation studies of ^{206}Po from liquid lead bismuth eutectic (LBE).

INTRODUCTION

Liquid lead alloys such as lead-bismuth eutectic (LBE) are considered to be used as target material in future spallation targets for neutron production. The main disadvantage of LBE is the formation of polonium, especially ^{210}Po under neutron bombardment. Because ^{210}Po is an alpha emitter, it is of great radiological concern due to its toxicity when inhaled or ingested. Therefore, its release from a spallation source into the environment is of special interest. Neuhausen et al. [1] investigated the evaporation behavior ^{206}Po from LBE under Ar/7%H_2 at ambient pressure over the temperature range of 500 - 1200K. Though polonium production in pure lead or the recently proposed lead gold eutectic (LGE) is 100 to 1000 times less compared to LBE, it still forms a considerable radio-hazard. To assess this hazard and to gain a better general understanding of Po mass transfer, a comparison of Po release from different lead based alloys is undertaken. The present study focuses on the evaporation behavior of ^{206}Po from liquid lead and liquid lead-gold eutectic (LGE).

EXPERIMENTAL SETUP

For evaporation studies of ^{206}Po from liquid lead and LGE the transportation method [2] was used. The sample was settled on a quartz tissue within a quartz boat, the boat was placed in a quartz tube and the tube was put into a furnace. As carrier gas, 7%H_2/Ar was supplied. For further purification, the gas flow was conducted over Pd pellets and Sicapent® before entering the quartz tube. In order to catch possible volatile species, an activated charcoal filter was attached at the exhaust of the system and to prevent the diffusion of ambient air into the device, a washing bottle filled with silicon oil was attached. To collect evaporated polonium for further thermochromatographic measurements a tantalum foil was placed directly behind the sample. A scheme of the setup is shown in Fig. 1. All samples had a mass between 600 and 900 mg. Experiments were conducted at temperatures from 873 K to 1273 K. The applied flux was 53 ml/min 7% H_2/Ar.

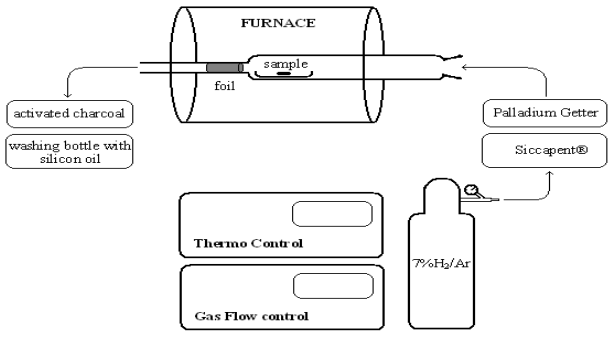

Fig. 1: Schematic setup.

PROCEDURE

The procedure for each experiment was as follows: Before each run the sample was measured by γ-spectroscopy and then put into the quartz tube. The quartz tube was positioned within the oven. The sample in the tube was situated in the cooler region downstream of the oven. In this way, the gadget was allowed to establish the desired temperature within the heated region of the quartz tube for 20 minutes. Then, the position of the tube was changed so that the sample was situated in the center of the furnace with the preset temperature. After one hour the experiment was stopped by again changing the position of the tube and transferring the sample into the non heated region, where it was allowed to cool down until solidification. The sample was taken out and measured again by γ-spectroscopy. The release of polonium from the sample was calculated from the difference of the activity between the two measurements before and after each experiment.

RESULTS AND DISCUSSION

Compared to Polonium release data from LBE from Neuhausen [1], the evaporation process of ^{206}Po from liquid lead and liquid LGE seems to be very similar (Fig.2). One future aim of this study is the further improvement of this method for determining the vapor pressure of evaporated polonium over the liquid metal. Together with thermo-chromatographic investigations of polonium we hope to get a clearer picture of polonium evaporation and deposition processes important for the licensing of future lead-alloy based nuclear facilities.

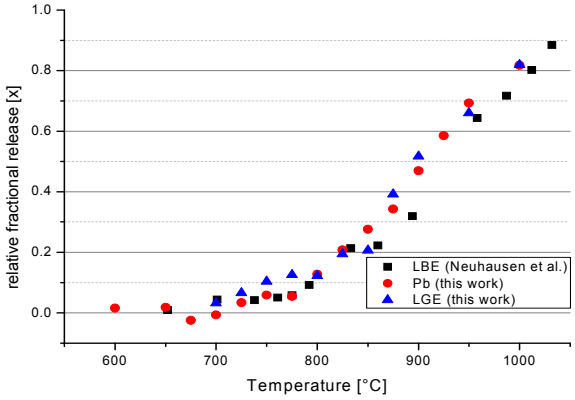

Fig. 2: Relative release of ^{206}Po from lead, LGE and LBE.

REFERENCES

[1] J. Neuhausen et al., Radiochimica Acta, **92**(12): p. 917. (2004).

[2] C.B. Alcock and G.W. Hooper, Physical Chemistry of Process Metallurgy, Part I, p. 325 (1959).

THERMOCHROMATOGRAPHIC INVESTIGATION OF POLONIUM-206

M. Rizzi (Univ. Bern & PSI), J. Neuhausen, R. Eichler, D. Schumann (PSI)

^{206}Po from evaporation experiments was recycled and used for thermochromatographic investigations to gain a deeper knowledge of the gas phase chemistry of polonium. First results seem to confirm the existence of a species more volatile than elemental polonium.

INTRODUCTION

The formation of polonium-210 in lead-based spallation targets induced by neutron bombardment is of great radiological concern due to its toxicity when inhaled or ingested. To understand the processes that can lead to its transfer to the vapor phase, evaporation experiments from different lead based alloys were performed [1,2,3]. Larson investigated the evaporation of ^{210}Po from a pool of molten lead bismuth eutectic (LBE) under different atmospheres [3] and found an increased volatility for polonium under moist conditions and in the presence of hydrogen, which he attributed to the formation of the volatile hydride H_2Po. The aim of this work is the confirmation of such volatile species involved in polonium evaporation using thermochromatographic studies of ^{206}Po in different atmospheres.

EXPERIMENTAL SETUP

Polonium samples were obtained by deposition of evaporated polonium from release experiments [4] onto tantalum foil. Activities of ^{206}Po on Ta-foil varied from some Becquerel up to kBq. These samples were put into a furnace with a linear negative temperature gradient between 1000°C to 100°C. The applied gas flow rates were 20ml/min in case of hydrogen atmosphere and 35ml/min in case of helium atmosphere. For gas purification, a furnace with tantalum getter operated at 960°C was attached in front of the column. To ensure that no volatile species would escape from the system, an activated charcoal filter was attached at the end of the column. Thermochromatographic measurements lasted for at least one hour and up to three hours. Polonium deposition was detected by γ-spectroscopy with a High Purity Germanium (HPGe) detector.

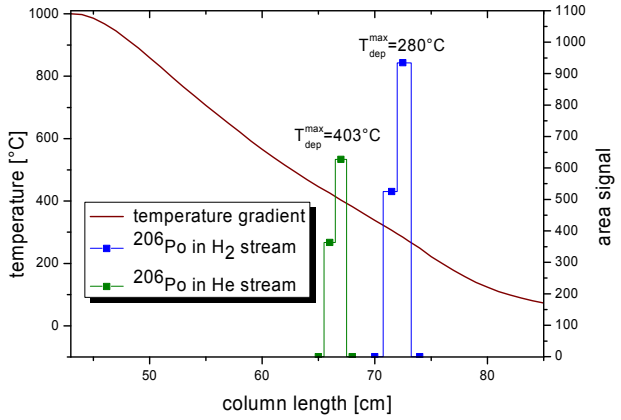

Fig. 1: Thermochromatography of ^{206}Po in He- and H_2-atmospheres (2 h experiments).

RESULTS AND DISCUSSION

The experimental results obtained for helium and hydrogen atmospheres differ significantly. As shown in Fig. 1, in experiments with a duration of 2 h in a helium atmosphere, Po is deposited at around 400 °C, while under hydrogen atmosphere a transport to about 280°C is observed. The variation of experiment time revealed that a slow transport of polonium from 400 °C to lower deposition temperatures occurred in a hydrogen atmosphere, as shown in Fig. 2. This indicates that in presence of hydrogen an unstable volatile species is formed that is slowly transported to its final position. For experiment times longer than 2 h, no further transport was observed.

In order to explore the nature of the formed volatile polonium species, further thermochromatographic experiments under varying experimental conditions, i.e. different atmospheres, gas flow rates, column materials and starting materials, need to be undertaken. We are confident that this method is a useful supplement to our Po evaporation experiments helping us to understand the process of Po mass transfer under different conditions, which is of crucial importance for accident scenarios of future lead alloy based nuclear systems.

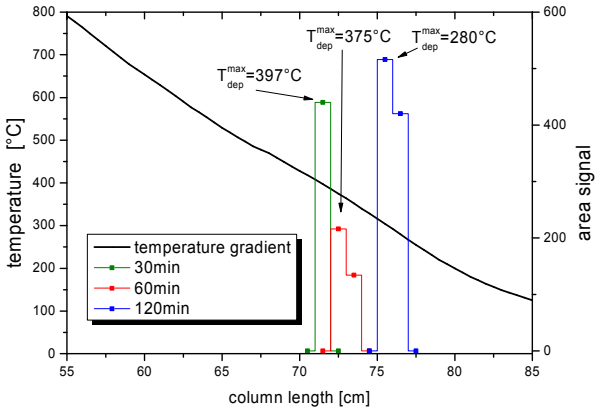

Fig. 2: Thermochromatography of ^{206}Po in H_2 atmosphere with different experiment times.

REFERENCES

[1] Buongiorno et al., Radiochimica Acta, **91**(3): p. 153 (2003).
[2] J. Neuhausen et al., Radiochimica Acta, **92**(12): p. 917 (2004).
[3] C. Larson, Master Thesis, Massachusetts Institute of Technology (2002).
[4] M. Rizzi et al., this report, p. 41.

PYROCHEMICAL EXTRACTION OF RADIONUCLIDES FROM THE LEAD-BISMUTH ISOLDE TARGET IRRADIATED WITH PROTONS

S. Heinitz (Univ. Bern & PSI), J. Neuhausen, D. Schumann (PSI), B. Hammer (Univ. Bern & PSI)

A lead-bismuth target irradiated with protons at the ISOLDE facility at CERN served as the first reference material for investigations of the nuclide inventory and the chemical behavior of radionuclides in irradiated LBE. We have investigated the separation of radionuclides present in the solidified metal by pyrochemical extraction using molten hydroxides.

INTRODUCTION

The knowledge of the chemistry in liquid metals used in nuclear facilities as coolant or target material is very important for safe and reliable operation. In order to study a real lead-bismuth eutectic (LBE) target irradiated with protons, an experiment was performed at the ISOLDE facility at CERN to analyze the release of volatile nuclear reaction products formed within the liquid metal under irradiation. Approximately 500 g of LBE were irradiated with 1 – 1.4 GeV protons for two weeks between 2004 and 2005 (see [1] for further details). This target was later transferred to PSI and serves now as a reference material for investigations on the chemical behavior of spallation products and their inventory in LBE.

We have applied a pyrometallurgical technique using molten hydroxides to identify the extraction performance for different radionuclides present in the ISOLDE LBE target. Using γ-spectroscopy we were able to identify 10 different radionuclides and analyze their extraction performance.

EXPERIMENTAL

A 462.3 mg sample was cut from the bulk LBE of the ISOLDE target and a γ-spectrum was recorded using an HPGe detector. The sample was then transferred into the extraction device described in [2] and fused with 0.9 g of eutectic NaOH/KOH. The extraction was performed at 300°C for one hour under a nitrogen stream. Afterwards, both phases were separated while molten and γ-spectra were recorded for the LBE and the NaOH/KOH sample, the latter previously being dissolved in 20 ml of distilled water. The LBE weight loss was determined to be 2.0 mg. The presence or absence of gamma lines in the corresponding spectra recorded before and after the experiment revealed the behavior of different elements towards the NaOH/KOH melt.

RESULTS

In total, 10 radionuclides of 7 different elements were identified in the γ spectra of the initial LBE sample: ^{60}Co, ^{101}Rh, ^{102m}Rh, ^{108m}Ag, ^{110m}Ag, ^{133}Ba, ^{172}Hf, ^{172}Lu, ^{173}Lu, and ^{207}Bi. Except for ^{172}Lu, which is the radioactive daughter of the ^{172}Hf isotope, all radionuclides have half-lifes $T_{1/2} > 1$ y. Short-lived isotopes are missing in the spectra since they all have decayed due to the long decay time of approx. 5 years. Other radioisotopes present in the sample, e.g. ^{208}Po, ^{148}Gd, or ^{129}I, may only be detected by other techniques like α-spectroscopy or accelerator mass spectroscopy (AMS).

A part of the recorded spectra for the LBE sample before and after the experiment as well as for the (Na,K)OH phase is shown in figure 1. Initially all radionuclides may be found within the starting LBE material. After performing the extraction experiments, certain elements stay in the liquid metal, while others are transferred to the hydroxide phase by oxidation.

In agreement with another study [3] performed with pure bismuth, Ag and Rh do not transfer to the hydroxide phase since they are not oxidized under the given conditions. They stay dissolved in the liquid metal and are not observed in the (Na,K)OH spectrum.

The isotopes ^{60}Co, ^{133}Ba, ^{172}Hf, ^{172}Lu, and ^{173}Lu were quantitatively extracted into the hydroxide phase. For ^{60}Co and ^{133}Ba this finding is in agreement with the study presented in [3], whereas for the mother-daughter pair ^{172}Hf/^{172}Lu and ^{173}Lu we observed a different behavior. Both elements do not transfer into the hydroxide phase from metallic bismuth, but are easily removed from LBE under inert conditions. Either this effect is influenced by the presence of lead in LBE or by traces of oxygen due to the long storage time of the ISOLDE target under ambient conditions exposing it to oxygen present in air. The weight loss for the sample indicates that approx. 0.5% of its total weight was present as oxides, because they easily dissolve in the alkaline melt. Possibly Lu and Hf were already oxidized before the extraction experiment. More detailed investigations on this effect have to be performed in the future.

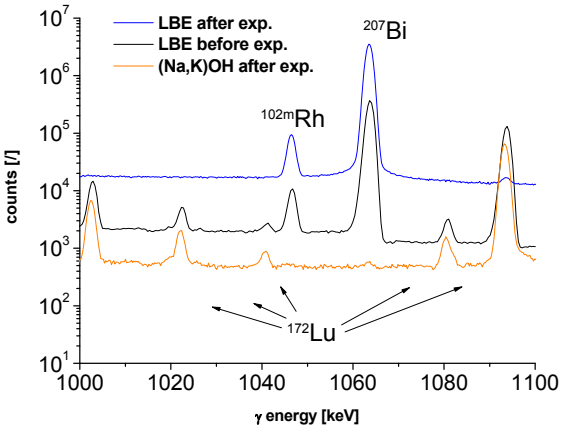

Fig. 1: Part of the γ-spectra recorded for LBE and (Na,K)OH before and after the extraction experiment.

REFERENCES

[1] Y. Tall, PhD thesis, University of Nantes (2008).
[2] S. Heinitz et al., Ann. Rep. Lab. of Radio- & Environ. Chemistry, Uni. Bern & PSI (2008), pp. 39-41.
[3] S. Heinitz et al., this report, p. 44.

PYROCHEMICAL EXTRACTION OF RADIONUCLIDES FROM BISMUTH IRRADIATED WITH AN ARGON BEAM

S. Heinitz (Univ. Bern & PSI), J. Neuhausen, A. Serov (Univ. Bern & PSI), R. Eichler, D. Schumann (PSI)

In order to study the pyrochemical purification of liquid metals by hydroxide melts, we have performed an extraction experiment of a Bi sample irradiated with Ar ions. From the variety of nuclides produced by different nuclear reactions we were able to qualitatively analyze the extraction performance for 30 elements by γ-spectroscopy.

INTRODUCTION

The use of molten sodium/potassium hydroxide in industrial metallurgy for the purification of crude lead or bismuth is known for almost 100 years. This pyrochemical technique was recently applied for the extraction of hazardous polonium from lead-bismuth eutectic (LBE) used as coolant or target material in nuclear facilities [1]. To extend this chemical knowledge to other elements present as impurities in liquid metals used in nuclear facilities, we have studied the performance of hydroxide melts for the extraction of various radionuclides from bismuth previously irradiated with an Ar beam.

EXPERIMENTAL

The irradiation of seven 0.1 mm thick bismuth foils with 300 MeV ^{40}Ar was performed at the PSI PHILLIPS cyclotron. The main purpose was the production of ^{209}At for thermochromatographic experiments [2]. For the separation of ^{209}At all foils were joined and heated to 1000°C for 30 min in a pure He stream.

The remaining Bi sample weighting 3.04 g was analyzed by gamma spectroscopy to identify its nuclide inventory. It was then given into the extraction device described in [3] and fused with 1.03 g of eutectic NaOH/KOH mixture. The extraction was performed for 2h at 350°C under nitrogen stream. Then both phases were separated while molten and a γ-spectrum was recorded for each phase with an HPGe detector. Analysis of the spectra recorded before and after the experiment enables a qualitative statement about the performance of NaOH/KOH for the extraction of radionuclides present in the Bi sample.

RESULTS

In the chart given in figure 1 all elements that were detected by γ-spectroscopy are highlighted in color. Elements marked green were successfully extracted from bismuth, red coloration indicates no or poor transfer.

The extraction performance of an element depends upon its oxidation potential compared to that of Bi. Since lanthanides or steel forming elements (Sc-Co, Y-Mo) show higher affinity toward oxygen, they may be successfully extracted into the alkaline melt. The less easily oxidized metals stay in the Bi phase. Members of the chalcogen group are transferred to the alkaline phase by reduction [3].

It is important to note that the behavior of different elements toward a pyrochemical extraction is also strongly dependent on their chemical form. As the Bi sample was previously heated to 1000°C, various processes (e.g. oxidation) could influence the chemical nature and the distribution of the trace elements within the Bi sample. Oxidized species could be enriched at the surface and hence be more easily extracted.

REFERENCES

[1] E.I. Yefimov et al., Mat. Res. Soc. Symp. Proc., **506**, 679 - 686 (1998).
[2] A. Serov, PhD thesis, University of Bern (2010).
[3] S. Heinitz et al., Ann. Rep. Lab. of Radio- & Environ. Chemistry, Uni. Bern & PSI (2008), pp. 39-41.

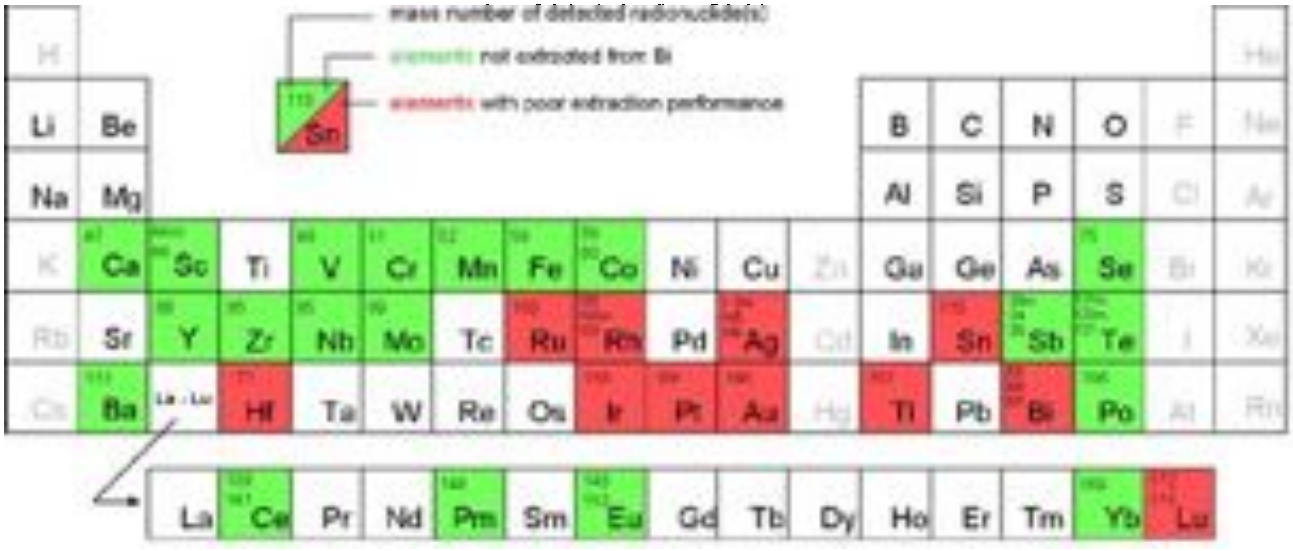

Fig. 1: Chart of detected elements indicating their extraction performance. Elements given in grey were evaporated by the 1000°C treatment.

POLONIUM SEGREGATION IN LEAD-BISMUTH EUTECTIC – IMPROVED MEASUREMENTS

S. Heinitz (Univ. Bern & PSI), S. Lüthi, A. Vögele, J. Neuhausen, D. Schumann (PSI)

In order to understand the segregation behavior of polonium in lead-bismuth eutectic, an improved sample preparation and measurement procedure was developed to eliminate deviations resulting from crystallization and sample geometry issues.

INTRODUCTION

The enrichment of polonium on surfaces of neutron irradiated solid samples of lead-bismuth eutectic (LBE) has been observed several years ago [1]. This effect has a significant influence on the risk assessment of nuclear facilities using LBE as coolant or target material, since polonium may become airborne even in solidified LBE by self-sputtering effects. Attempts to understand and to quantify the kinetics of polonium diffusion suffered from several issues due to low reproducibility and crystallization effects of liquid LBE samples [2]. In order to eliminate these problems, we have developed an improved method for sample preparation and surface activity measurements.

EXPERIMENTAL

To obtain many samples of identical geometry and surface properties, LBE cylinders (h = 10 mm, r = 3.5 mm) were prepared according to the following procedure: a LBE rod (L = 30 cm) was cast by pouring liquid inactive LBE into a glass tube sealed on one side under a nitrogen atmosphere. The metallic alloy is solidified by slow crystallization from bottom to top. Afterwards the glass tube is broken and the metal rod is cut in identical cylinders of 10 mm length. Both sides of each cylinder are trimmed with a microtome.

The samples were annealed in a resistance oven for at least two weeks at 50, 80, or 110°C, depending on the temperature at which the diffusion studies are performed later. After the annealing process, two different procedures where used to introduce polonium into the lead-bismuth cylinder. One batch of samples was irradiated at the PSI NAA neutron activation facility for 30 min at a flux of 5 x 10^{13} n*cm^{-2} s^{-1}. The samples were stored to allow a proper decay of the intermediate ^{210}Bi isotope. For another batch of samples polonium was deposited on the top and bottom surfaces of LBE from 100 µl of a 1M HNO_3 solution containing 560 Bq/ml ^{210}Po.

All samples are then placed inside a resistance oven at the temperature of their previous annealing. The surface activity of ^{210}Po is recorded twice per week by α-spectroscopy. A plastic tube serves as shielding to eliminate the contribution of α-emissions from the lateral surface of the cylinders.

RESULTS

The results of measurements performed at 50 and 110°C are given in figure 1. For neutron activated samples, a surface enrichment is observed as a function of time due to segregation of polonium. This results in higher counting rates in the α-spectrometer. In contrast, after deposition of polonium on the surface of inactive LBE, a pronounced lowering of the total count rates with time is observed indicating the diffusion of Po into the bulk. This was confirmed by depth profiling of non-annealed samples.

The segregation behavior of polonium for different temperatures given in figure 1 contradicts the findings reported in [2]. For higher temperatures less surface enrichment of Po is found in the present study, whereas the opposite is observed for experiments in [2]. More experiments have to be done to clarify this circumstance.

It should be stressed that the role of many parameters on the diffusion of polonium are still unclear. From analysis of the α-spectra a clear influence of a lead/bismuth oxide layer on the polonium segregation was found. This should be considered in case a surface treatment of LBE is performed, e.g. by HNO_3 during Po deposition. Moreover, various impurities in LBE may significantly change the segregation behavior within LBE. In order to understand the influence of these parameters on the dynamics of polonium in LBE and to deduce values for the diffusion constant under different conditions, in addition to the diffusion studies described here, further studies using analysis techniques such as radiography, TEM imaging, and depth profiling in combination with chemical analysis of the specimens will be performed.

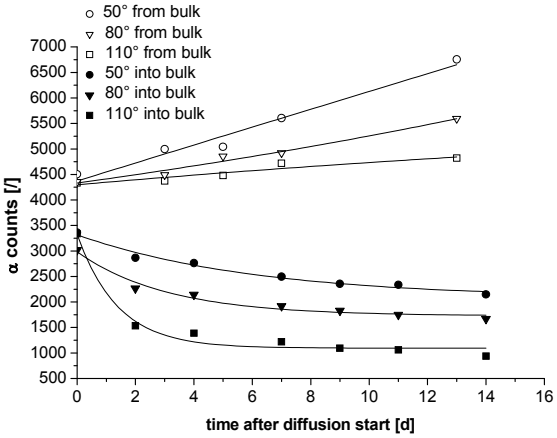

Fig. 1: The function of surface activity variation with time of cylinders where polonium was introduced by neutron activation (segregation *from bulk* to surface) or by spontaneous deposition (diffusion from surface *into bulk*); for comparison, three different temperatures are shown.

REFERENCES

[1] J. Neuhausen et al., Ann. Rep. Lab. of Radio- & Environ. Chemistry, Uni. Bern & PSI (2006), p. 43.

[2] S. Heinitz et al., Ann. Rep. Lab. of Radio- & Environ. Chemistry, Uni. Bern & PSI (2009), p. 59.

RADIOCHEMICAL ANALYSIS OF CONCRETE SAMPLES FROM ACCELERATOR WASTE; PART I: SAMPLE DESCRIPTION AND γ-ANALYSIS

D. Schumann (PSI), D. Kiselev, S. Teichmann, (PSI/GFA), H.-A. Synal, P. Kubik (ETHZ)

For the decommissioning and disposal of shielding concrete from accelerator facilities, the Swiss authorities require information on the radionuclide inventory. Descriptions of two sample sets and results on γ-spectrometry are given.

The concrete samples called "E" were taken from the floor below the former Target M, a rotating graphite wheel which was hit by 590 MeV protons for meson production. The beam dose on the target was approximately 2.92 Ah.
The target was positioned at 1.5 m above the floor level. The floor below Target M consisted of concrete covered with a 60 cm thick iron plate for shielding. After removing the iron plate, our samples were taken both from the beam entrance side (1.10 m distance from Target M) and exit (3.44 m distance from Target M) side by performing two core drillings, both with a diameter of 16 cm. From each of the obtained two 50 cm long pillars, 5 small equidistant samples were taken, as is illustrated in Figure 1.

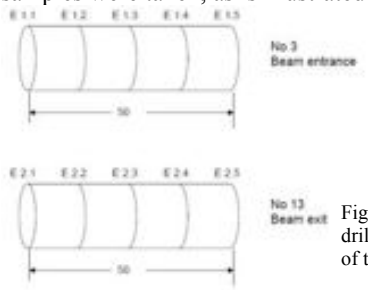

Fig.1: Depiction of the two drilling cores and the positions of the sample taking

The second sample set named "B" stems from the environment of the former BX2 beam dump, which served as a logging target for the 72 MeV injector cyclotron. The accumulated beam current was 1.74 Ah. It consisted of a copper block, followed by steel and lead shielding flush with a 30 cm thick concrete shielding block. 6 samples were taken at several positions of the concrete shielding. Details of the sample description shown in Figure 2 are taken from reference [1].

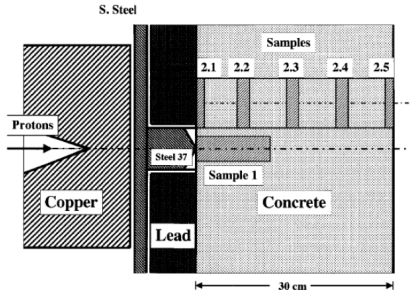

Fig. 2: (taken from [1]): Layout of the design of the BX2 beamdump

In Table 1, the results of the γ-measurements are summarized. For comparison, the values published in [1] for the sample 1 of the BX2 target, located about 14 cm away from beam entrance in beam direction, is given. Considering the proton beam energy of 72 MeV, with a range in copper of less than 8 mm, it is expected, that radionuclide production in the concrete shielding was mainly induced by secondary neutrons and not by protons penetrating the steel and lead shielding. This is confirmed by the fact that sample 1, which is located on the beam axis, shows similar values as samples 2.2.1 and 2.2.2, which are located away from the beam axis. With increasing depth, corresponding to a decreasing neutron field, the amount of induced activity becomes lower, which is clearly visible for all measured radionuclides. Sample B2.2.2 shows in most of the cases a higher activity than B2.2.1, which is located directly behind the lead shielding where the neutrons are not yet thermalized.
The values for the E-samples are generally lower than the B values (see [2].

[1] R. Weinreich et al., J. Radioanal. Nucl. Chem, 261 319 (2004).
[2] D. Schumann et al., this report, p.47.

Tab.1: γ-spectroscopic measurements of all concrete samples (calibrated to May/2003, with exception of sample 1: July/2003); *: values taken from [1]

sample	^{152}Eu	^{60}Co	^{44}Sc	^{133}Ba	^{154}Eu	^{134}Cs	^{144}Ce	^{22}Na
	[Bq/g]	[Bq/g]	[Bq/g]	[Bq/g]	[Bq/g]	[Bq/g]	[Bq/g]	[Bq/g]
E1.1	8.18	2.04	0.09	0.13				
E1.2	4.61	0.81	0.22					
E1.3	4.74	1.02	0.37					
E1.4	0.765	0.51	0.27					
E1.5	0.278	0.49	0.24					
E2.1	5.92	1.12						0.73
E2.2	6.78	1.15	0.12					
E2.3	3.18	0.75						0.26
E2.4	1.36	0.60	0.31					
E2.5	0.73	0.32	0.23					
B2.2.1	2646	712		18.2	320..6	156.3	84.3	
B2.2.2	2949	1421		27.3	302.5	167.9		
B2.2.3	1676	508		11.5	160.0	80.5		
B2.2.4	987	247		4.21	88.0	51.7		
B2.2.5	866	243		4.12	73.7	47.9		
sample 1	2616*	586*		15*	305*	229*		290*

RADIOCHEMICAL ANALYSIS OF CONCRETE SAMPLES FROM ACCELERATOR WASTE. PART II: CHEMICAL TREATMENT AND RESULTS OF α-SPECTROSCOPY AND ACCELERATOR MASS SPECTROMETRY MEASUREMENTS (AMS)

D. Schumann (PSI), D. Kiselev, S. Teichmann (PSI/GFA), H.-A. Synal, P. Kubik (ETHZ)

For determining long-lived radionuclides, concrete has to be chemically treated. Results on the α-emitters ^{238}U and $^{239/240}Pu$ as well as the very long-lived isotopes ^{10}Be, ^{26}Al, ^{36}Cl, and ^{129}I are given.

The description of the sample characteristics as well as the sample taking positions are given in [1].

Chemical treatment

About 1 g of each sample was milled in a ball mill.

^{238}U, $^{239/240}Pu$: An identical procedure as described in [2] was applied including the separation of the actinides by using ion exchange with BioRad and UTEVA columns as well as the sample preparation for the α-measurement [3].

^{26}Al and ^{10}Be: After adding 2mg of stable Al and Be carrier, respectively, decomposition with aqua regia was used as described in [4]. Finally, the solution was evaporated to dryness and the residue dissolved in 1 M HNO_3. Further treatment for the isolation of the isotopes and final purification were carried out following the procedure described in [5].

^{36}Cl and ^{129}I: Because chlorine-containing acids cannot be used for the decomposition in this case, hot-water-digestion as described in [6] was applied in a slight modification: Instead of water, 1M HNO_3 was used for the leaching. Samples were boiled together with 10 mg of stable chlorine and iodine carrier, respectively, and 20 ml acid solution in a tight three-neck vessel under a nitrogen flow which leads the volatiles into the corresponding adsorption vessels, as described in [5]. The halogens are precipitated with $AgNO_3$. After washing, re-precipitation and drying, the samples are ready for AMS measurements.

Results

From the results in Table 1 it can be seen that the samples from the BX2 target have generally much higher radionuclide inventories than the samples from the target M floor, although the received beam dose of target M is a factor 1.7 higher.

Tab. 1: Results of the AMS- and α-measurements. *: values taken from [2] for comparison

sample	^{129}I	^{26}Al	^{10}Be	^{36}Cl	$^{239/240}Pu$	^{238}U
	[mBq/g]	[mBq/g]	[mBq/g]	[mBq/g]	[mBq/g]	[mBq/g]
E1.1	$6.2\cdot10^{-4}$	$1.7\cdot10^{-2}$		82	0.347	12.72
E1.2	$4.3\cdot10^{-4}$		$4.0\cdot10^{-3}$	-		
E1.3	$9.1\cdot10^{-4}$		$1.0\cdot10^{-3}$	10		
E1.4	$7.0\cdot10^{-4}$	$8.3\cdot10^{-3}$	$1.2\cdot10^{-3}$	0.4		
E1.5	$8.2\cdot10^{-4}$		$5.1\cdot10^{-3}$	0.3	0.071	13.10
E2.1	$6.2\cdot10^{-4}$	$6.3\cdot10^{-1}$	$8.4\cdot10^{-2}$	34.6	0.286	11.28
E2.2	$3.1\cdot10^{-4}$	$3.7\cdot10^{-1}$	$8.5\cdot10^{-2}$	64.3		
E2.3	$3.2\cdot10^{-4}$	$1.6\cdot10^{-1}$	$4.1\cdot10^{-2}$	32.5		
E2.4	$7.2\cdot10^{-4}$	$1.7\cdot10^{-1}$	$3.3\cdot10^{-2}$	13.2		
E2.5	$3.5\cdot10^{-4}$			5.7	0.028	13.95
Sample 1	$1.2\cdot10^{-3}$	9.0	$9.6\cdot10^{-1}$	-		
B2.2.1	$2.0\cdot10^{-2}$		2.9	-	32.4*	13.1*
B2.2.2	$2.4\cdot10^{-2}$	11.8	1.5	6148	30.7*	14.7*
B2.2.3	$4.3\cdot10^{-2}$		$7.0\cdot10^{-1}$	-	11.9*	8.2*
B2.2.4	$2.8\cdot10^{-2}$		$4.8\cdot10^{-1}$	-	12.3*	12.9*
B2.2.5	$5.5\cdot10^{-2}$	4.7	$3.0\cdot10^{-1}$	-	5.66*	14.7*
0					<0.18*	8.24*

The following issues explain the differences:

- *Distance of the samples from the Target*

E-samples have a distance from the target of 1.5 m from the floor + 1.1 m or 3.4 m, respectively, from the target plus 60 cm iron shielding for the nearest (E1.1 and E2.1.) B-samples have a distance from the target of 14 cm for the nearest (sample 1).

- *Shielding*

E-samples are shielded with 60 cm iron. B-samples are shielded by around 7 cm iron (sample 1) or lead (all other samples)

- *Design and material of target*

BX2 is a compact thick copper target, where the 72 MeV proton beam is completely stopped. A high production rate of secondary particles has to be expected. Target M is a 0.5 cm thick rotating carbon wheel. Most 590 MeV protons penetrate the material; only a few percent interact with carbon to produce mesons and secondary neutrons (the beam is further transported to a second graphite target for meson production). Carbon with a low atomic number is less efficient for neutron production in comparison to copper, in the forward direction.

Conclusions

Uranium is a natural component in normal concrete. We find a more or less constant value in all samples (average 12.7±2.0 mBq/g, corresponding to around 1-1.5 ppm as given in the literature [7]). The plutonium is produced in nuclear reactions with secondary neutrons. Its content in the B-samples exceeds the limits given in the Swiss radiation Protection Act of 1994 (20 mBq/g) for the innermost samples. In the updated version of 2009, this limit is given as 40 mBq/g, which is not exceeded by any of the samples. The E-samples also do not exceed the limits concerning Pu.

None of the measured radionuclides including the γ-emitters [1] represent a safety issue. The long-lived components even do not exceed the exemption limits.

REFERENCES

[1] D. Schumann et al., this report, p. 46.
[2] R. Weinreich et al., J. Radioanal. Nucl. Chem, 261 319 (2004).
[3] S. Bajo et al., Radioanal. Nucl. Chem. 242 745 (1999).
[4] X. Hou, Radiochemical Analysis for Nuclear Waste Management in Decommissioning, NKS-B RadWaste report, July 2010 (ISBN 078-87-7893-292-1).
[5] D. Schumann et al., NIM B 264 83-95 (2007).
[6] http://www.tfb.ch/htdocs/Files/VSS/VSS546d.pdf.
[7] M. Peehs, T. Walter, S. Walter, in: Ullmanns Encyclopedia of Industrial Chemistry, 5th completely Revised Edition, Bol.A27, B. Elvers and S Hawkins (Eds.), VCH Verlagsgesellschaft mbH, Weinheim 1996, p. 289.

EXTRACTION OF ASTROPHYSICALLY INTERESTING RADIONUCLIDES FROM IRRADIATED STAINLESS STEEL SAMPLES

M. Bunka (Univ. Bern & PSI), D. Schumann, M. Ayranov, S. Koechli (PSI)

^{44}Ti, ^{53}Mn, and selected other long-lived radionuclides are attractive for several scientific applications. Proton irradiated stainless steel materials at PSI contain those isotopes. For the extraction and purification of ^{44}Ti and ^{53}Mn from the complex stainless steel 316L matrix a multistep separation system is developed and optimized.

INTRODUCTION

^{44}Ti is a neutron-deficient radionuclide with a half-life of 60.4 years, among others being of interest for the study of nuclear processes in astrophysics. It is produced in supernovae explosions and can be observed by γ–satellites in the space thanks to the γ-radiation of its short-lived daughter nuclei ^{44}Sc (3.97 h, 1157 keV). For the understanding of processes occurring in the stars, the knowledge of the cross sections of the formation and destruction reactions of ^{44}Ti, such as ^{40}Ca(α, γ)^{44}Ti, ^{44}Ti(p,γ)^{45}V; ^{44}Ti(α, p)^{47}V, are mandatory.

^{53}Mn with a half-life of $3.7 \cdot 10^6$ y is a so-called "cosmic clock", allowing studies of the long-term development of elements in stars. Here, also the cross sections of the corresponding nuclear reactions have to be known, and additionally, the high uncertainty of the half-life values represent a problem.

For all these investigations, the availability of sample material is a precondition, and unfortunately, they cannot be produced in considerable amounts so easily. One possibility is the exploitation of accelerator waste, irradiated with high-energetic protons [1,2]. At PSI, several activated materials suitable for such purposes are available. We report here on the use of irradiated steel as a possible source.

EXPERIMENTAL

The material – stainless steel (SS) grade 316L (**Fig.1**) originates from the former PIREX gas chamber of the biomedical application station. The sample weight is 12 kg and contains about 100 MBq ^{44}Ti and ~2 GBq ^{60}Co [2].

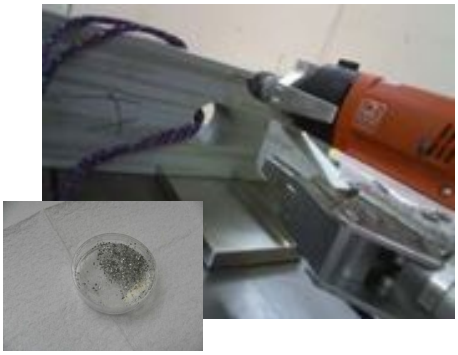

Fig. 1: Stainless steel sample

SS 316L contains 65% Fe, 18% Cr, 13% Ni, 2,6% Mo, 1,4% Mn, 0,035% Co and 0,013% Ti. To separate the desired elements Mn and Ti from all other elements a multistep separation is developed (**Fig.2**).

After the dissolution of SS in 8M HCl and couple mL of conc. HNO_3, extraction with diethyl ether is performed to separate the great part of iron and molybdenum. Next step is the precipitation with concentrated NH_3. Then the precipitate containing Fe, Ti, Cr, and Mn is dissolved in HCl and precipitated with sodium hydroxide and hydrogen peroxide. The precipitate containing Fe, Mn, and Ti is dissolved in 8M HCl and the extraction with diethyl ether repeated. For the determination of element concentrations ICP-OES is used.

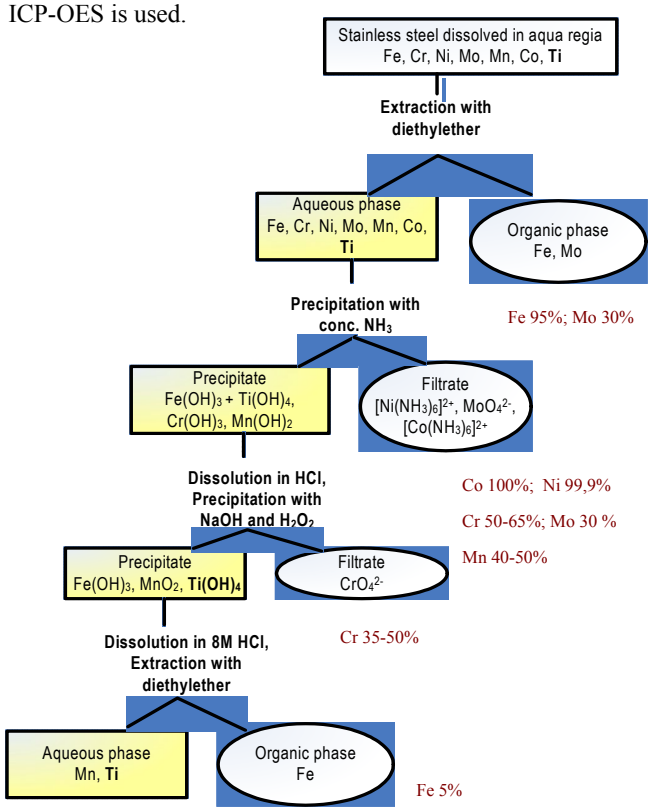

Fig. 2: Separation scheme

RESULTS AND DISCUSSION

Using this separation scheme experiments with up to 500 mg SS 316L samples were carried out. After the second extraction with diethyl ether Co and Mo are not found in the aqueous phase anymore. The decontamination factor for Cr and Fe is 10^4, for Ni $3 \cdot 10^3$, respectively. The chemical yields are 40-55% for Mn and 80-90% for Ti. A final separation of Mn and Ti can be obtained using ion exchange chromatography.

REFERENCES

[1] D. Schumann et al., J. Phys. G, 35 (2008) 014046.
[2] M. Ayranov, D. Schumann, Ann. Rep. Lab. of Radio- & Environ. Chemistry, Uni. Bern & PSI (2009), p. 49.

ION EXCHANGE FOR THE SEPARATION OF ^{44}Sc FROM ^{44}Ti

M. Bunka (Univ. Bern & PSI), D. Schumann, M. Ayranov (PSI)

To separate scandium-44 from its parent titanium-44 and other contaminants ion exchange as radionuclide generator system can be used. Anion and cation exchange columns DOWEX 1X8 and DOWEX 50WX8 are tested to find the optimal separation system for scandium.

INTRODUCTION

The ^{44}Ti/^{44}Sc radionuclide pair is suitable for radionuclide generator system for medical applications, because ^{44}Sc is a positron emitter with a half-life of 3,97 h allowing for a much longer patient investigation than the conventional positron emission tomography (PET) nuclides like ^{18}F or ^{68}Ga [2]. On the other hand, the long half-life of the mother nuclide enables an application time of several decades. Moreover, the chemistry of Sc concerning medical application is already extensively studied, due to the application of ^{47}Sc for therapeutic radionuclide cancer treatment. Several criteria are relevant for radionuclide generators, such as high purity of the daughter eluate, low breakthrough of titanium, long-term stability, eluate chemical form suitable for further application etc. In the present study the ion exchange technique was evaluated as ^{44}Ti/^{44}Sc generator system [1, 2].

EXPERIMENTAL

For the separation of ^{44}Sc from ^{44}Ti the anion exchanger DOWEX 1X8 (D1; 100-200 mesh, 2 mL column) and the cation exchanger DOWEX 50WX8-200 (D50; 2 mL column) are tested. ^{44}Ti solution with an activity of about 10 kBq (0,5M HCl) is evaporated and fumed with HF solution twice, dissolved in 1M HF and passed through the column D1. Ti and Sc are adsorbed and scandium is eluted with HNO_3/HF and HCl/HF solutions.

The ^{44}Ti solution (about 10 kBq) in 0,5M HCl is passed through the D50 column, where Ti and Sc are adsorbed. First, titanium is eluted with HCl or HCl/H_2O_2 solution. Scandium remains on the column under these conditions and is eluted with HCl, HNO_3, or H_2SO_4/$(NH_4)_2SO_4$ solution.

RESULTS AND DISCUSSION

In **Fig. 1** the γ-spectra of the D1 column before the separation (red), after elution of Sc (blue) and of the eluate containing scandium-44 (green) is shown. No ^{44}Sc is detected on the column after the separation. The eluate is free of contaminants and contains only ^{44}Sc. No ^{44}Ti breakthrough can be detected in the eluate.

For the elution of ^{44}Sc from D1 several concentration ranges of HNO_3/HF and HCl/HF are used. Measured yields of ^{44}Sc in the eluates are given in **Tab. 1**. The best elution systems with an elution efficiency of 98-99% and minimal volume of eluate are 0,5M HCl/1M HF and 0,6M HCl/1M HF. After about one day scandium is grown back in on the column and is in equilibrium with titanium. So, scandium can be eluted again with the mother's activity.

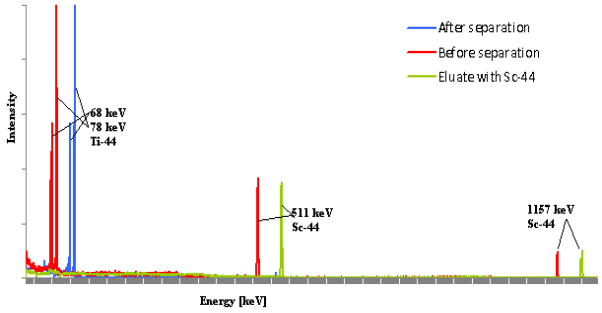

Fig. 1: γ-spectra of DOWEX 1X8 column with ^{44}Ti and ^{44}Sc in equilibrium and after elution with 0,4M HCl/1M HF solution; eluate with ^{44}Sc.

Tab. 1: Yields of ^{44}Sc in the eleuates (DOWEX 1X8)

Conc. of HNO_3/HF	**% of ^{44}Sc** in x mL of eluent	**Conc. of HCl/HF**	**% of ^{44}Sc** in x mL of eluent
0,1M/0,4M	92% in 14 mL	0,15M/1M	95% in 14 mL
0,15M/0,4M	96% in 11 mL	0,2M/1M	98% in 12 mL
0,2M/0,4M	95% in 6 mL	0,3M/1M	98% in 8 mL
0,25M/0,4M	98% in 5 mL	0,4M/1M	98% in 6 mL
0,2M/0,5M	97% in 7 mL	0,5M/1M	99% in 5 mL
0,2M/1M	97% in 7 mL	0,6M/1M	98% in 5 mL
		0,5M/0,5M	96% in 6 mL
		0,5M/1,5M	97% in 5 mL
		0,4M/0,5M	98% in 6 mL

Using D50 for the separation ^{44}Ti can be eluted from the column with 16 mL of 1M HCl; 10 mL of 1,75M HCl; 10 mL of 1,75M HCl/H_2O_2 solution. Scandium remains on the column and is eluted with HCl, HNO_3, H_2SO_4, or mixed H_2SO_4/$(NH_4)_2SO_4$ solution (**Tab. 2**). The elution efficiency of Sc using D1 is better compared to D50.

Tab. 2: Yields of ^{44}Sc in the eleuates (DOWEX 50WX8)

Eluent	**% of ^{44}Sc** in x mL of eluent
0,5M H_2SO_4	25% in 15 mL
4M HCl	32% in 9 mL
6M HCl	45% in 10 mL
7M HNO_3	79% in 10 mL
0,025M H_2SO_4/3M $(NH_4)_2SO_4$	64% in 10 mL
0,025M H_2SO_4/1M $(NH_4)_2SO_4$	75% in 10 mL

REFERENCES

[1] D. Schumann et al., Ann. Rep. Lab. of Radio- & Environ. Chemistry, Uni. Bern & PSI (2006), p. 41.
[2] D. V. Filosofov et al., Radiochim. Acta, 98, 149-156 (2010).

SINQ COOLING WATER – SOURCE OF n.c.a. RADIONUCLIDES

M. Ayranov, D. Schumann, R. Dressler (PSI), A. Kalt, F. Heinrich, O. Morath, R. Lüscher (PSI/NUM)

SINQ cooling water is used as a source for the separation of TBq activity of ^{7}Be. The prepared sample is sufficiently pure and suitable to be used as a second calibration point for the determination of the ^{10}Be half-life. Together with ^{7}Be, a number of valuable isotopes, such as ^{54}Mn, ^{83}Rb, ^{88}Y, ^{85}Sr etc, are isolated in n.c.a. form.

INTRODUCTION

^{7}Be as well as ^{10}Be are key radionuclides for investigations of several astrophysical processes and phenomena. One of the "hot topics" is the half-life of ^{10}Be, where the literature values differ from 1.34 to $1.51 \cdot 10^{6}$ a [1, 2]. Therefore, a more accurate determination of the ^{10}Be half-life is needed.

One possibility is the use of Liquid scintillation counting (LSC) for the determination of the activity and Multi Collector Inductively Coupled Mass Spectrometry (MC-ICP-MS) for measuring the number of atoms. The mass discrimination correction of the ICP-MS requires at least 2 isotopes of known amounts. Since beryllium has only one stable isotope ^{9}Be, ^{7}Be can be used successfully as the second calibration point.

Another application of ^{7}Be is the study of key reactions concerning the solar neutrino flux, in particular the reaction ^{7}Be(p,γ)^{8}B [3].

^{7}Be is produced in considerable amounts in the cooling water (D_2O) of the SINQ facility at PSI by spallation reactions on ^{16}O with the generated fast neutrons. In table 1 the highest measured activity concentrations of the most populated radionuclides in the water of three different SINQ cooling loops are presented. By-products can be nearly neglected, so that this cooling water establishes an ideal source for highly active ^{7}Be-samples.

Tab. 1: Radionuclide inventory in the SINQ cooling loops.

Cooling loop	Activity, Bq/g					
	^{7}Be	^{3}H*	^{22}Na	^{54}Mn	^{88}Y	^{83}Rb
Target	4400	25	800	0.1	0.6	2.3
Target window	480	23	0.4	0.05	-	-
Moderator	930	21	4	0.1	-	-

*Tritium activity is in MBq/g

EXPERIMENTAL

An ion exchange filter containing 1 liter of the mixed-bed ion exchanger LEWATIT was installed as a by-pass in the target cooling loop for 6 weeks – figure 1. The collected activity of ^{7}Be was in the range of few TBq [4]. Due to the high dose rate a separation system was designed and installed in a hot-cell, figure 2. After a cooling period of 12 months the ion exchanger was transferred to the hot cell for separation of ^{7}Be.

Fig. 1: Filter device installed in the SINQ cooling workshop.

Fig. 2: Hot-cell remote controlled separation system.

The radiochemical separation of beryllium and accompanying radionuclides is performed by combination of cation and anion exchange. The description and selectivity of the procedure have been published previously[5].

RESULTS

The separated radionuclides and their activities, decay corrected for the end of sampling, are presented in table 2.

Tab. 2: Radionuclides extracted from the SINQ cooling water

Activity, MBq							
^{7}Be	^{22}Na	^{54}Mn	^{88}Y	^{83}Rb	^{65}Zn	^{85}Sr	^{75}Se
1.2	540	15	16	12	0.2	110	3

*^{7}Be activity is in TBq

At the end of the experiment, 5 GBq ^{7}Be or 0.4 mg, are separated. This amount is sufficient to perform the ICP-MS measurement.

In addition, significant activities of valuable radionuclides are separated.

REFERENCES

[1] R. Middleton et al., Nucl. Instr. Meth. Phys. Res. Sect. B, **82,** 399, (1993).
[2] G. Korschinek et al., Nucl. Instr. Meth. Phys. Res. Sect. B, **268** , 187, (2010).
[3] L. T. Baby et al., Phys. Rev. Lett.**, 90**, *2*, 022501.1, (2003).
[4] D. Schumann et al., Ann. Rep. Lab. of Radio- & Environ. Chemistry, Univ. Bern & PSI (2008).
[5] M. Ayranov et al., Ann. Rep. Lab. of Radio- & Environ. Chemistry, Univ. Bern & PSI (2009).

RE-DETERMINATION OF THE ^{60}Fe HALF-LIFE: FIRST RESULTS

M. Ayranov, M. Bunka, R. Dressler (PSI), I. Günther-Leopold (PSI/NES), St. Heinitz (PSI), N. Kivel (PSI/NES), S. Lüthi, D. Schumann, T. Stowasser, A. Vögele, D. Wittwer (PSI)

First results on γ- measurements of ^{60}Fe samples to confirm the recently obtained new half-life are presented.

INTRODUCTION

The recently performed re-determination of the ^{60}Fe half-life – (2.62±0.04) Ma [1] – showed a deviation from the so far accepted value $t_{1/2}$ = (1.49±0.27) Ma [2] of more than 1 Ma. This discrepancy demands a repetition of the measurement. Therefore, a new ^{60}Fe sample was prepared using the target used for the determination of the neutron capture cross section [3].

EXPERIMENTAL

The ^{60}Fe, fixed on a carbon backing [4], was dissolved in 7 M HCl and ^{60}Co was separated by extracting the iron into methyl isobutyl ketone and back extraction into 0.1 M HCl. The procedure was repeated several times. The solution was divided into four parts. Two samples are currently used for the γ-measurement of the half-life determination, one at the University of Vienna, the other one at PSI. The third sample is used for the determination of the number of atoms per gramm liquid and the last part is used as target material for the measurement of the thermal neutron capture cross section. About 80% of the original target material could be recovered during the chemical procedures, i.e. a total number of 3.5×10^{15} atoms ^{60}Fe is expected in each of the samples used for the γ-measurements and 1.7×10^{15} atoms ^{60}Fe in the sample used for the MC-ICP-MS and for the thermal neutron capture cross section measurements, respectively.

The ^{60}Fe solution used for γ-spectroscopic investigations at PSI was transferred into a serum vial (11 mm outer diameter) and filled up to 4 ml using diluted acid (0.1 M HCl). A HPGe well detector with closed well end (crystal length 53 mm, diameter 60 mm; core length 40 mm, diameter 19 mm; active volume ~132 cm^3) is used for the measurements. The serum vial fits perfectly into the well opening. A reference sample containing (157.6±3.4) Bq ^{60}Co and (7.3±1.6) Bq ^{241}Am (with k=2 expanded standard uncertainties, reference date 2.10.2009) is measured for 4 h alternating to the 160 h measurements of the ^{60}Fe sample fixing the gain and offset of the spectroscopic hardware using a digital stabilizer. The activities of ^{60}Co and ^{241}Am are determined using a total efficiency calibrated detector. Therefore, the uncertainties of these values are rather large. The first measurement of the ^{60}Fe sample started in August.

RESULTS

Fig. 1 shows a measurement using the ^{60}Co-^{241}Am reference source, the completed first measurement of the ^{60}Fe (started 4 h after finishing the last purification) and a snap shot 4 h after start of this measurement. It can be clearly seen that the activity of ^{60}Co was very low after the last purification. The initial ^{60}Fe and ^{60}Co activities were deduced from a fit of the performed measurements to be 32 Bq/g and 85 mBq/g,

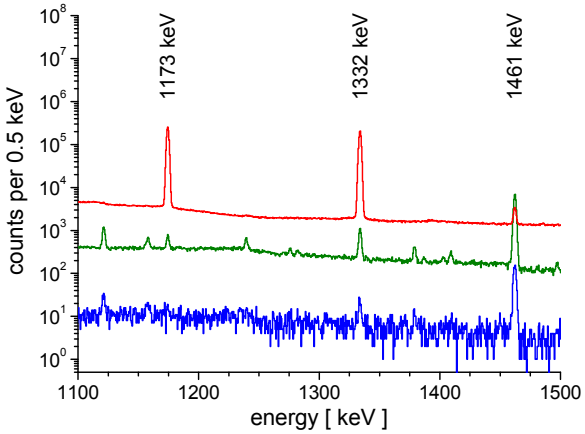

Fig. 1: From top to bottom: 48 h γ-spectra of ^{60}Co-^{241}Am reference sample (red, digital stabilizer on), first 160 h measurement of ^{60}Fe sample (green, digital stabilizer hold), and snap shot of this measurement after 4 h. The γ-lines of ^{60}Co and ^{40}K are indicated.

respectively. The uncertainties of these values are about 10%, depending on the uncertainty of the ^{60}Co activity in the reference source and the reached quality of the peak area determination and the resulting fit quality. The additional population of the 1332 keV line via a 0.24% branch of ^{60m}Co leads to an enhanced count rate of this γ-line compared to the ^{60}Co reference measurement. This is depicted in Fig. 2 via the count-rate ratios of the 1173 keV and the 1332 keV ^{60}Co γ-line.

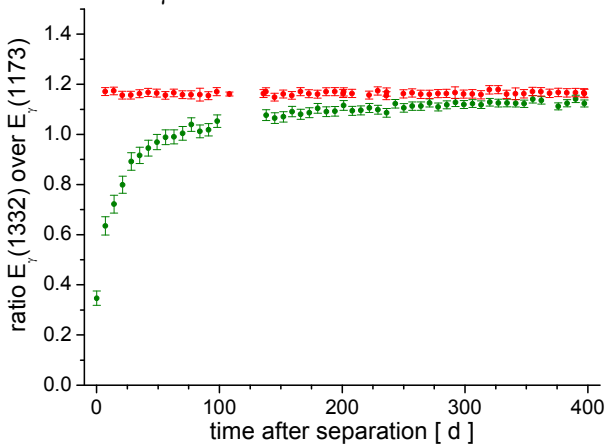

Fig. 2: Count-rate ratios of the 1173 keV and the 1332 keV ^{60}Co γ-line of the ^{60}Co-^{241}Am reference source (red) and the ^{60}Fe sample in dependence of the time after the last chemical separation.

REFERENCES

[1] G. Rugel et al., Phys. Rev. Lett. **103,** 072502 (2009).
[2] W. Kutschera et al., Nucl. Instr. Meth. **B5,** 430 (1984).
[3] E. Uberseder et al., Phys. Rev. Lett. **102,** 151101, (2009).
[4] D. Schumann et al., Nucl. Instr. Meth. **A613,** 347 (2010).
[5] T. B. Coplen et al., Pure Appl. Chem., **74,** 1987 (2002).

CHARACTERISATION AND CALIBRATION OF WEAK ^{44}Ti SOURCES FOR ASTROPHYSICAL APPLICATIONS

D. Schumann (PSI), K. Schmidt, D. Bemmerer (FZD)

Five ^{44}Ti calibration sources supplied by Paul-Scherrer-Institute have been characterized concerning their activity distribution as well as the absolute activities. Now, calibration sources for nuclear astrophysics experiments with an uncertainty of ± 1.2 % are available.

INTRODUCTION

The radioactive nuclide ^{44}Ti ($T_{1/2}$ 58.9 ys) is believed to be produced in supernova explosions. By observing the γ-rays from the decay of this nuclide with the INTEGRAL satellite - the first space observatory that can simultaneously observe objects in gamma rays, X-rays, and visible light - one can find a signature of supernova explosion that has taken place in the last few centuries. So far the ^{44}Ti decay radiation has been observed only for one supernova remnant called Cassiopeia A [1]. Several other remnants of recent supernovae studied did not show the expected emission, which leads to the question whether the currently accepted supernova models are correct [2].

Nuclear reaction rates determined in the laboratory are one important aspect of these models. Dedicated sensitivity studies have shown that the ^{40}Ca(α,γ)^{44}Ti reaction plays an important role in this context [3]. In order to obtain results as precise as possible, well-characterized calibration sources are necessary.

EXPERIMENTAL

Five ^{44}Ti calibration sources – three point and two area sources - were prepared by evaporating radionuclide-containing diluted nitric acid on tantalum plates. The sources were covered with a 200 nm thick gold layer afterwards in order to protect the surface. One example is shown in Fig.1 (point source P60). Unfortunately, the evaporation method does not give uniform distributions. Therefore, a careful characterization of the total activity and distribution is necessary.

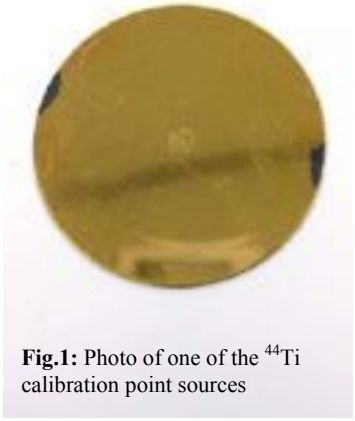

Fig.1: Photo of one of the ^{44}Ti calibration point sources

The absolute activity was determined with a standard γ-spectrometer using high-precision ^{60}Co, ^{137}Cs, and ^{88}Y calibration sources from Amersham and PTB, respectively. For the determination of the activity distribution the image plate system was used, a method based on photo luminescence measurements, allowing for a very high resolution. Details of these measurements can be found in [4].

RESULTS AND DISCUSSION

In Fig.2, the activity distributions of the point source P60 and the area source F320 are shown as examples, determined with the image plate method. While the activity distribution of the point source is similar to the model of a point source, the area source is not distributed as expected, but forms a kind of ring in the peripheric region.

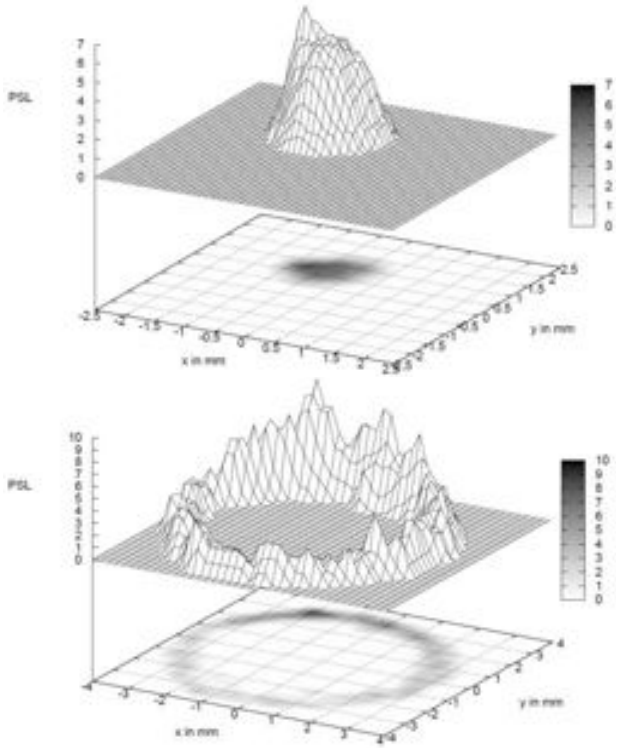

Fig. 2: Image plate pictures for the distribution of ^{44}Ti in the point source P60 (above) and the area source F320 (below); intensity scale is linear.

Table 1 shows the results of the high precicion γ-measurements. The low uncertainties are reached using high-precision calibration sources and correction of the summing effect.

Tab. 1: Measured ^{44}Ti activities

source	activity [Bq]
P-60 (point source)	35.5±0.4
P-160 (point source)	67.5±0.8
P-690 (point source)	498±6
F-130 (area source)	137.1±1.7
F-320 (area source)	225±3

The manufactured calibration sources are applicable for the ongoing activation experiment. However, due to the non-uniform distribution in case of the area source, other sample preparing methods like electro-deposition should be taken into consideration.

REFERENCES

[1] M. Renaud et al., Astrophys. J. Lett. 647, L41 (2006).
[2] L.-S.The et al., Astron. Astrophys. 450, 1037 (2006).
[3] G. Magkosios et al., Astrophys. J. Suppl. Ser. 191, 66 2010.
[4] K. Schmidt, Praktikumsbericht FZD, 2010.

PREPARATION OF A ^{207}Bi CALIBRATION SOURCE FROM IRRADIATED LEAD

D. Schumann, T. Stowasser (PSI), R. Nolte, M. Ehlert (PTB Braunschweig)

About 260 kBq of ^{207}Bi were separated from irradiated lead from the SINQ target 4. The ^{207}Bi serves as a calibration source for γ-spectrometry.

INTRODUCTION

Proton–irradiated lead targets from the SINQ facility represent a unique and valuable pool for the retrieval of rare exotic and expensive radionuclides. Due to the long irradiation time – usually a target is standing in the beam for two years - and the high proton intensity of up to 2.4 mA, high specific activities can be expected.

One of the radionuclides, which are very useful as a calibration source for γ-spectrometry, is ^{207}Bi. With its relatively long half-live of 31.5 ys and three γ-lines up to 1800 keV, it is best-suited for several applications requiring high-energy calibration points. Moreover, from lead as target material, the production of stable Bi is not expected, giving the possibility to produce even carrier-free samples.

In previous works, we determined the radionuclide content of 2 typical samples from the SINQ target 4 [1]. We have found ^{207}Bi activities up to $3 \cdot 10^7$ Bq/g, making the entire project very prospective.

EXPERIMENTAL

Around 10 mg of a lead sample from SINQ target 4 were dissolved in 10 ml 7M HNO_3 and evaporated, till a precipitation of $Pb(NO_3)_2$ occurred. The supernatant solution was decanted and evaporated to dryness. The residue was dissolved in 3M HNO_3 and passed through a lead-specific ion exchange column (Eichrom) in order to remove traces of lead, as described earlier [2]. The eluate was again evaporated and the activity dissolved in 1 M HNO_3. This solution was loaded onto a cation exchange column (DOWEX50x8, 200-400 mesh, H^+ form). Afterwards, the column was washed with 10 ml 1M HNO_3. Then, the Bi-fraction could be eluted with 6 ml 0.4 M HCl. After this treatment, the ^{207}Bi fraction showed only a slight contamination with ^{108m}Ag. In order to remove these impurities, in a final purification step 1mg La was added and concentrated ammonia solution was used to precipitate the hydroxide. Whereas ^{207}Bi was found completely in the precipitate, silver stayed as ammonia complex in solution. To get rid of the lanthanum, the precipitate was dissolved in 1M HNO_3 once more and the purification procedure using the ion exchange column was repeated as described before.

RESULTS AND DISCUSSION

In Fig.1a, the γ-spectrum of the lead sample without any chemical treatment is shown. Besides the desired ^{207}Bi, the main contaminations are ^{172}Lu/^{172}Hf, ^{173}Lu, ^{194}Au/^{194}Hg, ^{102m}Rh, ^{202}Tl/^{202}Pb, $^{58/60}$Co, ^{106}Ru, ^{108m}Ag, ^{125}Sb, ^{133}Ba, and ^{44}Sc/^{44}Ti (not all marked). After the first chemical treatment nearly all other radionuclides with exception of ^{108m}Ag (Fig.1b) are already removed. Silver should in principle stay on the DOWEX50 column, due to the formation of unsoluble AgCl in HCl-containing solution. However, the solubility product of $1.77 \cdot 10^{-10}$ mol^2/l^2 would require an Ag concentration of at least $4.4 \cdot 10^{-9}$ mol/l, which is not reached in carrier free concentration ranges. Therefore, Ag^+ as a singly-charged cation is eluted first from the column together with Bi.

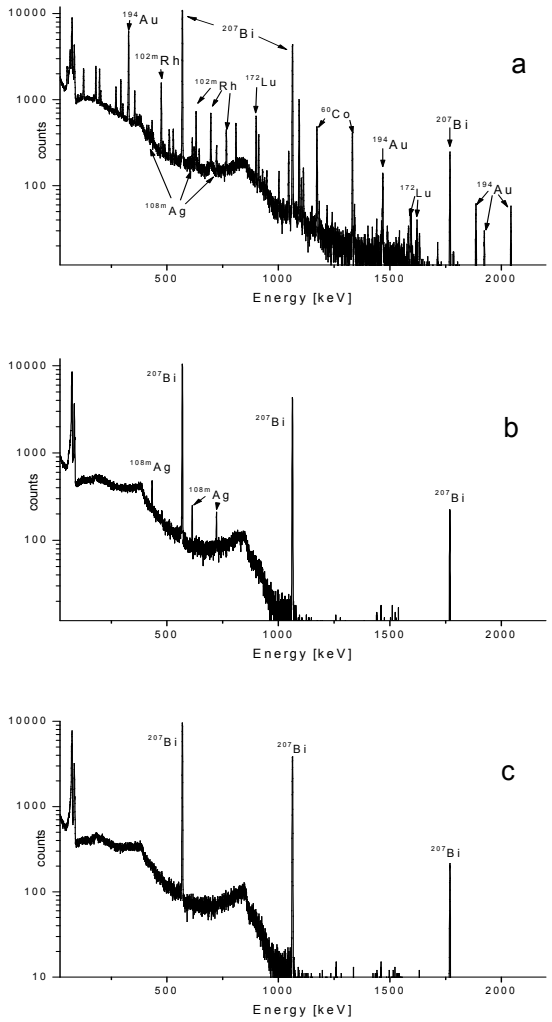

Fig. 1a-c: γ-spectra of the ^{207}Bi sample: a) without chemical treatment, b) after first separation, c) final product.

After the final purification step, also silver had been completely removed. The final sample contains ~260 kBq. With the availability of more sample material from SINQ targets in the near future, we can now think about the establishment of a routine production of such rare and valuable radionuclides.

REFERENCES

[1] D. Schumann et al., Ann. Rep. Lab. of Radio- & Environ. Chemistry, Uni. Bern & PSI (2007), p. 45.

[2] D. Schumann et al., ND2004, Santa Fe, AIP Vo.769, p. 1517.

CONSECUTIVE DETERMINATION OF URANIUM, ^{226}Ra, ^{210}Pb AND ^{210}Po IN SURFACE WATER SAMPLES

M. Ayranov, D. Schumann, R. Dressler (PSI)

A fast procedure for determination of natural uranium and its decay products ^{226}Ra, ^{210}Po, and ^{210}Pb in surface water samples, based on spontaneous deposition co-precipitation and extractive chromatography is presented. The activities of uranium and polonium were determined by low-level alpha spectrometry, and liquid scintillation spectrometry was applied for the determination of radium and lead.

INTRODUCTION

Due to the importance of water for human life, its quality has to be controlled [1]. For the determination of natural uranium and ^{238}U decay products in a variety of water samples, different radiochemical techniques, ion exchange, co-precipitation, electrochemical separation and solvent extraction have been applied [2]. These methods are complicated, time consuming and producing toxic organic wastes. In order to develop simple, fast and sensitive methods for sequential determination of ^{nat}U, ^{226}Ra, ^{210}Po, and ^{210}Pb in water samples, we examined the combination of spontaneous deposition; co-precipitation and extraction chromatography.

EXPERIMENTAL

The radiochemical procedure is presented in figure 1. As the first step, polonium is separated by spontaneous deposition on copper disks. Next, uranium and lead are collected together by co-precipitation with $Fe(OH)_3$ and purified by extraction chromatography, respectively on

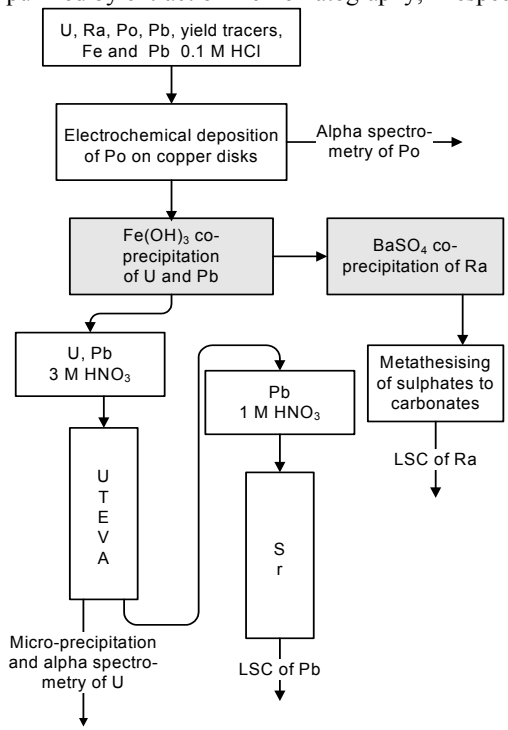

Fig. 1: Radiochemical separation synopsis.

UTEVA and Sr-Spec columns [3]. Separation and determination of ^{210}Pb and ^{210}Po is described in detail elsewhere [4]. Radium remains in the solution after $Fe(OH)_3$ filtering, and is separated by co-precipitation with $BaSO_4$. The sulphate is converted to carbonate and dissolved in 0.1 M HCl. The solution containing ^{226}Ra is directly mixed with the scintillation cocktail OptiPhase HiSafe 3 and measured by LSC (Tri-Carb 3110TR, PerkinElmer). The instrument uses pulse shape analyses technology to separate the alpha spectrum from the beta spectrum. Alpha sources of uranium are prepared by micro-precipitation with NdF_3. The precipitation is collected on 0.1 μm filters (Gelman Sc. Product) and mounted on a stainless steel plate for alpha spectrometry, performed on PIPS detectors (Canberra) with 900 mm^2 active surface.

RESULTS

The minimum detectable activities (LD) for sample sizes of 1000 ml and a chemical yield of 90 % for uranium, 88 % for polonium and 85 % for radium and lead respectively, are presented in Table 1.

Tab. 1: Minimum detectable activities.

Radionuclide	LD, mBq/l
^{238}U	0.2
^{234}U	0.2
^{226}Ra	1.9
^{210}Po	0.2
^{210}Pb	2.5

The method developed was tested by standard addition of different activities to real water samples. The results showed good correspondence between expected and measured values. The proposed method proved to be accurate, reproducible and faster than the commonly used procedures for routine low-level radioactivity control of uranium, radium, lead and polonium in environmental water samples.

REFERENCES

[1] Guidelines for drinking-water quality, 3nd Ed., Vol. 1, World Health Organization, Geneva, 2008.
[2] H. Surbeck, The Sci. Tot. Environ. **173/174**, 91 (1995).
[3] Eichrom Technologies Inc. http://www.eichrom.com/products/tech/
[4] M. Ayranov et al., Ann. Rep. Lab. of Radio- & Environ. Chemistry, Univ. Bern & PSI (2009).

SEPARATION OF GROUP 4 AND 5 ELEMENTS USING EXTRACTION

D. Schumann, S. Lüthi, T. Stowasser (PSI)

The extraction of group 4 and 5 elements into MIBK as model for the behavior of Db and Rf has been studied. Systems are identified allowing for a group 4/5 separation as well as for a differentiation between Nb and Ta.

INTRODUCTION

The discovery of the superheavy elements 115 and 113 in 2003 [1], followed by a confirmation experiment in 2004 [2,3], were important milestones regarding the acceptance of the synthesis of superheavy elements via fusion reactions using a ^{48}Ca beam on actinide targets at JINR (Dubna, Russia). The chemistry experiment [2,3], aimed to identify the atomic number of the long-lived spontaneous fissioning isotope terminating the decay chain as Db (or Rf, in the case that EC decay takes place prior to the terminating SF event) was criticized for two drawbacks: a) α-spectra had not been shown, due to the high β-background circumventing the identification of possible actinide contamination and b) no differentiation between Db and Rf could be made, so that the nature of the terminating isotope and, therewith, the end of the decay chain is eventually unclear [4]. The first problem had been solved by measuring the α-spectra and SF events of a representative sample again 3 years after the experiment and demonstrating the absence of any possible actinide contamination [5]. For the second point, an additional experiment is necessary and proposed here, allowing for a confident assignment of the final decay product either as member of group 4 or 5.

SELECTION OF THE CHEMICAL SYSTEM

The chemical system applied in the "chemistry confirmation experiment" [2] allows for a safe and quick isolation of the members of the groups 4 and 5 together, using precipitation and ion exchange on a cation exchanger from 1 M HF solution. An additional separation step has to be applied to separate these two groups. We have selected liquid-liquid extraction from HF/HCl containing aqueous solutions into methylisobutylketone (MIBK) for several reasons: 1) a quick mixing of the final 1M HF solution containing the isotopes of interest with additional HF and HCl solution is possible to get the necessary start concentration, 2) only one single separation step will be necessary and 3) both fractions can easily be evaporated in order to get samples for α- and SF spectrometry.

EXPERIMENTAL

The isotopes ^{181}Hf, ^{182}Ta, and ^{95}Zr were produced by neutron activation of the stable elements using the NNA-facility at SINQ (PSI). ^{95}Nb is produced as the decay product of ^{95}Zr. Stock solutions containing less than 10^{-6} mol/l of the stable elements, respectively, were prepared in order to simulate low carrier conditions like in the real superheavy element experiments.

Concentration ranges from 0.5-20 M HF and 0-5M HCl were studied by shaking 10 ml of the aqueous solution with up to 10 ml MIBK. The distribution of the radionuclides was determined by γ-spectrometry.

RESULTS AND DISCUSSION

The first aim of the studies was to find conditions where the members of group 4, Zr and Hf, remain in the aqueous solution, and Ta and Nb are completely extracted into the organic phase. Fig.1 shows an example for a suitable extraction system.

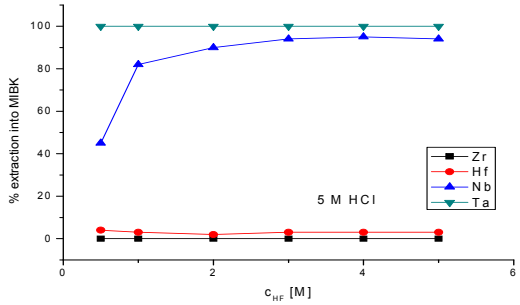

Fig. 1: Extraction behaviour of group 4 and 5 elements into MIBK from 5M HCl solutions containing various amounts of HF.

Earlier experiments studying the chemical properties of Db using the short-lived isotopes $^{262/263}$Db showed similarities more with the lighter homolog Nb than with Ta [6]. The availability of the long-lived ^{268}Db ($T_{1/2}$=36h) allows now to find out, whether this difference is caused by relativistic effects as proposed in [6] or kinetically founded. For this, a system with lower acid concentrations should be selected, where Nb remains in the aqueous phase (see Fig.2), and the time dependence of the distribution has to be studied.

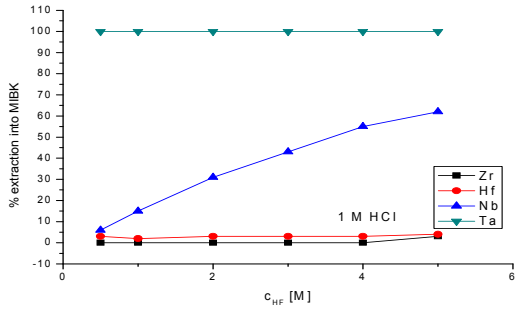

Fig. 2: Extraction behaviour of group 4 and 5 elements into MIBK from 1M HCl solutions containing various amounts of HF.

REFERENCES

[1] Y. T. Oganessian et al., Phys. Rev. C 69, 021601(R) (2004).
[2] S.N. Dmitriev et al., Mendeleev Comm. **15** 1 2005.
[3] D. Schumann et al., Radiochimica Acta **93** 727 2005.
[4] M. Gupta et al., Nuclear Data Sheets 106 (2005) 251–366.
[5] R. Dressler et al., Phys. Rev. C 79, 054605 (2009).
[6] J.V. Kratz et al., Radiochim. Acta 48 (1989) 121.

IRRADIATION-INDUCED MODIFICATION OF DIAMOND COLOURS

R. Dressler (PSI), G. Bosshart (Horgen ZH), R. Eichler, D. Piguet, D. Schumann, A. Vögele (PSI)

The generation of green colour in white diamond using proton and α-particle beams was studied. The color shift of type Ia and type IIa diamonds applying α-particles, protons, neutrons, electrons and γ-quanta is discussed.

INTRODUCTION

The artificial color modification of nearly white diamonds was studied under neutron irradiation using the PNA installation of the SINQ at PSI [1]. During these experiments, typical doses of about 2.3×10^{17}/cm^2 thermal neutrons were applied. However, neutrons with kinetic energy up to 590 MeV are present in addition to thermal ones. Only a small part of these neutrons contribute to the colour modification, because the displacement threshold energy (T_m) to produce permanent vacancies in type IIa diamonds varies from 37.5 eV [100] to 45.0 eV [111] and 47.6 keV [110], depending on the direction of the incident particles relative to the crystallographic directions [2]. For neutrons and protons, these energies correspond to incident kinetic energies (E_{inc}) of 112.5 eV, 135.0 eV, and 142.8 eV, respectively, using the non-relativistic limit of the following equation [3], whereas M denotes the mass of the target atom ^{12}C and m the mass of the incident particle.

$$T_m = \frac{2\cdot m}{M}\cdot\frac{E_{inc}+2\cdot mc^2}{mc^2}\cdot E_{inc} \approx \frac{4\cdot m}{M}\cdot E_{inc}$$

Therefore, the effective neutron-flux for modifications of the diamond color at the PNA station must be estimated using neutron-flux calculations based on the MCNPX transport code [4]. The calculated data of the NAA station compare very well with our experimental results. We assume that the calculations of the PNA station can also be used to estimate the neutron-flux of $E_{inc} > 112.5$ eV. A mean fluence value of 4×10^{16}/cm^2 for this neutron-flux was deduced in the case of the irradiations described in [1].

Here we report on a continuation of these experiments using the proton- and α-particle beams of the PHILLIPS cyclotron at PSI. It is expected, that these particles cause similar vacancies and color alterations in diamonds than neutrons. For protons, E_{inc} will be the same as for neutrons. In the case of α-particles, E_{inc} will be 50.0 eV, 60.0 eV, and 63.5 eV, respectively, due to the four times higher mass.

RESULTS

Different diamonds were exposed during 0.25 h and 14.5 h to the delivered particle beams in the NEC area 1. The primary proton energies used were 50 MeV, 45 MeV, and 25 MeV, respectively, whereas the applied doses varied between 4.7×10^{14}/cm^2 and 1.1×10^{16}/cm^2. A primary beam energy of 75 MeV and applied doses from 1.0×10^{15}/cm^2 to 3.3×10^{15}/cm^2 were used in the case of α-particles. The beams passed a 20 µm Be vacuum window and a 6 mm N_2 cooling gas to save the integrity of the windows foils before entering the crystals.

Fig. 1 shows a diamond irradiated with protons of 25 MeV primary beam energy, additionally degraded with 1.5 mm Al to an entrance-energy of 17 MeV into the crystal. At this energy, the range of protons in diamond is 1.1 mm. The saturation of the green colour increases from the bottom face (the entrance of the beam) and sharply rises into the Bragg peak, visible as an almost black band. This behaviour can be well reproduced using the SRIM-2010 code [5] calculating the vacancy formation density (T_m = 45.0 eV).

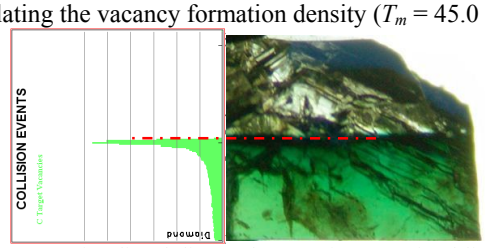

Fig. 1: Proton irradiated diamond PC5-2 in transmitted light. The effective proton energy was 17 MeV and the applied dose 3.0×10^{15}/cm^2. Results of SRIM-2010 calculations are shown for comparison. The position of the Bragg peak is depicted at a penetration depth of 1.1 mm.

Colorimetric analysis of the samples showed small hue differences for the various beam particles but large ones between the two diamond types. A compilation of these results is given in Tab. 1. Prior to irradiation, all samples under investigation were virtually free of natural radiation phenomena and showed either faint yellow hues (type Ia) or near-colourless hues (type IIa). For type Ia diamonds, the hues observed after α-, proton-, and electron-irradiation were located near 550 nm (yellowish-green) whereas for type IIa diamonds the colour shifts are considerably larger than for type Ia stones and the hues accordingly more blue-green (523-497 nm). In the case of neutron irradiations almost identical colours of yellowish-green for both diamond types were observed. Exposures of some samples to intense Bremsstrahlung- and γ–radiation of ^{60}Co (3 MCi at 3.5 m distance) with doses from 9 MGy/cm^2 to 34 MGy/cm^2 at Leoni Studer-Hard, Däniken, did not show any visible colour alterations. GR1 lattice damage, however, was noticed by Raman PL for both X-ray and gamma treatments.

Tab. 1: Diamond hues before and after irradiations.
Average values are enclosed in ‹›-brackets. Wavelengths of 500 nm, 520 nm, and 570 nm correspond to colors of blue-green, green and yellow-green, respectively.

Radiation	Type Ia	Type IIa
	main hues *before* irradiation	
non-irradiated	(573-580) nm	578.3 nm
	main hues *after* irradiation	
α-particles	‹553.5› nm	516.7 nm
neutrons	‹551.8› nm	‹559.6› nm
protons	555.7 nm	523.3 nm
electrons	‹549.2› nm	‹497.0› nm
γ-ray	‹579.3› nm	575.8 nm
X-ray	‹573.9› nm	578.5 nm

REFERENCES

[1] G. Bosshart et al., Ann. Rep. Lab. of Radio- & Environ. Chemistry, Uni. Bern & PSI (2009), p. 52.
[2] J. Koiken, et al., Appl. Phys. Lett. 60 (1992) 1450.
[3] F. Seitz, J.S. Koehler, Prog. Solid State Phys. 2 (1956) 305.
[4] L. Zanini, et al., PSI-Bericht 08-04 ISSN 1019-0643 (2008).
[5] J.F. Ziegler, J.P. Biersack, M.D. Ziegler, ISBN 096542071X

A NEW R&D RADIOPHARMACEUTICAL LABORATORY AT THE INSEL HOSPITAL

K. Zhernosekov (PSI), T. Krause (INSELSPITAL), K. von Bremen, C. Dumas, N. Ceccomancini (SWAN), S. Braccini (Univ. Bern), A. Türler (Univ. Bern & PSI)

The Laboratory for Radiochemistry and Environmental Chemistry (Univ. Bern & PSI) in collaboration with SWAN Isotopen AG is building and equipping a modern research and development laboratory for the small-scale production of radiopharmaceuticals to be launched in 2011.

Ongoing development in radiopharmaceutical science is significantly increasing the potential of nuclear medicine and molecular imaging. Beyond the successful application in nuclear oncology, novel radiopharmaceuticals are intensively involved for clinical research in cardiology and neurology. Long-term, immediate access to commercially unavailable radiotracers is, however, an essential factor for implementation of such innovative clinical trials. Here, in-house production of radiopharmaceuticals represents a key advantage in further clinical research development.

The Laboratoray for Radiochemistry and Environmental Chemistry (LCH) in collaboration with SWAN Isotopen AG is building and equipping a new research and development radiopharmaceutical laboratory on the premises of the INSEL university hospital. SWAN Isotopen AG is an innovative small enterprise responsible for the planning, construction, and management of a professional commercial radioisotope and radiopharmaceutical production in Bern.

Fig. 1: The new building at INSEL university hospital (currently under construction).

The new building (Figure 1) will comprise a production division and new patient wards for nuclear medicine and oncology/palliative medicine. The core of the radionuclides and radiopharmaceuticals production is a multifunctional cyclotron Cyclone® 18/9 by IBA, equipped with an external beam line, which is giving additional flexibility in performance of target irradiations (Figure 2). The machine provides 18 MeV protons and 9 MeV deuterons with current intensities up to 100 and 40 µA, respectively.

Fig. 2: Cyclotron IBA Cyclone® 18/9, fitted with Vectio® external beam line for advanced research.

Besides the commercial production site a modern radiopharmaceutical laboratory of the University of Bern will be setup in the new building, enabling the small-scale production of injectable radiopharmaceuticals for innovative clinical research. There are, however, strict regulations for the preparation of radiopharmaceuticals utilized in clinical trials. The tracers need to be produced according to the current Good Manufacturing Practice (cGMP), whereas handling of the radioactivity involves adherence to regulation on radiation protection. The laboratory will correspond to class B radiation protection standards, while ensuring high air quality of grade C environment (clean room). Configuration of the facility is supposed to provide maximum flexibility and multifunctionality for handling a variety of diagnostic and therapeutic radionuclides and carrying out radiochemical and radiolabeling processes under GMP-conditions. For these tasks up-to-date shielded workstations (hot cells) with a grade C to A rating were purchased from Tema Sinergie (Faenza, Italy) for the laboratory layout (Figure 3).

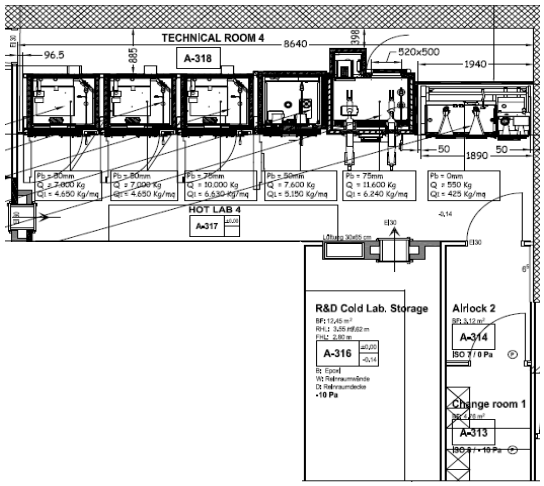

Fig. 3: The laboratory layout. Six workstations are integrated into the clean room. The laboratory links to personnel airlock and a small QC/ storage room.

Four multifunctional research hot cells and a dedicated hot cell for aseptic processing and dispensing of the injectable radiopharmaceuticals will be installed. In addition, a sterile isolator is suitable for processing of microbiologically hazardous samples or for the aseptic preparation of inactive solutions and precursors. The radionuclides for radiolabeling reactions are supposed to be produced by irradiation of liquid and solid targets at the in-house cyclotron or at external facilities as well as by radionuclide generator systems. The new radiopharmaceuticals laboratory will be launched in 2011.

PRODUCTION OF ^{161}Tb IN QUALITY AND QUANTITY SUITABLE FOR MEDICAL APPLICATIONS

H.J. Dorrer (Univ. Bern & PSI), K. Zhernosekov (PSI), U. Köster (ILL), A. Hohn (PSI), R. Schibli (ETHZ & PSI), A. Türler (Univ. Bern & PSI)

The novel therapeutic radionuclide ^{161}Tb was produced with quality and in quantities necessary for preparation of ^{161}Tb-radiopharmaceuticals. The radionuclide could be effectively isolated from massive ^{160}Gd-targets by means of cation exchange chromatography. The method is the basis for further development of ^{161}Tb-labeled radiopharmaceuticals.

INTRODUCTION

^{161}Tb is due to its physical and chemical properties a promising candidate for targeted radionuclide therapy in nuclear oncology. It emits low energy β^--particles and additionally a significant amount of conversion- and Auger electrons, providing high energy transfer to a small volume. Thus, a high therapeutic effect of this radiolanthanide can be expected. ^{161}Tb also emits low-energy γ-photons which are suitable for imaging purposes by means of a gamma camera. The radionuclide is supposed to be applied for radiolabeling of biomolecules such as peptides, antibodies or vitamins and must be produced with high specific activity, chemical and radiochemical purity [1, 2].

EXPERIMENTAL

Up to 15 mg of highly enriched ^{160}Gd (98.2 %) were irradiated at the high flux reactor at ILL (Grenoble, France), with a thermal neutron flux of $8 \cdot 10^{14}$ cm^{-2}s^{-1} for 7 days, resulting in up to 20 GBq ^{161}Tb at EOB. After about 10 days cooling and transport period the irradiated samples were transported to PSI.

The isolation of ^{161}Tb from the massive ^{160}Gd-target was performed on a chromatographic column of 300 x 9 mm dimension, filled with a strong acidic cation exchange resin in its NH_4^+-form. The irradiated target material was dissolved and loaded on the column. The separation was performed by isocratic elution of the column with α-HIBA (α- hydroxyisobutyric acid) solutions adjusted with ammonia to pH = 4.75. The ^{161}Tb was obtained in about 10 ml of the eluent. This fraction was mixed with 2 ml of 1 M HCl solution and loaded on a secondary cation exchange column of 12 x 5 mm dimensions. The column was finally stripped with 4 ml 4 M HCl. The obtained fraction of radioactivity was evaporated under nitrogen flow to dryness and redissolved in 300 µl of 0.04 M HCl.

For evaluation of the preparations quality the radionuclide was used for radiolabeling of peptide DOTA-Tyr3-octreotate (DOTATATE). Up to 200 MBq ^{161}Tb and 1.4 to 5.6 nmol of DOTATATE were used for radiolabeling reaction. The reaction mixtures (65 µl total volume, pH 4.5) were incubated at 95 °C for 30 minutes. The radiolabeling yield was monitored by HPLC. The product was additionally analyzed by means of LC-ESI-TOF.

RESULTS AND DISCUSSION

The developed one-step column separation of ^{161}Tb(III)/Gd(III) allows obtaining not less than 90 % of the radionuclide with the content of the target material reduced by a factor of at least 10^6 (Figure 1).

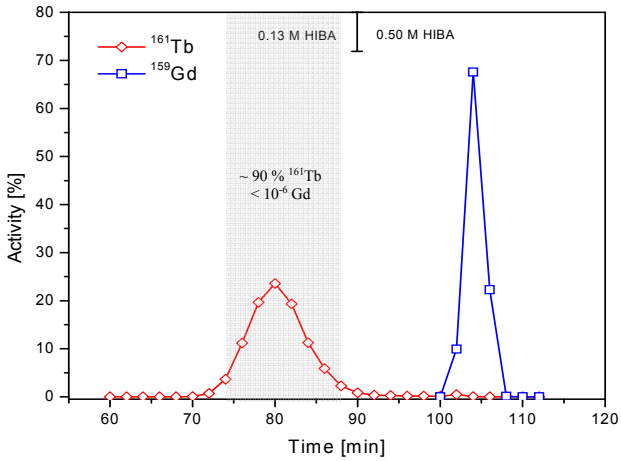

Fig. 1: Model processing of 20 mg Gd-target on the chromatographic column.

Based on the strategy, a semi-automated procedure was installed in a hot cell, where it allows an effective processing of high active targets within one day only.

Up to 7 GBq ^{161}Tb (dose useful for therapeutic applications) could be produced at PSI. The radionuclide was successfully utilized in radiolabeling reactions. Thus ^{161}Tb-DOTA-peptide could be prepared with > 98 % labeling yield and specific activity, corresponding to a ^{161}Tb to the tracer molar ratio of 1:10. LC-ESI-TOF mass spectrometry allowed identification of the ^{161}Tb-DOTATATE and detection of only minor levels of general metallic impurities such as Zn(II) and Fe(III), finally evidencing the high quality of the ^{161}Tb preparations obtained.

CONCLUSIONS

We established an efficient method for production of ^{161}Tb at PSI. The availability of the radionuclide with high quality provides the basis for the development of novel therapeutic ^{161}Tb-radiopharmaceuticals.

ACKNOWLEDGEMENTS

This work was supported by the Swiss South African Joint Research Programme (SSAJRP). We thank Ernst Schaub and Walter Hirzel for technical support and Alexander Voegele for irradiations of samples at SINQ.

REFERENCES

[1] S. Lehenberger et al., article submitted in 2010.
[2] National Nuclear Data Center, http://www.nndc.bnl.gov/.

^{14}C SOURCE APPORTIONMENT OF DICARBOXYLIC ACIDS AND HUMIC-LIKE SUBSTANCES IN ATMOSPHERIC AEROSOLS

S. Fahrni (Univ. Bern & PSI), S. Szidat, E. Vogel (Univ. Bern), L. Wacker (ETHZ), M. Rzaca, H. Puxbaum, H. Bauer (TU Wien)

Dicarboxylic acids, such as oxalic acid, and humic-like substances (HULIS) are important constituents of atmospheric aerosols due their abundance and their ability to influence cloud condensation processes. In order to quantify the contributions of fossil vs. biogenic and biomass-burning contributions, we applied specific radiocarbon (^{14}C) analysis to oxalic acid and HULIS. The results emphasize the importance of biomass burning particularly during winter but also contributions of fossil sources to these compounds.

INTRODUCTION

Dicarboxylic acids (DCAs) in carbonaceous aerosols have received great attention in the last decades [1]. The research on these compounds is strongly motivated by their hydrophilicity, which is related to the ability to influence cloud condensation processes. Through their abundance in continental as well as in marine air and their influence on the cloud formation, DCAs play a role in the global radiation balance. Another interesting fraction of carbonaceous particles comprises the compound class of humic-like substances (HULIS). This fraction contributes greatly to the total mass of carbonaceous aerosols as it was found to account for 20–50% of the organic carbon fraction [2]. HULIS are interesting due to their mere abundance as well as their ability to influence cloud formation. Even though DCAs and HULIS were studied extensively in many studies, a clear attribution to the sources was not possible yet, as correlations with atmospheric tracers allowed only qualitative and semi-quantitative source apportionment.

In order to provide quantitative information on sources of both DCAs as well as HULIS, ^{14}C source apportionment is a promising method: carbon from fossil, i.e. radiocarbon-free sources is distinguished from carbon of biogenic and biomass-burning emissions, which are on the contemporary radiocarbon level.

EXPERIMENTAL

The method for the separation of DCAs comprises water extraction and preparative 2D-chromatography by means of ion chromatography and HPLC separation [3].

Separation of HULIS samples was performed at the technical University of Vienna with a method developed by Limbeck et al. [4]. Filters were extracted with 0.1 N NaOH and acidified to enable their retention on a solid phase extraction column. HULIS were eluted from the column with methanol and eluates were mixed with diluted nitric acid. Then the solutions were loaded onto a strong anion exchange column and eluted with diluted ammonia. These fractions were collected in PFA vials and were transported to the University of Bern for further processing. The aqueous solutions were concentrated under a flow of nitrogen and concentrated HULIS solutions were transferred to clean quartz vessels. The concentrates were dried and resuspended with 1 M HCl in order to remove carbonates. Hydrochloric acid was dried as well and samples were ready for combustion.

Samples from both, DCAs and HULIS, were combusted and ^{14}C was analyzed in the resulting CO_2 with the gas feeding system at the small accelerator mass spectrometry facility MICADAS at ETH Zürich.

RESULTS

A first set of radiocarbon values was generated from highly loaded aerosol filters (Figure 1). DCAs other than oxalic acid were not yet measured as the carbon amount of the less abundant compounds was not found to be sufficient for ^{14}C measurements. First results on oxalic acid show a generally higher non-fossil contribution to this compound than for the organic carbon (OC) fraction. The main findings for HULIS suggest residential wood heating as the major source of this compound class during winter. Slightly higher fossil contributions are observed during summer.

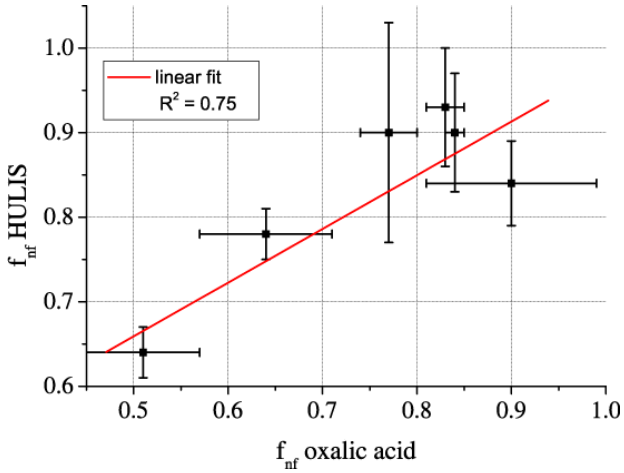

Fig. 1: A small set of data for radiocarbon results from OC, oxalic acid and HULIS.

A significant correlation between the non-fossil fractions (f_{nf}) of oxalic acid and HULIS was found, indicating common sources. A combination with other techniques such as aerosol mass spectrometry measurements and a determination of levoglucosan may help to subdivide non-fossil contributions further into biogenic and biomass burning contributions.

REFERENCES

[1] K. Kawamura & I. Kaplan, Environ. Sci. Technol., **21**, 105-110 (1987).
[2] S. Zappoli et al., Atmos. Environ., **33**, 2733–2743 (1999).
[3] S.M. Fahrni et al., Radiocarbon, **52**, 752-760 (2010).
[4] A. Limbeck et al., Anal. Chem., **77**, 7288-7293 (2005).

IMPROVING A GAS ION SOURCE FOR ^{14}C AMS

S. Fahrni (Univ. Bern & PSI), L. Wacker, H.-A. Synal (ETHZ), S. Szidat (Univ. Bern)

For more than 4 years, gaseous samples of 1 to 50 µg carbon have been routinely measured with the gas ion source of the small AMS (Accelerator Mass Spectrometer) facility MICADAS at ETH Zurich. The applied measurement technique offers a simple and fast way of ^{14}C measurements without the need of sample graphitization. A major drawback of gaseous ^{14}C measurements, however, is the relatively low negative ion current in comparison to graphitized samples. This results in longer measurement times and lower precision. In December 2009, we installed a new, improved Cs sputter ion source at MICADAS and began to optimize conditions for the measurement of gaseous samples. With the improved settings, higher precision and faster measurements have been achieved.

INTRODUCTION

Common sample sizes in ^{14}C AMS range from a few milligrams down to about 100 micrograms of carbon. The vast majority of samples for radiocarbon measurements with accelerator mass spectrometry are converted to graphite as this material offers high negative ion yields and high currents [1]. In the graphitization of small (<100 µg) and especially of ultra-small (<10 µg) samples, however, problems arise due to the increasing influence of contaminations and unreliable outcomes of the graphitization reaction [2]. In order to circumvent the graphitization of samples in this low size range, Ruff et al. set up a CO_2 feeding system for the AMS facility MICADAS [3]. Measurements with gaseous samples of 2 to 50 µg C were established and many users have measured their samples with this gas handling system. The relatively low ionization yield and the resulting low negative ion currents, however, limited the quality of the measurements in comparison to graphitized samples. With a new ion source installed at MICADAS, tests were conducted in order to improve the performance of gaseous measurements.

EXPERIMENTAL

In order to improve the performance of ^{14}C analysis of small samples, settings at the ion source and at the gas handling system were systematically checked for their effect on the ionization and C^- currents.

RESULTS

Significantly higher negative ion currents were achieved in the course of the improvements. From initially 3 µA, C^- currents were increased up to 12-15 µA for average samples. Figure 1 shows that higher C^- currents and faster measurements depend crucially on the increased heating of the cesium reservoir to higher temperatures, which intensifies the sputtering of the target with Cs^+ ions. Average ionization yields of gas samples were increased by a factor of 2 and are now in the range of 8% for average samples. This is comparable to the approximately 10% ionization yield achieved with larger graphite targets at MICADAS in normal operation. Additionally, a higher flow of helium as a CO_2 carrier and a few modifications at the ion source allowed to strongly increase the yield of samples in the low microgram range.

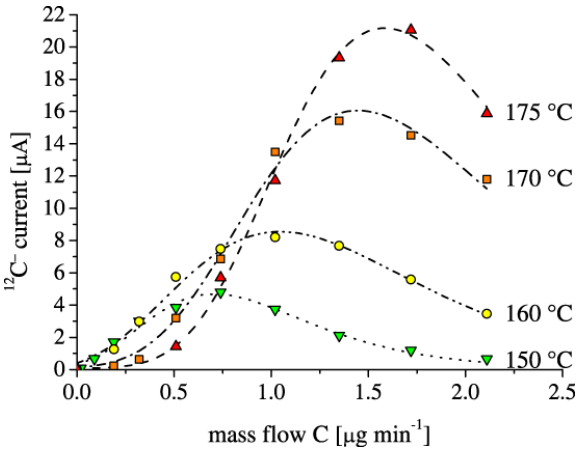

Fig. 1: Currents and ionization yields depending on the carbon mass flow rate and the Cs reservoir temperature.

Furthermore, it is now possible to double the sample throughput with the new conditions. This was achieved by a higher carbon mass flow, shorter target cleaning before the measurements and through an automated and software-controlled handling of samples. An example of a resulting measurement course is illustrated in Figure 2.

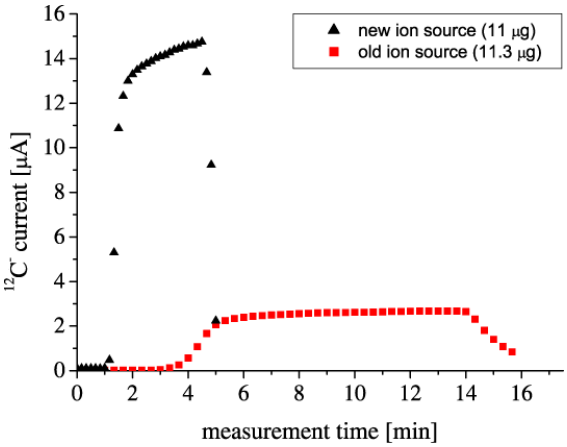

Fig. 2: Current courses before (red squares) and after the improvements (black triangles).

REFERENCES

[1] J. Southon and G. M. Santos, NIMB **259**, 88-93 (2007).
[2] R. Drosg et al., NIMB, **259**, 340-344 (2007).
[3] M. Ruff et al., Radiocarbon **49**, 307–314 (2007).

CAN 3-D MODELS EXPLAIN THE OBSERVED FRACTIONS OF FOSSIL AND NON-FOSSIL CARBON IN AND NEAR MEXICO CITY?

A. Hodzic, S. Madronich, J.L. Jimenez (Univ. Colorado), J.D. Fast (PNNL), A.S.H. Prévôt (PSI/LAC), S. Szidat (Univ. Bern)

The 3-D model simulations have been applied to the Mexico City metropolitan area during March 2006 and compared with aerosol ^{14}C and aerosol mass spectrometry measurements to investigate the origin of elevated levels of non-fossil carbon aerosols observed in this urban area.

INTRODUCTION

Organic aerosols (OA), composed of a complex mixture of primary (POA, emitted in the particle phase) and secondary (SOA, formed due to chemical reactions of organic vapors) compounds, account for a large fraction of the submicron particulate mass [1]. Despite their ubiquity, the sources and formation processes of OA are still largely controversial with major consequences on our ability to predict and regulate OA levels. Over the past several decades radiocarbon analyses have provided insights into the relative contribution of fossil (index "f") and non-fossil (index: "nf") sources of carbonaceous aerosols at different locations by measuring the ^{14}C in ambient aerosol samples [2]. Receptor modeling based on aerosol mass spectrometry is another source-attribution approach, which distinguishes hydrogenated and oxygenated OA (HOA and OOA, respectively) aiming at an experimental separation of POA and SOA [3]. In this work, both approaches are applied in combination and compared to 3-D chemistry-transport model results for the Mexico City metropolitan area [1] to investigate the origin of elevated levels of non-fossil carbonaceous aerosols in this highly urbanized region.

METHODS

Aerosol samples from quartz fiber filters were analyzed for ^{14}C content and, simultaneously, aerosol mass spectrometry data were acquired during March 2006 at an urban location in Mexico City [4]. Additionally, the mesoscale chemical transport model CHIMERE was run over the Mexico City region at both regional (35×35 km^2) and urban (5×5 km^2) grid scales [1] using the SOA formation concept of [5].

RESULTS

Using the 3-D model, concentrations of POA, SOA, and primary biological aerosol particles (PBAP) were calculated for fossil and non-fossil sources considering urban (urb), biomass-burning (BB), and biogenic (biog) emissions. This dataset was compared to ^{14}C and aerosol mass spectrometry measurements for episodes of low and high biomass-burning contribution (Fig. 1). Measurement results indicate that biomass burning organic aerosol represents about 5 and 18% of OA during low and high biomass burning, respectively. According to this method, the estimated fraction of non-fossil OOA accounts for ~35% of the OA and it is larger than the fossil fraction (8-12%). Primary organic species (HOA) from fossil fuel burning represents about 30%.

Model predictions show a somewhat different OA apportionment. The main difference is the larger proportion of fossil secondary organics (25-30%), with a 15% higher model prediction, whereas the non-fossil fraction is about 5-10% lower in the model. The amount of primary organic aerosols from fossil and non-fossil sources is close to the observations. The discrepancies between observation and simulation are subject to further investigation.

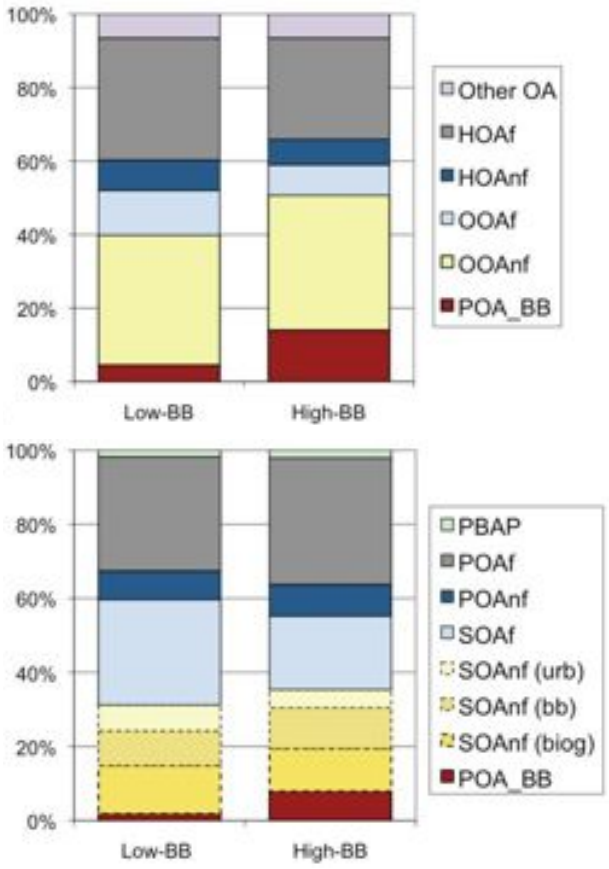

Fig. 1: Source-specific contributions to organic PM10 aerosols at Mexico City as derived from the combination of ^{14}C and aerosol mass spectrometry measurements (top) and as predicted by model simulation (bottom) [1].

REFERENCES

[1] A. Hodzic et al., Atmos. Chem. Phys., **10**, 10997 (2010).
[2] S. Szidat, Chimia, **63**, 157 (2009).
[3] N.L Ng et al., Atmos. Chem. Phys., **10**, 4625 (2010).
[4] A.C. Aiken et al., Atmos. Chem. Phys., **10**, 5315 (2010).
[5] A.L. Robinson et al., Science, **315**, 1259 (2007).

THE OC/EC ANALYZER SUNSET: A NEW SAMPLE PREPARATION SYSTEM FOR THE ^{14}C DETERMINATION IN DIFFERENT FRACTIONS OF AEROSOLS

Y.L. Zhang (Univ. Bern & PSI), N. Perron, A.S.H. Prevot (PSI/LAC), L. Wacker (ETHZ), S. Szidat (Univ. Bern)

$^{14}C/^{12}C$ values of carbonaceous aerosol particles give a unique and absolute measure of the contemporary-to-fossil carbon source ratio, which can be used for apportionment of biogenic and anthropogenic emissions. Here, we present a new sample preparation system by connecting a commercial OC/EC analyzer with cryogenic traps. The final goal is to achieve an optimized thermal method for the isolation of EC and OC for ^{14}C measurements

The carbonaceous aerosol (total carbon, TC), which comprises the large fractions of elemental carbon (EC) and organic carbon (OC), badly affects climate and human health [1]. However, there is a large uncertainty about detailed apportionment and quantification of its sources due to the vast number of origins and chemical compounds associated with aerosols. Radiocarbon measurements have proved to be a useful isotopic tracer for distinguishing contemporary and non-fossil emissions [2, 3].

Since OC and EC are influenced by very different sources [3], this method requires a clear separation of both fractions, which is not trivial. On the one hand, some thermal unstable OC compounds may char during the combustion at low temperature, which will produce additional, apparent EC. On the other hand, some non-refractory EC may be removed prematurely together with recalcitrant OC at intermediate temperature. As a result, the ^{14}C measurement of EC may then be biased.

Thus, a major improvement in sample preparation is necessary. In order evaluate the extent of charring during analysis, we performed sample preparation with a new commercial Sunset thermo-optical OC/EC Analyzer. This instrument is dedicated for laboratory analysis and equipped with a NDIR CO_2 detector. It monitors the optical properties of the filters by a 660-nm tuned-diode laser during the thermal treatment. The gas flow parameters of the thermo-optical OC/EC Analyzer Sunset were adjusted and stabilized to 65 mL/min of pure O_2. CO_2 resulting from the sample analysis is collected in previously designed cryogenic traps [4] after quantification by the NDIR cell. The set-up is sketched in Fig.1.

As the major advantage compared to the previous setup [4], the Sunset OC/EC Analyzer allows online optical monitoring of the filters during analysis. Charring was significantly reduced to less than 5% when analyzing the water-extracted filters under pure O_2 for summer and winter filters from Gothenburg (Sweden), Moleno, and Zurich (Switzerland).

A four-step O_2 method was developed in order to isolate pure EC and OC for ^{14}C measurement [5]. This procedure was proven to be optimized for summer filters yielding more than 70% pure EC for ^{14}C measurements. However, it is not possible to achieve a quantitative separation of OC and EC for some winter filters, as the more refractory fraction of OC (or brown carbon) and wood-burning EC often have similar properties [1].

In the future, the thermal program of the Sunset Analyzer will be investigated on a variety of filters from different campaigns to find out the best method for OC/EC separation for ^{14}C measurement.

REFERENCES

[1] U. Pöschl, Angew. Chem. Int. Ed., **44**, 7520-7540 (2005).
[2] L.A. Currie, Radiocarbon, **42**, 115-126 (2000).
[3] S. Szidat et al., Atmos. Chem. Phys., **9**, 1521-1535 (2009).
[4] S. Szidat et al., Nucl. Instr. Meth. Phys. Res B, **223-224**, 829-836 (2004).
[5] N. Perron, Radiocarbon-supported source apportionment of carbonaceous aerosols, PhD thesis, Univ. Bern (2010).

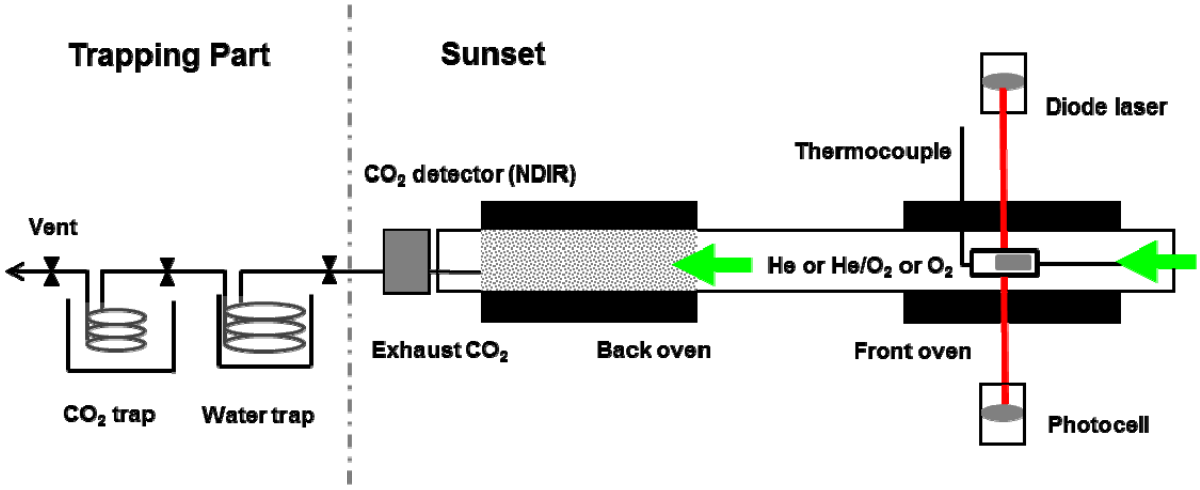

Fig. 1: A new sample preparation system by coupling a commercial Sunset OC/EC Analyzer with cryogenic traps.

A NEW ^{14}C AMS LABORATORY AT THE UNIVERSITY OF BERN

S. Szidat (Univ. Bern), M. Schwikowski, A. Türler (Univ. Bern & PSI), T. Stocker, M. Leuenberger (KUP, Univ. Bern), M. Grosjean (OCCR, Univ. Bern), W. Zeller (BAG)

Precise determinations of the radionuclide ^{14}C have widespread applications in many branches of natural sciences, ranging from geochemistry, archeology, and climate science to biomedical and pharmacological applications. In order to strengthen ^{14}C-based research in our laboratory and at the University of Bern in general, an accelerator mass spectrometry (AMS) system MICADAS will be installed on site.

Radiocarbon (^{14}C) is a long-lived radioisotope with many scientific applications. The University of Bern has a long history of experience in precise ^{14}C measurements based on the conventional counting laboratory founded by Hans Oeschger more than 50 years ago [1]. Due to the demanding procedure involved in preparing the counting gas from the organic samples and to the long counting time to obtain reliable statistics, the throughput and required carbon mass of this technique both are the limiting factors. Because the University of Bern decided to continue the high-precision ^{14}C studies, an update of the facility is urgently needed accommodating an increasing number of ^{14}C measurements requested by the various institutes or their collaborators.

During the last two decades, enormous technical development on accelerator mass spectrometry (AMS) has been achieved with the breakthrough of the small instrument MICADAS by ETH Zurich [2]. This small unit (see Fig. 1) can readily compete with the conventional counting method regarding precision but is significantly superior regarding its low requirements of sample amounts and process time [3]. Therefore, we will establish a new ^{14}C laboratory at the University of Bern based on the AMS technique. For this, a dedicated MICADAS instrument will be set up in collaboration with ETH Zurich. It shall become operational at Bern in 2012.

This ^{14}C laboratory will focus on the development of hyphenated analytical systems [4], the source apportionment of carbonaceous particles [5], and dating of mid-latitude glacier ice [6] within the Laboratory of Radiochemistry and Environmental Chemistry. Furthermore, the ^{14}C laboratory will become available to ^{14}C applications of climate-change research within the Oeschger Centre. Moreover, it will be open to analytical service measurements.

ACKNOWLEDGEMENTS

Funding of the following institutions is acknowledged: Swiss National Science Foundation (project 206021_133817), Swiss Federal Office of Public Health (BAG), and University of Bern (contributing parties: the University Board of Directors, the Department of Chemistry and Biochemistry, and the Oeschger Centre for Climate Change Research). We are very grateful to the Laboratory of Ion Beam Physics at ETH Zurich for collaboration with the installation of MICADAS.

REFERENCES

[1] F.G. Houtermans and H. Oeschger, Helv. Phys. Acta, **31**, 117-126 (1958).
[2] H.-A. Synal et al., Nucl. Instrum. Meth. Phys. Res. B, **259**, 7-13 (2007).
[3] H.-A. Synal and L. Wacker, Nucl. Instrum. Meth. Phys. Res. B, **268**, 701-707 (2010).
[4] N. Perron et al., Radiocarbon, **52**, 761-768 (2010).
[5] S. Szidat, Chimia, **63**, 157-161 (2009).
[6] M. Sigl et al., J. Glaciol., **55**, 985-996 (2009).

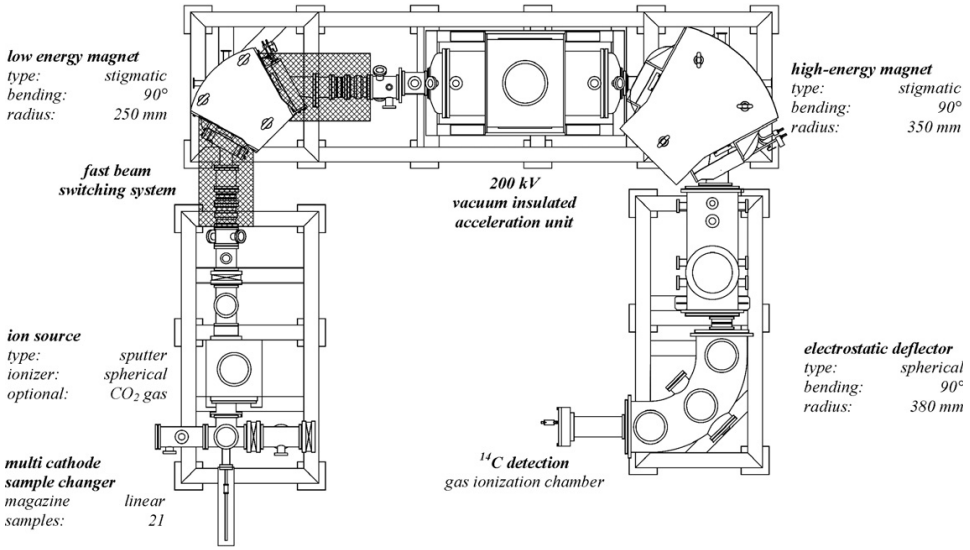

Fig. 1: The layout of the ^{14}C AMS system MICADAS [2] as it will be installed at the University of Bern.

^{210}Pb DATING OF THE Mt. HUTTON ICE CORE FROM NEW ZEALAND

H.W. Gäggeler, L. Tobler (PSI), S. Szidat, E. Vogel (Univ. Bern), U. Morgenstern, J. Thomson, K. McBeth, N. Bertler (GNS Science, Lower Hutt, New Zealanad), B. Anderson, A. Mackintosh, L. Kees (Victoria Univ. Wellington, New Zealand), P. Mayewski, D. Dixon (Univ. Maine, USA), S. Kang, X. Gao, Y. Zhang (Institute of Tibetian Plateau Research, Beijing, China)

^{210}Pb activitiy concentrations were measured along an ice core retrieved in June 2009 from a glacier in New Zealand. Except for the uppermost snow layer, the entire core consisted of solid ice. The measured very low and constant background values of ^{210}Pb suggests for the ice an age of more than 168 years.

INTRODUCTION

Glaciers in New Zealand are temperate and it is not clear whether they are suited as archive of air constituents that serve as climate indicators (e.g. sulphate) or as proxy of past temperatures e.g via δ^{18}O. However, given the fact that there are very few ice archives in the Southern Hemisphere (besides Antarctica) a reconnaissance study was performed in Aoraki Mt. Cook National Park and three firn/ice cores drilled in 2009.

The Mt. Hutton core (43.60559S¸170.38971E; 2760 m asl;; length 33.3 m) was drilled on June 26, 2009 and reached bedrock. The drill site is on the Eastern slope of the N-S oriented mountain chain, known to have a very strong W-E negative gradient in precipitation rates. This core is expected to indicate the integrity of ice as a climate archive in the Southern Alps. The site is very exposed with cold basal ice. Immediately below this year's winter snow solid ice was found, without a gradual firn-ice transition. Therefore, it is likely that this core is not a continuous record and that at least the recent years are missing.

EXPERIMENTAL

1m long segments were melted at GNS, the liquid samples acidified with 20 mL HCl_{conc}. 2 g of $NH_4OH.HCl$ was added as well as 80 µL ^{209}Po tracer. Deposition of Po on 15 mm Ag discs immersed in the liquid was achieved during approx. 8 hours at 95 °C in 0.5 L Erlenmeyer flasks using a magnetic stirrer. Then, the Ag discs were transferred to Bern University for α-counting. The ^{210}Pb activity concentrations were deduced from the measured ^{210}Po activities via its 5.3 MeV α-line assuming secular equilibrium (which may not have been reached for the uppermost sample yet) and taking into account the chemical yield deduced from the ^{209}Po tracer. The described separation procedures deviates from that applied at Bern University for many years [1].

RESULTS

The uppermost snow layer contained a ^{210}Pb activity concentration of 132 mBq/L. Below the snow layer, all ^{210}Pb activity concentrations of the ice samples were constant with an average value of 0.72 mBq/L, except for the lowermost sample with an increased value of 5.9 mBq/L (Fig. 1), possibly caused by high amounts of mineral dust close to bedrock (supported ^{210}Pb). Samples from 13 to 23 m were not analysed.

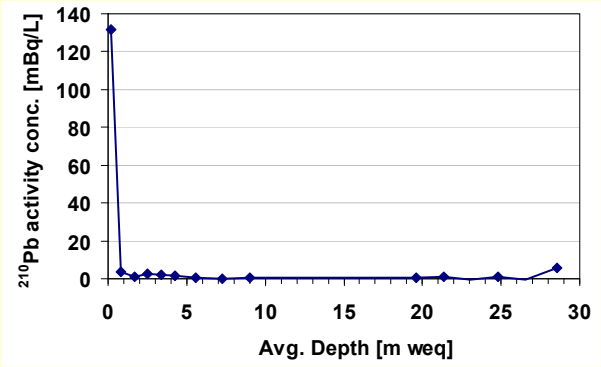

Fig. 1: ^{210}Pb activity concentrations measured along the Mt. Hutton core.

No increased ^{210}Pb activity concentrations were found throughout the core at e.g. minor dirt layers (as is usually observed at temperate glaciers in the European Alps [1])

If the drop of the ^{210}Pb activity concentration between the uppermost snow layer and the ice is assumed to be caused by radioactive decay only, then a minimum age of 168 years results for the ice.

It would therefore be highly desirable to analyze the ice body with a technique able to date ice of higher age: such a technique exists with the measurement of ^{14}C contained in aerosol samples scavenged by snow precipitation from the atmosphere [2].

ACKNOWLEDGEMENTS

Support during the experimental work at GNS by Bob Ditchburn and Roger Tremain is highly appreciated. H.G. acknowledges the hospitality at GNS by Alex Malahoff.

REFERENCES

[1] H.R. von Gunten, E. Rössler, H.W. Gäggeler, Z. Gletscherkunde und Glazialgeologie, **18**, 37 (1982).

[2] T.M. Jenk, S. Szidat, D. Bolius, M. Sigl, H.W. Gäggeler, L. Wacker, M. Ruff, C. Barbante, C.F. Boutron, M. Schwikowski, J. Geophys. Res. **114**, D14305 (2009).

^{210}Pb DATING OF THE BAKER AND ANNETTE ICE CORES FROM NEW ZEALAND

H.W. Gäggeler, L. Tobler (PSI), S. Szidat, E. Vogel (Univ. Bern), U. Morgenstern, J. Thomson, K. McBeth, N. Bertler (GNS Science, Lower Hutt, New Zealanad), B. Anderson, A. Mackintosh, L. Kees (Victoria Univ. Wellington, New Zealand), P. Mayewski, D. Dixon (Univ. Maine, USA), S. Kang, X. Gao, Y. Zhang (Institute of Tibetian Plateau Research, Beijing, China)

^{210}Pb activity concentrations of two firn/ice cores were measured which were retrieved in 2009 from glaciers in New Zealand. The ^{210} Pb activity concentrations along the Baker and the Annette cores exhibit roughly exponential decay resulting in unexpected low accumulation rates of 33 and 22 cm w.eq./year, respectively. On the other hand, the surface ^{210}Pb activity concentrations are unexpectedly high with values of 172 and 184 mBq/L, respectively.

INTRODUCTION

As outlined in [1], a reconnaissance study was performed in 2009 to explore the potential of New Zealand glaciers as climate archive. This study describes the dating of two firn/ice cores drilled on the Annette plateau and on the Baker glacier field at Aoraki Mt. Cook National Park.

THE ANNETTE CORE

On 16 June 2009 a 44.5 m deep drill was performed until a water conduit was intercepted which filled the borehole up to a level of 13 m. The site is at an elevation of only 2220 m asl at 43.75385S/170.0572E, very wind exposed and has a glacier thickness of c. 100 m.
The samples were processed and analyzed as described in [1]. The measured ^{210}Pb activity concentrations are depicted in Fig. 1 reflecting an exponential decrease, which is surprising given the very temperate nature of the glacier. The surface activity concentration amounts to 184 mBq/L, the accumulation rate to only 22 cm w.eq./y. The age at a depth of 44.5 m (=36.9 m w.eq.) is 1841 assuming that the exponential decrease is due the decay of ^{210}Pb.

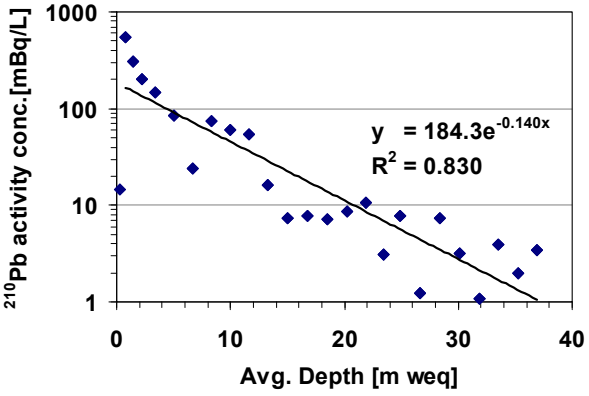

Fig. 1: ^{210}Pb activity concentrations along a firn/ice core from the Annette plateau.

THE BAKER CORE

On 30 June 2009 a 30.7 m core was drilled at 2360 m asl and 43.57248S/170.31552E. This site has a low exposure to the sun. Through the top 30 m we surprisingly obtained very good quality firn/ice, dry and cold, with a gradual firn-ice transition between about 15 and 20 m. No significant meltlayers were visible. At 30 m, however, we encountered wet layers and stopped drilling.
Fig. 2 depicts the density profile underlying the good quality of the core. Fig. 3 shows the ^{210}Pb activity concentrations which nicely reflect an exponential decrease. The surface activity is 172 mBq/L; the accumulation rate 33 cm m w.eq./y. The age at the bottom of the 30.7 m long core (=22.48 m w.eq.) is 1943 assuming that the observed decrease is due to the radioactive decay of ^{210}Pb only.

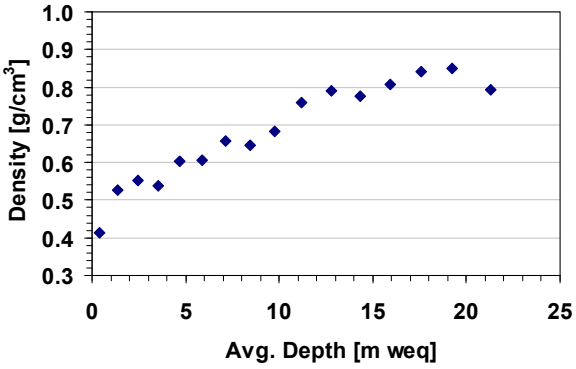

Fig. 2: Density (in g/cm^3) profile along the Baker core (in m w.eq.).

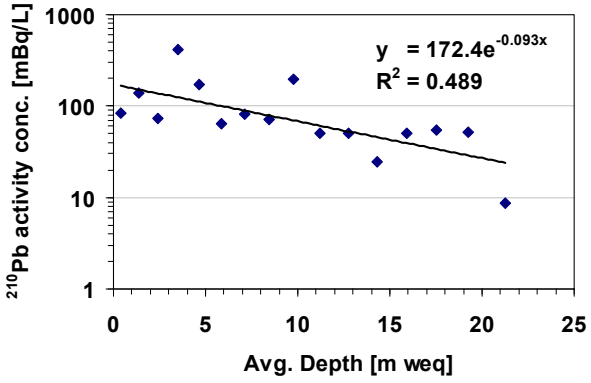

Fig. 3: ^{210}Pb activity concentrations from the Baker core.

REFERENCE

[1] H.W. Gäggeler et al., this report, p. 64.

LIST OF PUBLICATIONS

HEAVY ELEMENTS

L.-L. Andersson, D. Rudolph, P. Golubev, R.-D. Herzberg, R. Hoischen, E. Merchán, D. Ackermann, Ch.E. Düllmann, K. Eberhardt, J. Even, J. Gerl, F.P. Heßberger, E. Jäger, J. Khuyagbaatar, I. Kojouharov, J.V. Kratz, J. Krier, N. Kurz, W. Prokopowicz, M. Schädel, H. Schaffner, B. Schausten, E. Schimpf, A. Semchenkov, A. Türler, H.-J.Wollersheim, A. Yakushev, P. Thörle-Pospiech, W. Hartmann, A. Hübner, B. Lommel, B. Kindler, J. Steiner
TASISpec – A highly efficient multi-coincidence spectrometer for nuclear structure investigations of the heaviest nuclei
Nucl. Instrum. Methods Phys. Res. Sect. A: **622** (1)**:** 164-170 (2010).

C. E. Düllmann, M. Schädel, A. Yakushev, A. Türler, K. Eberhardt, J. V. Kratz, D. Ackermann, L. L. Andersson, M. Block, W. Brüchle, J. Dvorak, H. G. Essel, P. A. Ellison, J. Even, J. M. Gates, A. Gorshkov, R. Graeger, K. E. Gregorich, W. Hartmann, R. D. Herzberg, F. P. Heßberger, D. Hild, A. Hübner, E. Jäger, J. Khuyagbaatar, B. Kindler, J. Krier
Production and decay of element 114: High cross sections and the new nucleus Hs-277
Phys. Rev. Lett. **104** (25): 252701 (2010).

R. Eichler, N. V. Aksenov, Y. V. Albin, A. V. Belozerov, G. A. Bozhikov, V. I. Chepigin, S. N. Dmitriev, R. Dressler, H. W. Gäggeler, V. A. Gorshkov, G. S. Henderson, A. M. Johnsen, J. M. Kenneally, V. Y. Lebedev, O. N. Malyshev, K. J. Moody, Y. T. Oganessian, O. V. Petrushkin, D. Piguet, A. G. Popeko, P. Rasmussen, A. Serov, D. A. Shaughnessy, S. V. Shishkin, A. V. Shutov, M. A. Stoyer, N. J. Stoyer, A. I. Svirikhin, E. E. Tereshatov, G. K. Vostokin, M. Wegrzecki, P. A. Wilk, D. Wittwer, A. V. Yeremin
Indication for a volatile element 114
Radiochim. Acta **98** (3): 133-139 (2010).

R. Graeger, D. Ackermann, M. Chelnokov, V. Chepigin, C. E. Düllmann, J. Dvorak, J. Even, A. Gorshkov, F. P. Heßberger, D. Hild, A. Hübner, E. Jäger, J. Khuyagbaatar, B. Kindler, J. V. Kratz, J. Krier, A. Kuznetsov, B. Lommel, K. Nishio, H. Nitsche, J. P. Omtvedt, O. Petrushkin, D. Rudolph, J. Runke, F. Samadani, M. Schädel, B. Schausten, A. Türler, A. Yakushev, Q. Zhi
Experimental study of the U-238(S-36,3-5n)Hs-269-271 reaction leading to the observation of Hs-270
Phys. Rev. C **81** (6): 061601 (2010).

A. Hermann, J. Furthmüller, H. W. Gäggeler, P. Schwertfeger
Spin-orbit effects in structural and electronic properties for the solid state of the group-14 elements from carbon to superheavy element 114
Phys. Rev. B **82** 155116 (2010).

K. Nishio, S. Hofmann, F. P. Hessligberger, D. Ackermann, S. Antalic, Y. Aritomo, V. F. Comas, C. E. Düllmann, A. Gorshkov, R. Graeger, K. Hagino, S. Heinz, J. A. Heredia, K. Hirose, H. Ikezoe, J. Khuyagbaatar, B. Kindler, I. Kojouharov, B. Lommel, R. Mann, S. Mitsuoka, Y. Nagame, I. Nishinaka, T. Ohtsuki, A. G. Popeko, S. Saro, M. Schädel, A. Türler, Y. Watanabe, A. Yakushev, A. V. Yeremin
Nuclear orientation in the reaction S-34 + U-238 and synthesis of the new isotope Hs-268
Phys. Rev. C **82** (2): 024611 (2010).

A. Türler
Chemical experiments with superheavy elements
CHIMIA **64:** 293-298 (2010).

D. Wittwer, F. S. Abdullin, N. V. Aksenov, Y. V. Albin, G. A. Bozhikov, S. N. Dmitriev, R. Dressler, R. Eichler, H. W. Gäggeler, R. A. Henderson, S. Hübener, J. M. Kenneally, V. Y. Lebedev, Y. V. Lobanov, K. J. Moody, Y. T. Oganessian, O. V. Petrushkin, A. N. Polyakov, D. Piguet, P. Rasmussen, R. N. Sagaidak, A. Serov, I. V. Shirokovsky, D. A. Shaughnessy, S. V. Shishkin, A. M. Sukhov, M. A. Stoyer, N. J. Stoyer, E. E. Tereshatov, Y. S. Tsyganov, V. K. Utyonkov, G. K. Vostokin, M. Wegrzecki, P. A. Wilk
Gas phase chemical studies of superheavy elements using the Dubna gas-filled recoil separator - stopping range determination
Nucl. Instrum. Methods Phys. Res. Sect. B: Atoms **268** (1): 28-35 (2010).

SURFACE CHEMISTRY

T. Bartels-Rausch, M. Brigante, Y. F. Elshorbany, M. Ammann, B. D'Anna, C. George, K. Stemmler, M. Ndour, J. Kleffmann
Humic acid in ice: Photo-enhanced conversion of nitrogen dioxide into nitrous acid
Atmos. Environ. **44** (40): 5443-5450 (2010).

J. N. Crowley, M. Ammann, R. A. Cox, R. G. Hynes, M. E. Jenkin, A. Mellouki, M. J. Rossi, J. Troe, T. J. Wallington
Evaluated kinetic and photochemical data for atmospheric chemistry: Volume V - Heterogeneous reactions on solid substrates
Atmos. Chem. Phys. **10** (18): 9059-9223 (2010).

T. Huthwelker, V. Zelenay, M. Birrer, A. Krepelova, J. Raabe, G. Tzvetkov, M. G. C. Vernooij, M. Ammann
An in situ cell to study phase transitions in individual aerosol particles on a substrate using scanning transmission X-ray microspectroscopy
Rev. Sci. Instrum. **81** (11): 113706-9 (2010).

M. Kerbrat, T. Huthwelker, T. Bartels-Rausch, H. W. Gäggeler, M. Ammann
Co-adsorption of acetic acid and nitrous acid on ice
Phys. Chem. Chem. Phys. **12** (26): 7194-7202 (2010).

M. Kerbrat, T. Huthwelker, H. W. Gäggeler, M. Ammann
Interaction of nitrous acid with polycrystalline ice: Adsorption on the surface and diffusion into the bulk
J. Phys. Chem. C **114** (5): 2208-2219 (2010).

C. E. Kolb, R. A. Cox, J. P. D. Abbatt, M. Ammann, E. J. Davis, D. J. Donaldson, B. C. Garrett, C. George, P. T. Griffiths, D. R. Hanson, M. Kulmala, G. McFiggans, U. Pöschl, I. Riipinen, M. J. Rossi, Y. Rudich, P. E. Wagner, P. M. Winkler, D. R. Worsnop, C. D. O' Dowd
An overview of current issues in the uptake of atmospheric trace gases by aerosols and clouds
Atmos. Chem. Phys. **10** (21): 10561-10605 (2010).

A. Křepelová, T. Huthwelker, H. Bluhm, M. Ammann
Surface chemical properties of eutectic and frozen NaCl solutions probed by XPS and NEXAFS
Chem. Phys. Chem. **11** (18): 3859-3866 (2010).

A. Křepelová, J. Newberg, T. Huthwelker, H. Bluhm, M. Ammann
The nature of nitrate at the ice surface studied by XPS and NEXAFS
Phys. Chem. Chem. Phys. **12** (31): 8870-8880 (2010).

M. E. Monge, B. D'Anna, L. Mazri, A. Giroir-Fendler, M. Ammann, D. J. Donaldson, C. George
Light changes the atmospheric reactivity of soot
Proc. Nat. Acad. Sci. 107(15):6605-6609. PNAS: 10.1073/pnas.0908341107 (2010).

B. R. Pinzer, M. Kerbrat, T. Huthwelker, H. W. Gäggeler, M. Schneebeli, M. Ammann
Diffusion of NOx and HONO in snow: A laboratory study
J. Geophys. Res. **115** (D3): D03304 (2010).

A. Rouvière, M. Ammann
The effect of fatty acid surfactants on the uptake of ozone to aqueous halogenide particles
Atmos. Chem. Phys. **10** (23): 11489-11500 (2010).

A. Rouvière, Y. Sosedova, M. Ammann
Uptake of ozone to deliquesced KI and mixed KI/NaCl aerosol particles
J. Phys. Chem. A **114** (26): 7085-7093 (2010).

V. Zelenay, M. Ammann, A. Křepelová, M. Birrer, G. Tzvetkov, M. G. C. Vernooij, J. Raabe, T. Huthwelker
Direct observation of water uptake and release in individual submicrometer sized ammonium sulfate and ammonium sulfate/adipic acid particles using X-ray microspectroscopy
J. Aerosol Sci. **42** (1): 38-51 (2010).

ANALYTICAL CHEMISTRY

J. Gabrieli, P. Vallelonga, G. Cozzi, P. Gabrielli, A. Gambaro, M. Sigl, F. Decet, M. Schwikowski, H. W. Gäggeler, C. Boutron, P. Cescon, C. Barbante
Post 17th-century changes of European PAH emissions recorded in high-altitude alpine snow and ice
Environ. Sci. Technol. **44** (9): 3260-3266 (2010).

P. Ginot, U. Schotterer, W. Stichler, M. A. Godoi, B. Francou, M. Schwikowski
Influence of the Tungurahua eruption on the ice core records of Chimborazo, Ecuador
Cryosphere **4** (4): 561-568 (2010).

T. Kellerhals, S. Brütsch, M. Sigl, S. Knüsel, H. W. Gäggeler, M. Schwikowski
Ammonium concentration in ice cores: A new proxy for regional temperature reconstruction?
J. Geophys. Res. **115** (D16): D16123 (2010).

T. Kellerhals, L. Tobler, S. Brütsch, M. Sigl, L. Wacker, H. W. Gäggeler, M. Schwikowski
Thallium as a tracer for preindustrial volcanic eruptions in an ice core record from Illimani, Bolivia
Environ. Sci. Technol. **44** (3): 888-893 (2010).

M. Schwikowski, A. Eichler
Alpine glaciers as archives of atmospheric deposition.
in *Alpine waters* **6**, Bundi, U. (Editor), Springer-Verlag: Berlin Heidelberg**,** p. 141-150 (2010).

M. Trachsel, M. Grosjean, I. Larocque-Tobler, M. Schwikowski, A. Blass, M. Sturm
Quantitative summer temperature reconstruction derived from a combined biogenic Si and Chironomid record from varved sediments of lake Silvaplana (south-eastern Swiss Alps) back to AD 1177
Quat. Sci. Rev. **29** (19-20): 2719-2730 (2010).

RADWASTE ANALYTICS

M. Ayranov, D. Schumann
Preparation of Al-26, Ni-59, Ti-44, Mn-53 and Fe-60 from a proton irradiated copper beam dump
J. Radioanal. Nucl. Chem. **286** (3): 649-654 (2010).

St. Bister, F. Koenn, M. Bunka, J. Birkhan, T. Lüllau, B. Riebe, R. Michel
Uranium in water of the Mulde River
J. Radioanal. Nucl. Chem. **286**:367–372 (2010).

D. Schumann, M. Ayranov
Preparation of Fe-60, Be-7, Ti-44 and other samples for nuclear physics experiments
J. Phys. Conf. Ser. **202** (1): 012034 (2010).

D. Schumann, J. Neuhausen, I. Dillmann, C. Domingo Pardo, F. Käppeler, J. Marganiec, F. Voss, S. Walter, M. Heil, R. Reifarth, J. Goerres, E. Uberseder, M. Wiescher, M. Pignatari
Preparation of a Fe-60 target for nuclear astrophysics experiments
Nucl. Instrum. Methods Phys. Res., Sect. A **613** (3): 347-350 (2010).

M. Wohlmuther, Y. Dai, D. Gavillet, K. Geissmann, D. Kuster, R. Meier, J. Neuhausen, D. Schumann, A. Strinning, P. Suter, S. Teichmann, R. Thermer, K. Thomsen, W. Wagner, J. Züllig, Ch. Zumbach, B. Binkert, F. Bugmann, R. Emch, R. Erne, D. Gubler, Ch. Hösli, R. Keller, R. Leuzinger, D. Moosmann, Ch. Schörck, A. Wegmüller
MEGAPIE on the way to PIE
Proceedings of the International Topical Meeting on Nuclear Research Applications and Utilization of Accelerators, AccApp09, 4-8 May 2009, Vienna, Austria, IAEA Proceedings Series, IAEA-I3-CN-173, ISBN 978-92-0-150410-4, ISSN 1991-2374, January 2010.

ENVIRONMENTAL RADIONUCLIDES UNIVERSITÄT BERN

A. C. Aiken, B. de Foy, C. Wiedinmyer, P. F. DeCarlo, I. M. Ulbrich, M. N. Wehrli, S. Szidat, A. S. H. Prevot, J. Noda, L. Wacker, R. Volkamer, E. Fortner, J. Wang, A. Laskin, V. Shutthanandan, J. Zheng, R. Zhang, G. Paredes-Miranda, W. P. Arnott, L. T. Molina, G. Sosa, X. Querol, J. L. Jimenez
Mexico city aerosol analysis during MILAGRO using high resolution aerosol mass spectrometry at the urban supersite (T0) – part 2: Analysis of the biomass burning contribution and the non-fossil carbon fraction
Atmos. Chem. Phys. **10** (12): 5315-5341 (2010).

S. Fahrni, H. W. Gäggeler, I. Hajdas, M. Ruff, S. Szidat, L. Wacker
Direct measurements of small C-14 samples after oxidation in quartz tubes
Nucl. Instrum. Methods Phys. Res., Sect. B **268** (7-8): 787-789 (2010).

S. Fahrni, M. Ruff, L. Wacker, N. Perron, H. W. Gäggeler, S. Szidat
A preparative 2D-chromatography method for compound-specific radiocarbon analysis of dicarboxylic acids in aerosols
Radiocarbon **52:** 752-760 (2010).

A. Hodzic, J. L. Jimenez, A. S. H. Prévôt, S. Szidat, J. D. Fast, S. Madronich
Can 3-D models explain the observed fractions of fossil and non-fossil carbon in and near mexico city?
Atmos. Chem. Phys. **10** (22): 10997-11016 (2010).

M. Nemec, L. Wacker, I. Hajdas, H. W. Gäggeler
Alternative methods for cellulose preparation for AMS measurementnt
Radiocarbon **52**: 1358-1370 (2010).

M. Nemec, L. Wacker, H. W. Gäggeler
Optimization of the graphitization process at AGE-1
Radiocarbon **52**: 1380-1393 (2010).

N. Perron, S. Szidat, S. Fahrni, M. Ruff, L. Wacker, A. S. H. Prevot, U. Baltensperger
Towards on-line C-14 analysis of carbonaceous aerosol fractions
Radiocarbon **52** 761-768 (2010).

M. Ruff, S. Fahrni, H. W. Gäggeler, I. Hajdas, M. Suter, H.-A. Synal, S. Szidat, L. Wacker
On-line radiocarbon measurements of small samples using elemental analyzer and MICADAS gas ion source
Radiocarbon **52** (4): 1645-1656 (2010).

M. Ruff, S. Szidat, H. W. Gäggeler, M. Suter, H. A. Synal, L. Wacker
Gaseous radiocarbon measurements of small samples
Nucl. Instrum. Methods Phys. Res., Sect. B **268** (7-8): 790-794 (2010).

Y.L. Zhang, D. Liu, C.D. Shen, P. Ding, G. Zhang
Development of a preparation system for the radiocarbon analysis of organic carbon in carbonaceous aerosols in China
Nucl. Instr. Meth. Phys. Res. B **268**, 2831-2834 (2010).

RADIONUCLIDE DEVELOPMENT – CHEMISTRY

K. Zhernosekov, S. Lehenberger, U. Köster, H. Dorrer, A. Hohn, R. Schibli, A. Türler
The low-energy beta(-) and electron emitter Tb-161 as alternative for Lu-177 for targeted radionuclides therapy
Nuclear Medicine and Biology **37** (6): 718-719 (2010).

K. Zhernosekov, S. Lehenberger, U. Köster, H. Dorrer, A. Hohn, R. Schibli, A. Türler (2010)
The low-energy β -and electron emitter ^{161}Tb as alternative for ^{177}Lu for targeted radionuclide therapy
pages 465-468
TECHNETIUM AND OTHER RADIOMETALS IN CHEMISTRY AND MEDICINE
Edited by U. Mazzi, W. C. Eckelman, W. A. Volkert, SGE Ditoriali, Padova, Italy.

REPORTS AND TECHNICAL NOTES

A. Fuchs, S. Heinitz, M. Jolkkonen, R. Moormann, J. Neuhausen, D. Schumann, L. Zanini
Environmental compliance report concerning the target material
EC-FP7 Project ESS-PP Deliverable D 8.1, Paul Scherrer Institut, Villigen, Switzerland, 2010.

F. Beer, R. Moormann, A. Fuchs, D. Kiselev, J. Neuhausen, P. Pacenti, M.G. Ortore, F. Carsughi, D. Schumann, J. Quiñones, F. Martin Fuertes, E. Gonzalez Romero, J. Garitaonandia, F. Albizu
Environmental compliance report concerning the radioactive inventory
EC-FP7 Project ESS-PP Deliverable D 8.2, Paul Scherrer Institut, Villigen, Switzerland, 2010.

J. Neuhausen
Final report on Po, I, Hg production and deposition
EC-FP6-IP EUROTRANS Deliverable D4.66, Paul Scherrer Institut, Villigen, Switzerland, 2010.

S. Heinitz, J. Neuhausen, C. Neuhausen, D. Schumann
The interaction of LBE with silicon oil
MEGAPIE Technical Report MPR-11-HS24-001/TM-24-10-02, Paul Scherrer Institut, Villigen, Switzerland, 2010.

CONTRIBUTIONS TO CONFERENCES, WORKSHOPS AND SEMINARS

HEAVY ELEMENTS

R. Eichler
Chemical investigation of element 114
Seminar of the Laboratory of Radiochemistry and Environmental Chemistry, Paul Scherrer Institute and University of Berne, Switzerland, 28 May, 2010.

R. Eichler
Chemistry with the newly discovered superheavy elements
Euchems'10, Nürnberg, Germany, 30 September, 2010.

R. Eichler
The chemical investigation of element 114: Up's and down's
International Chemical Congress of Pacific Basin Societies (Pacifichem), Honolulu, Hawaii, USA, 14-20 December, 2010.

H.W. Gäggeler
From Mendeleev's principle to Einstein's relativity: news from the chemistry of superheavy elements
Industrial Research Limited IRL, Lower Hutt, New Zealand, 19 March, 2010.

H.W. Gäggeler
From Mendeleev's principle to Einstein's relativity: news from the chemistry of superheavy elements
Institute for Nuclear Physics, ANU Canberra, Australia, 31 March, 2010.

H.W. Gäggeler
Recent achievements in chemical studies of heaviest elements
INPC'10, Vancouver, Canada, 04-09 July, 2010.

H.W. Gäggeler
Chemistry of heaviest elements
Int. Grad. School Basel-Graz-Tübingen, Liborhof (Todtmoos), Germany, 27-30 September, 2010.

A. Serov
Element 114 chemistry and what is next?
16th Radiochemical Conference, Marianske Lazne, Czech Republic, 18-23 April, 2010.

A. Serov
Thermochromatographic investigation of ^{113m}In, ^{125}Sb and ^{125m}Te in quartz columns
16th Radiochemical Conference, Marianske Lazne, Czech Republic, 18-23 April, 2010.

S. Söllradl
Prompt Gamma Activation Analysis at FRM II in Munich: Plans, Challenges and Examples after one year PhD
1st Year Graduate Student Symposium, University of Bern, Switzerland, 13 September, 2010.

A. Türler
Gas-phase chemistry of superheavy elements
Schleching: XLI Arbeitstreffen Kernphysik, Germany, 18-25 February, 2010.

A. Türler
Nucleon transfer reactions induced by A < 50 projectiles
IRIS Workshop, GSI Darmstadt, Germany, 01 March, 2010.

A. Türler
New nucleus ^{277}Hs: in between two islands of stability
16th Radiochemical Conference, Marianske Lazne, Czech Republic, 18-23 April, 2010.

A. Türler
Nuclear Structure and Reactions Near Doubly Magic ^{270}Hs
ARCEBS-10, Saha Institute of Nuclear Physics, Kolkata, India , 07-13 November, 2010.

A. Türler
Future heavy element plans at PSI
FDHES Workshop, Lawrence Berkeley National Laboratory, Berkeley, California, USA, 09-10 December, 2010.

A. Türler
Gas-phase chemistry of superheavy elements
FDHES Workshop, Lawrence Berkeley National Laboratory, Berkeley, California, USA, 09-10 December, 2010.

A. Türler
Research activities on superheavy element chemistry and physics at Paul Scherrer Institute and Bern University
Pacifichem 2010, Honolulu, Hawaii, USA, 15-20 December, 2010.

D. Wittwer
Gas phase chemical studies of superheavy elements using the Dubna gas-filled separator: The stopping range determination
16th Radiochemical Conference, Marianske Lazne, Czech Republic, 18-23 April, 2010.

D. Wittwer
Lanthanide target preparation on Noble metal backings - Release of transfer and fusion products from metal foils
Seminar of the Laboratory of Radiochemistry and Environmental Chemistry, Paul Scherrer Institute and University of Berne, Switzerland, 28 May, 2010.

R. Dressler
Chemical investigation of element 114: indication for a massive relativistic effect in chemistry
The International Nuclear Physics Conference 2010, Vancouver, British Columbia, Canada, 04-09 July, 2010.

R. Dressler
Chemical investigation of element 114: indication for a massive relativistic effect in chemistry
3rd International Conference on Frontiers in Nuclear Structure, Astrophysics and Reactions, Rhodes, Greece, 23-27 August, 2010.

SURFACE CHEMISTRY

M. Ammann
Phase transfer at the interface between chemistry and climate
ATCHEM Workshop 2010, University of Bayreuth, Germany 24-26 February, 2010.

M. Ammann, Y. Sosedova, O. Vesna, A. Rouvière, V. Zelenay, C. George
Feedbacks between organic aerosol oxidation and gas phase HO_x: A laboratory perspective
ATCHEM Workshop 2010, University of Bayreuth, Germany, 24-26 February, 2010.

M. Ammann
Uptake of nitric acid to tropospheric particles and implications for chemistry and climate
Seminar of the Institute for Atmospheric and Climate Science, ETH Zürich, Switzerland, 29 March, 2010.

M. Ammann
Flow tube perspective of organic aerosol aging: Condensed phase chemistry and photochemistry
European Geoscience Union General Assembly, Vienna, Austria, 02-07 May, 2010.

M. Ammann, A. Rouvière
Effect of fatty acid coatings on ozone uptake to deliquesced KI/NaCl aerosol particles
3rd Bi-Annual Symposium "Future Ocean", University of Kiel, Kiel, Germany, 13-16 September, 2010.

M. Ammann
The nature of ice surfaces under the effect of atmospheric trace gases
Seminar at MAXLAB, Lund, Sweden, 04 November, 2010.

T. Bartels-Rausch, G. Krysztofiak, A. Bernhard, M. Schläppi, M. Schwikowski, M. Ammann
Photochemistry of mercury and organics in sea ice – laboratory investigations
European Geoscience Union General Assembly, Vienna, Austria, 02-07 May, 2010.

T. Bartels-Rausch, G. Krysztofiak, A. Bernhard, M. Schläppi, M. Schwikowski, M. Ammann
Laboratory investigations of the light-driven mercury reduction in ice: The effect of organic matter
International Polar Year Oslo Science Conference, Oslo, Norway, 07-12 June, 2010.

M. Kerbrat, T. Bartels-Rausch, T. Huthwelker, M. Ammann
Adsorption of trace gases to ice surfaces: Surface, bulk and co-adsorbate effects
European Geoscience Union General Assembly, Vienna, Austria, 02-07 May, 2010.

A. Křepelová, J. Newberg, T. Huthwelker, H. Bluhm, M. Ammann
XPS studies on ice
Seminar of the Laboratory of Radiochemistry and Environmental Chemistry, Paul Scherrer Institute and University of Berne, Switzerland, 19 March, 2010.

S. Schreiber, M. Kerbrat, T. Huthwelker, M. Birrer, M. Ammann
Trace gas uptake on growing ice surfaces
International Polar Year - Oslo Science Conference, Oslo, Norway, 08-12 June, 2010.

S. Schreiber, M. Kerbrat, T. Huthwelker, M. Birrer, M. Ammann
Trace gas uptake in growing ice
Seminar of the Laboratory of Radiochemistry and Environmental Chemistry, Paul Scherrer Institute and University of Berne, Switzerland, 10 December, 2010.

Y. Sosedova, A. Rouvière, M. Ammann
Photoenhanced nitrous acid formation upon NO_2 uptake on tannic and gentisic acid films
European Geoscience Union General Assembly, Vienna, Austria, 02-07 May, 2010.

Y. Sosedova
Photoenhanced nitrous acid formation on the organic surfaces: Experiments based on HONO detection by LOPAP
Seminar of the Laboratory of Radiochemistry and Environmental Chemistry, Paul Scherrer Institute and University of Berne, 10 December, 2010.

T. Ulrich
Interactions of HO_2NO_2 with ice: The synthesis of HO_2NO_2
Seminar of the Laboratory of Radiochemistry and Environmental Chemistry, Paul Scherrer Institute and University of Berne, Switzerland, 30 April, 2010.

T. Ulrich, T. Bartels-Rausch, S. Leutwyler, M. Ammann
The adsorption of HO_2NO_2 on ice
International Polar Year - Oslo Science Conference, Oslo, Norway, 08-12 June, 2010.

T. Ulrich
The adsorption of HNO4 on ice - a coated wall flow tby study
1st Year Graduate Student Symposium, University of Bern, Switzerland, 13 September, 2010.

V. Zelenay
Soot, water and XAS: An X-ray microspectroscopy study on water uptake in single soot particles
Seminar of the Laboratory of Radiochemistry and Environmental Chemistry, Paul Scherrer Institute and University of Berne, Switzerland, 19 March, 2010.

V. Zelenay, A. Křepelová, Y. Rudich, T. Huthwelker, M. Ammann
Tracking the morphology of fulvic acids during water uptake
European Geoscience Union General Assembly, Vienna, Austria, 02-07 May, 2010.

V. Zelenay
Mapping morphology upon water uptake in single particles using microspectroscopy
SLS Seminar 'Liquids and Gases', Paul Scherrer Institut, Villigen, Switzerland, 03 August, 2010.

ANALYTICAL CHEMISTRY

A. Ciric, G. Cassasa, M. Schwikowski
ENSO-related accumulation variability derived from Mercedario ice core
II International Symposium "Reconstructing Climate Variations in South America and the Antarctic Peninsula over the last 2000 years", Valdivia, Chile, 27-30 October, 2010.

A. Eichler, M. Schwikowski, S. Brütsch, S. Olivier, T. Papina, W. Tinner
A 750 year ice core record of past biogenic emissions and wild fires from Siberian boreal forests
EGU General Assembly 2010, Vienna, Austria, 03-07 May, 2010.

A. Eichler, M. Schwikowski
Reconstruction of air pollution from high-alpine ice cores
OCCR WP3 meeting on Climate Responses & Impacts, Gurten, Switzerland, 29 October, 2010.

A. Eichler
A 750 year ice core record of past biogenic emissions and wild fires from Siberian boreal forests
Seminar of the Laboratory of Radiochemistry and Environmental Chemistry, Paul Scherrer Institute and University of Berne, Switzerland, 19 November, 2010.

J. Gabrieli, P. Vallelonga, G. Cozzi, M. Sigl, F. Decet, M. Schwikowski, H. Gäggeler, C. Boutron, P. Cescon, C. Barbante
Post 17th-Century changes of European PAH emissions recorded in high-altitude Alpine snow and ice
14th Alpine Glaciology Meeting, Milano, Italy, 25–26 March, 2010.

H.W. Gäggeler
On the way to quantify human impact on climate: pollution records and climate information from alpine ice cores
Geological and Nuclear Science GNS, Avalon, Lower Hutt, New Zealand, 10 February, 2010.

P.-A. Herren
First results from an ice core of the Mongolian Altai
Seminar of the Laboratory of Radiochemistry and Environmental Chemistry, Paul Scherrer Institute and University of Berne, Switzerland, 30 April, 2010.

P.-A. Herren
Reconstruction of past climate from an ice core of the Mongolian Altai
9th International NCCR Climate Summer School "Adaptation and Mitigation: Responses to Climate Change", Grindelwald, Switzerland, 29 August – 03 September, 2010.

I. Mariani, T. Jenk, M. Sigl, M. Schwikowski
Ice core proxies as indicators of moisture source areas for the Alps
14th Alpine Glaciology Meeting, Milano, Italy, 25–26 March, 2010.

I. Mariani, M. Sigl, J. Gabrieli, D. Bolius, C. Barbante, C. Boutron, M. Schwikowski
Increased frequency of Saharan dust storms in the last decades confirmed by the Colle Gnifetti ice core record
Int. Workshop on Weather and Climate Extremes During the Past 100 years, Diessenhofen, Switzerland, 07-09 June, 2010.

I. Mariani
Ice core proxies as indicators of moisture source areas for the Alps
9th International NCCR Climate Summer School "Adaptation and Mitigation: Responses to Climate Change", Grindelwald, Switzerland, 29 August – 03 September, 2010.

S. Maus, S. Haase, J. Büttner, T. Huthwelker, M. Schwikowski, A. Vähätalo
Ion fractionation and pore space geometry in young sea ice from Kongsfjorden, Svalbard
Int. Symposium on Sea Ice in the Physical and Biogeochemical System, Tromsø, Norway, 31 May – 04 June, 2010.

C. Mayer, A. Lambrecht, N. Frank, M. Schwikowski, C. Smiraglia
Accumulation conditions in a high elevated basin of the Karakoram
EGU General Assembly 2010, Vienna, Austria, 03-07 May, 2010.

M. Schläppi, P.A. Santibañez, A. Rivera, G. Cassasa, M. Schwikowski
Accumulation rates derived from Pio XI ice core, Southern Patagonian Icefield
II International Symposium "Reconstructing Climate Variations in South America and the Antarctic Peninsula over the last 2000 years", Valdivia, Chile, 27-30 October, 2010.

I. Schuck
A new Svalbard ice core
9th International NCCR Climate Summer School "Adaptation and Mitigation: Responses to Climate Change", Grindelwald, Switzerland, 29 August – 03 September, 2010.

I. Schuck
A new ice core from Svalbard - first results
Seminar of the Laboratory of Radiochemistry and Environmental Chemistry, Paul Scherrer Institute and University of Berne, Switzerland, 19 November, 2010.

M. Schwikowski, A. Ciric, T. Kellerhals
Regional temperature reconstruction from Andean ice cores
VICC2010, International Glaciological Conference Ice and Climate Change: A view from the South, Valdivia, Chile, 01-03 February, 2010.

M. Schwikowski, T. Kellerhals, S. Brütsch, M. Sigl, S. Knüsel, H.W. Gäggeler
Ammonium in ice cores – a new proxy for tropical South American temperature reconstruction
EGU General Assembly 2010, Vienna, Austria, 03-07 May, 2010.

M. Schwikowski, M. Sigl, H.W. Gäggeler, D. Divine, T.M. Jenk, J. Gabrieli, C. Barbante, C. Boutron
1000-year summer temperature reconstruction from an Alpine ice core
EGU General Assembly 2010, Vienna, Austria, 03-07 May, 2010.

M. Schwikowski, M. Sigl, H.W. Gäggeler, J. Gabrieli, C. Barbante, C. Boutron
Decadal variability of NAO during the last millennium inferred from Saharan dust in Alpine ice
EGU General Assembly 2010, Vienna, Austria, 03-07 May, 2010.

M. Schwikowski, I. Mariani
Ice core proxies as indicators of moisture source areas for the Alps
Climate Services Seminar MeteoSwiss, Zurich, Switzerland, 15 June, 2010.

M. Schwikowski
Deriving past climate changes from ice cores
Summer School on Monsoon Variability, Teleconnections, and Impacts on Mid to Low Latitude Glaciers, Obergurgl, Austria, 20-30 June, 2010.

M. Schwikowski
Ice cores from Alpine glaciers
Presentation during an excursion to the Jungfraujoch, The first Tibetan Plateau Research Young Scientists Fieldtrip to the Alps, Jungfraujoch, Switzerland, 03 August, 2010.

M. Schwikowski
Ice cores from high-alpine glaciers as regional climate archives
OCCR WP1&2 Joint Workshop, Gwatt, Switzerland, 17-18 August, 2010.

M. Schwikowski
Deriving past climate changes using ice cores from high-alpine glaciers
Seminar Institut für Planetare Geodäsie, TU Dresden, Dresden, Germany, 01 October, 2010.

M. Schwikowski, I. Schuck, A. Eichler, E. Isaksson, T. Martma
Preliminary results from the 2009 Lomonossovfonna ice core
Svalbard Ice Core Workshop, Uppsala, Sweden, 14-15 October, 2010.

M. Schwikowski, S. Brütsch, S. Knüsel, T. Kellerhals
Regional temperature reconstruction from Illimani ice core
II International Symposium "Reconstructing Climate Variations in South America and the Antarctic Peninsula over the last 2000 years", Valdivia, Chile, 27-30 October, 2010.

A. Zapf
Radiocarbon-dating of glacier ice
9th International NCCR Climate Summer School "Adaptation and Mitigation: Responses to Climate Change", Grindelwald, Switzerland, 29 August – 03 September, 2010.

RADWASTE ANALYTICS

M. Ayranov, D. Schumann
Preparation of ^{26}Al, ^{59}Ni, ^{44}Ti, ^{53}Mn and ^{60}Fe samples from a proton irradiated copper beam dump
Radchem2010, Marianske Lazne, Czech Republic, 18-22 April, 2010.

M. Ayranov, D. Schumann
Accelerator Wastes - Source of $^{44}Ti/^{44}Sc$ for PET application
International Workshop on bio-medical applications of micro-PET, Sevilla, Spain, 20-22 September, 2010.

M. Bunka
Preparative radiochemical separation of exotic radionuclides from accelerator waste
1st Year Graduate Student Symposium, University of Bern, Switzerland, 13 September, 2010.

T. Faestermann, I. Günther-Leopold, N. Kivel, K. Knie, G. Korschinek, M. Poutivtsev, G. Rugel, D. Schumann, R. Weinreich, M. Wohlmuther
Bestimmung der ^{60}Fe Halbwertszeit
9. Symposium Massenspektrometrische Verfahren der Elementspurenanalyse, Berlin, Germany, 06-08 September, 2010.

C. Fazio, A. Weisenburger, P. Vladimirov, A. Class, Th. Wetzel, K. Litfin, J. Van den Bosch, F. Javier Martin Muñoz, L. Brissonneau, J. Henry, F. Roelofs, L. Magielsen, P. Turroni, A. Ciampichetti, M. Tarantino, L. Mansani, D. Gorse, J. Abella, Y. Dai, J. Neuhausen, L. Zanini, H. Jeanmart, G. Gerbeth, A. Karbojian
Development and assessment of structural materials and heavy liquid metal technologies for transmutation systems (DEMETRA): Highlights on major results
OECD Nuclear Energy Agency International Workshop on Technology and components of accelerator driven systems, Karlsruhe, Germany, 15-17 March, 2010.

S. Heinitz, J. Neuhausen, D. Schumann
Is lead-gold eutectic a suitable spallation target material from the chemical point of view?
ICANS Grindelwald, Switzerland, 08-12 March, 2010.

S. Heinitz, J. Neuhausen, D. Schumann
Behaviour of polonium in lead - bismuth eutectic
3rd EuCheMS Chemistry Congress, Nürnberg, Germany, 29 August - 02 September, 2010.

S. Heinitz, J. Neuhausen, D. Schumann
Alkaline extraction of polonium from lead bismuth eutectic
International Conference on Nuclear Materials, ZKM, Karlsruhe, Germany, 04-07 October, 2010.

D. Kiselev, Y. Dai, S. Lüthi, J. Neuhausen, D. Schumann, S. Teichman
Nuclide inventory in proton irradiated lead –comparison of simulation and measurement
SATIF10, CERN, Geneve, Switzerland, 02-04 June, 2010.

J. Neuhausen, S. Heinitz, F. v. Rohr, D. Schumann, S. Lüthi, S. Horn, R. Dressler, B. Eichler, M. M. Marin Marmol, St. Keller, S. Müller, L. Zanini, V. Boutellier, M. Ruethi, J. Eikenberg
Behaviour of nuclear reaction products in liquid metal spallation targets: Summary of achieved results
International DEMETRA Workshop on Development and Assessment of Structural Materials and Heavy Liquid Metal Technologies for Transmutation Systems, Berlin, Germany, 02-04 March, 2010.

J. Neuhausen, D. Schumann, S. Heinitz, F. v. Rohr, S. Horn, S. Lüthi, L. Zanini, V. Boutellier, M. Rüthi, J. Eikenberg
Nuclear reaction product behaviour in liquid eutectic lead-bismuth alloy
OECD Nuclear Energy Agency International Workshop on Technology and components of accelerator driven systems, Karlsruhe, Germany, 15-17 March, 2010.

J. Neuhausen, D. Schumann, S. Heinitz, F. Von Rohr, S. Horn, S. Lüthi, L. Zanini, V. Boutellier, T. Stora, M. Rüthi, J. Eikenberg, E. Noah
Radiochemical aspects of liquid metal spallation targets
Tenth International Workshop on Spallation Materials Technology, Beijing, China, 18–22 October, 2010.

J. Neuhausen
Radiochemical aspects of liquid metal spallation targets
PSI/ SSM topical meeting on safety issues of a future ESS-facility, PSI, Villigen, Switzerland, 17–18 November, 2010.

G. Rugel, T. Faestermann, K. Knie, G. Korschinek, M. Poutivtsev, D. Schumann, N. Kivel, I. Günther-Leopold, R. Weinreich, M. Wohlmuther
Half-life of ^{60}Fe
DPG-Tagung, Bonn, Germany, 15-19 March, 2010.

G. Rugel, T. Faestermann, K. Knie, G. Korschinek, M. Poutivtsev, D. Schumann, N. Kivel, I. Günther-Leopold, R. Weinreich, M. Wohlmuther
Half-life of ^{60}Fe
NIC XI, Heidelberg, Germany, 19-23 July, 2010.

D. Schumann, M. Ayranov, R. Dressler
Achievements and perspectives of ERAWAST
EFNUDAT Paris, France, 25-27 May, 2010.

D. Schumann
Validation on the results from the post irradiation analysis of MEGAPIE samples
Annual meeting of the ANDES project, Madrid, Spain, 17-18 June, 2010.

D. Schumann
Nuclear chemistry for nuclear physics
INPC Vancouver, Canada, 05-09 July, 2010.

D. Schumann
Extraction of radionuclides from accelerator waste at PSI
FINUSTAR Rhodos, Greece, 23-27 August, 2010.

D. Schumann
Radiochemische Charakterisierung von Betonproben aus der Umgebung von Beschleunigeranlagen
SAAGA&RCA workshop Dresden, Germany, 06-09 September, 2010.

D. Schumann, S. Lüthi, T. Stowasser
^{14}C and ^{3}H determination of graphite target wheels
LSC2010, Paris, France, 06-10 September, 2010.

D. Schumann
High-power accelerator facilities - a new challenge for radiochemistry
International Workshop on bio-medical applications of micro-PET, Sevilla, Spain, 20-22 September, 2010.

L. Zanini, V. Boutellier, R. Bruetsch, D. Gavillet, J. Eikenberg, J. Krbanevic, H.P. Linder, M. Martin, J. Neuhausen, M. Ruthi, D. Schumann, A. Grimberg, I. Leya, E. Noah, T. Stora
Post-test analysis of a Pb/Bi target irradiated by protons of 1 GeV and 1.4 GeV energy at ISOLDE
OECD Nuclear Energy Agency International Workshop on Technology and components of accelerator driven systems, Karlsruhe, Germany, 15-17 March, 2010.

RADIONUCLIDE DEVELOPMENT

H.J. Dorrer
Production and evaluation of Terbium isotopes for medical use
1st Year Graduate Student Symposium, University of Bern, Switzerland, 13 September, 2010.

A. Türler
Neue (und alte) Radionuklide für therapeutische Anwendungen
7. Zuppinger Symposium der Berner Radium-Stiftung, Bern, Switzerland, 24 June, 2010.

A. Türler, R. Henkelmann, J. Moreno, E. Kabai, M. Harfensteller, A. Eursch, E. Huenges, M. Mentler, F. G. Parak, V. Bechtold
Cyclotron production of several GBq of ^{225}Ac via the ^{226}Ra(p, 2n) reaction
Pacifichem 2010, Honolulu, Hawaii, USA, 15-20 December, 2010.

K Zhernosekov, S. Lehenberger, H.J. Dorrer, A. Hohn, S. Cohrs, K. Zimmermann, E. Fischer, J. Grünberg, R. Schibli, A. Türler
The low-energy β-- and electron emitter ^{161}Tb as alternative for ^{177}Lu for targeted radionuclides therapy
Physics for health in Europe workshop
CERN, Genève, Switzerland, February, 2010.

K. Zhernosekov, S. Lehenberger, U. Köster, H.J. Dorrer, A. Hohn, R. Schibli, A. Türler
The low-energy β-- and electron emitter ^{161}Tb as alternative for ^{177}Lu for targeted radionuclides therapy
ISRS, International Symposium on Technetium and other Radiometals in Chemistry and Medicine, Bressanone, Italy, September, 2010.

K. Zhernosekov, A. Hohn, H.J. Dorrer, T.N. van der Walt, A. Türler, R. Schibli
Positron emitting radiolanthanides for PET: ^{140}Nd in vivo generator and ^{152}Tb
Workshop WIRP on innovative PET radionuclides, Nantes, France, July, 2010.

T. Nikula, U. Köster, B. Ponsard, K. Zhernosekov, P. Juntunen, L. Nikula
Reliable ^{99}Mo/^{99m}Tc-Generator Based on Medium-Specific-Activity ^{99}Mo
23rd Annual Congress of the European Association of Nuclear Medicine, October 9–13, 2010, Vienna, Austria
Eur. J. Nucl. Med. Mol. Imaging **37** (Suppl 2): 251 (2010).

K. Zhernosekov, M. Harfensteller, J. Moreno, O. Leib, O. Buck, A. Tuerler, R. Henkelmann, T. Nikula
Development of a novel metal-fee ^{68}Ge/^{68}Ga radionuclide generator system
23rd Annual Congress of the European Association of Nuclear Medicine, October 9–13, 2010, Vienna, Austria
Eur. J. Nucl. Med. Mol. Imaging **37** (Suppl 2): 251 (2010).

ENVIRONMENTAL RADIONUCLIDES UNIVERSITÄT BERN

D. Ceburnis, A. Garbaras, S. Szidat, A.S.H. Prevot, C. Facchini, C.D. O'Dowd
North Atlantic marine boundary layer organic aerosol: sources and fluxes
11th International Global Atmosphere Chemistry (IGAC) Conference, Halifax, Canada, 11-16 July, 2010.

D. Ceburnis, A. Garbaras, S. Szidat, S. Fahrni, N. Perron, L. Wacker, M. Rinaldi, A.S.H. Prevot, G. Jennings, V. Remeikis, C. Facchini, C.D. O'Dowd
Unambiguous origin of aerosol organic matter by ^{13}C and ^{14}C analysis
International Aerosol Conference 2010, Helsinki, Finland, 29 August - 03 September, 2010.

S. Fahrni, L.Wacker, M. Ruff, S. Szidat, H.-A. Synal
Improved measurements of gaseous ^{14}C samples at MICADAS
DPG Frühjahrstagung, Hannover, Germany, 08-12 March, 2010.

S. Fahrni
Improved measurements of gaseous ^{14}C samples at MICADAS
Seminar of the Laboratory of Radiochemistry and Environmental Chemistry, Paul Scherrer Institute and University of Berne, Switzerland, 30 April, 2010.

S. Fahrni, S. Szidat, H.W. Gäggeler, M. Ruff, L. Wacker
Source apportionment by compound-specific ^{14}C measurements of aerosol components
International Aerosol Conference 2010, Helsinki, Finland, 29 August - 03 September, 2010.

H.W. Gäggeler
Scientific and private reminiscences from a post-deadline sabbatical leave to New Zealand,
Seminar of the Laboratory of Radiochemistry and Environmental Chemistry, Paul Scherrer Institute and University of Berne, Switzerland, 17 December, 2010.

A. Hodzic, J.L. Jimenez, A.S.H. Prévôt, N. Marley, S. Madronich, S. Szidat
Can 3D models predict the observed fractions of modern and fossil carbon in and near Mexico City?
EGU, General Assembly 2010, Vienna, Austria, 02-07 May, 2010.

A. Hodzic, J.L. Jimenez, A.S.H. Prevot, S. Szidat, J.D. Fast, S. Madronich
Can 3D models explain the observed fraction of non-fossil carbon in Mexico City?
International Aerosol Conference 2010, Helsinki, Finland, 29 August - 03 September, 2010.

J. Liebl, S. Fahrni, R. Golser, W. Kutschera, K. Mair, A. Priller, P. Steier, I. Vonderhaid, L. Wacker, E.M. Wild
^{14}C AMS measurement and sample preparation methods of µg-sized carbon samples
DPG Frühjahrstagung, Hannover, Germany, 08-12 March, 2010.

M.C. Minguillón, N. Perron, X. Querol, S. Szidat, S. Fahrni, L. Wacker, C. Reche, M. Cusack, U. Baltensperger, A.S.H. Prévôt
Origin of fine carbonaceous particulate matter in the Western Mediterranean Basin: fossil versus modern sources
EGU, General Assembly 2010, Vienna, Austria, 02-07 May, 2010.

M.C. Minguillón, N. Perron, X. Querol, S. Szidat, S. Fahrni, L. Wacker, C. Reche, M. Cusack, U. Baltensperger, A.S.H. Prévôt
Carbonaceous particulate matter in the Western Mediterranean Basin: contribution of fossil versus modern sources
International Aerosol Conference 2010, Helsinki, Finland, 29 August - 03 September, 2010.

N. Perron, P. Lienemann, R. Gehrig, S. Szidat, S. Fahrni, M. Ruff, L. Wacker, A.S.H. Prévôt, U. Baltensperger
^{14}C-supported evidence of non-exhaust traffic resuspension in an Alpine valley
International Aerosol Conference 2010, Helsinki, Finland, 29 August - 3 September, 2010.

A.S.H. Prévôt, N. Perron, S. Szidat, V.A. Lanz, J. Sandradewi, M.R. Alfarra, A. Caseiro, U. Baltensperger
Comparison of several wood smoke markers and source apportionment methods for wood burning particulate mass
EGU, General Assembly 2010, Vienna, Austria, 02-07 May, 2010.

A.S.H. Prévôt, N. Perron, J. Sandradewi, M.R. Alfarra, S. Szidat, M.N. Wehrli, M. Ruff, S. Weimer, V.A. Lanz, E. Weingartner, A. Caseiro, A. Kasper-Giebl, H. Puxbaum, L. Wacker, U. Baltensperger
News on source apportionment methods for wood-burning particulate matter
International Aerosol Conference 2010, Helsinki, Finland, 29 August - 03 September, 2010.

S. Szidat, S. Fahrni, M. Ruff, N. Perron, L. Wacker, H.-A. Synal
Online ^{14}C analysis of ultra-small samples with accelerator mass spectrometry
16th Radiochemical Conference, Marianske Lazne, Czech Republic, 19-23 April, 2010.

S. Szidat
Compound-specific radiocarbon analysis: techniques and applications
Seminar Laboratory for Waste Management, Paul Scherrer Institut, Switzerland, 01 June, 2010.

S. Szidat
Sources of atmospheric carbonaceous aerosols
SCS Young Faculty Meeting 2010, University of Bern, Switzerland, 25 June, 2010.

S. Szidat
^{14}C and other environmental radionuclides - Research focus of the Szidat group
OCCR Work Package 1&2 Workshop, Gwatt, Switzerland, 17-18 August, 2010.

S. Szidat, N. Perron, Y. Zhang, S. Fahrni, M. Ruff, L. Wacker, M.C. Minguillon, A.S.H. Prevot, U. Baltensperger
Towards fast and reliable separation of OC and EC for ^{14}C-based source apportionment
International Aerosol Conference 2010, Helsinki, Finland, 29 August - 03 September, 2010.

S. Szidat
Offline- und Onlinemethoden zur ^{14}C-Messung von Kleinstproben
23. Seminar Aktivierungsanalyse und Gammaspektroskopie, Dresden, Germany, 06-08 September, 2010.

S. Szidat
Bestimmung von Feinstaubquellen mit Radiokohlenstoff
FZD-Kolloquium, Forschungszentrum Dresden-Rossendorf, Dresden, Germany, 08 September, 2010.

S. Szidat, S. Fahrni, M. Ruff, N. Perron, A.S.H. Prévôt, L. Wacker
Improved ^{14}C analysis of carbonaceous particulate matter
11th Int. Symp. on Environmental Radiochemical Analysis, Chester, U.K., 15-17 September, 2010.

S. Szidat
Analytics of ^{14}C, ^{210}Pb and other radionuclides
OCCR Work Package 3 Workshop, Bern, Switzerland, 29 October, 2010.

Y.L. Zhang, D. Liu, G. Zhang, C.D. Shen, P. Ding
A preparation system for OC/EC measurement of radiocarbon in China
The Society of Environmental Toxicology and Chemistry (SETAC), Asia/Pacific Annual Meeting, Guangzhou, China, 4-5 June, 2010.

Y.L. Zhang
Source appointment of aerosols by radiocarbon analysis
1st Year Graduate Student Symposium, University of Bern, Switzerland, 13 September, 2010.

Y.L. Zhang
Source appointment of aerosols by radiocarbon analysis
Seminar of the Laboratory of Radiochemistry and Environmental Chemistry, Paul Scherrer Institute and University of Berne, Switzerland, 19 November, 2010.

PUBLIC RELATIONS AND OUTREACH ACTIVITIES

Analytical Chemistry

Die Botschaft
1000-jähriges Eis, das als Geschichtsbuch dient
26 July 2010

Tages-Anzeiger
Ungewöhnliche Forschungsplätze: Spurensuche im Eis
03 August 2010

Bio Chemie am Samstag, Universität Bern
M. Schwikowski, P.-A. Herren, A. Zapf: Chemische Spuren im ewigen Eis
04 December 2010

Heavy Elements

Bio Chemie am Samstag, Universität Bern
A. Türler: Chemische Experimente mit superschweren Atomen
23 October 2010

Environmental Radionuclides Universität Bern

Homepage Department of Chemistry and Biochemistry, Uni Bern
Molecule of the month: What are the sources of oxalic acid in air-borne particulate matter?
http://www.dcb-server.unibe.ch/dcbneu/mom/mom_2010-12.html
December 2010

Homepage Oeschger Centre for Climate Change Research (OCCR), Uni Bern
A high-tech replacement for the Oeschger Counter
http://www.oeschger.unibe.ch/about/news/news_en.html?ID=9
December 2010

LECTURES AND COURSES

Prof. Dr. A. Türler
Universität Bern, FS2010:
Bachelor
- Instrumentalanalytik II (with others) (3 ECTS)
- Allgemeine Chemie (Einführung Radioaktivität) (with others) (4 ECTS)

Universität Bern, HS2010:
Bachelor
- Physikalische Chemie IV (with Prof. T. Wandlowski) (3,75 ECTS)
- Praktikum Phys. Chemie II (with others) (4 ECTS)
- Biochemische Methoden I (with others) (3 ECTS)

Master
- Nuclear and Radiochemistry (3 ECTS)
- Lab course: Nuclear and Radiochemistry at the PSI (with others) (4 ECTS)
- Seminar Radio- und Umweltchemie in collaboration with Paul Scherrer Institut (organized by D. Schumann)

Prof. Dr. M. Schwikowski
Universität Bern, FS2010:
Bachelor
- Instrumentalanalytik II (with others) (3 ECTS)

Universität Bern, HS2010:
Master
- Environmental Chemistry (with S. Szidat) (3 ECTS)

Dr. M. Ammann
ETH Zürich, FS2010:
- Atmospheric Interface Chemistry (3 ECTS)

Dr. T. Bartels-Rausch
HS2010:
- Lab course: Nuclear and Radiochemistry at the PSI (with Prof. A. Türler and S. Szidat) (4 ECTS)

Dr. R. Eichler
Universität Bern, HS2010:
- Praktikum Phys. Chemie II (with Prof. A. Türler) (4 ECTS)
- Lab course: Nuclear and Radiochemistry (with Prof. A. Türler and S. Szidat) (4 ECTS)

Dr. D. Schumann
- Seminar Radio- und Umweltchemie in collaboration with Paul Scherrer Institut

PD Dr. S. Szidat
Universität Bern, FS2010:
- Ergänzungen zur analytischen Chemie für Pharmazeuten (Vorlesung und praktische Übungen) (2 ECTS)

Universität Bern, HS2010:
- Chemie für Studierende der Veterinärmedizin (with C. Leumann) (4.5 ECTS)
- Environmental Chemistry (with M. Schwikowski) (3 ECTS)
- Praktikum Physikalische Chemie II (with others) (4 ECTS)
- Lab Course: Nuclear and Radiochemistry (with A. Türler and R. Eichler) (4 ECTS)

Dr. K. Zhernosekov
Universität Bern, HS2010:
- Nuclear and Radiochemistry (with Prof. A. Türler) (3 ECTS)

MEMBERS OF SCIENTIFIC COMMITTEES
EXTERNAL ACTIVITIES

Dr. Markus Ammann:
- Air-Ice Chemical Interactions (AICI), Member of Steering Committee
- Atmospheric Chemistry and Physics: member of editorial board
- Member of the IUPAC Subcommittee on gas kinetic data evaluation
- PSI internal research commission (FoKo), member

Dr. Robert Eichler:
- PSI internal research commission (FoKo), member
- Associate Editor of the International Journal of Modern Physics E (IJMPE)
  World Scientific Publishing 2010

Dr. Dorothea Schumann:
- Member of the Nuklearforum Schweiz
- Member of the Schweizerische Gesellschaft der Kernfachleute
- Member of the PSI internal Neutron Source Development Group

Prof. Dr. Margit Schwikowski:
- Member of the Coordinating Committee of the Pages/IGBP initiative LOTRED SA
  (Long-Term climate Reconstruction and Diagnosis of (southern) South America)
- Schweizerische Gesellschaft für Schnee, Eis und Permafrost (SEP), board member
- Member of the Oeschger Centre for Climate Change Research (OCCR)

PD Dr. Sönke Szidat:
- Member of the Oeschger Centre for Climate Change Research (OCCR)
- Treasurer of the Bernese Chemical Society (Berner Chemische Gesellschaft, BCG)

Prof. Dr. Andreas Türler:
- Eidgenössische Kommission für Strahlenschutz und Überwachung der Radioaktivität (KSR), member
- Research Center Dresden-Rossendorf (FZD), member of the advisory board
- GSI Helmholtzzentrum für Schwerionenforschung GmbH, member of the General Program Advisory Committee (G-PAC) and GSI Users Group, member of the Executive Committee (UEC)
- Forschungs-Neutronenquelle Heinz Maier-Leibnitz (FRM-II), member of the committee on instrumentation
- Gesellschaft Deutscher Chemiker (GDCh), Fachgruppe Nuklearchemie, Vorstands-Beirat
- Radiochimica Acta, member of the advisory board

DOCTORAL THESIS

Nolwenn Perron

Radiocarbon-supported source apportionment of carbonaceous aerosols

Prof. Dr. U. Baltensperger / PSI
Prof. Dr. H.W. Gäggeler / PSI & Uni Bern
May 2010

Alexey Serov

On the chemical investigation of superheavy elements (Z>110)

Dr. R. Eichler / PSI
Prof. Dr. H.W. Gäggeler / PSI & Uni Bern
October 2010

Manuel Schläppi

Accumulation rates and chemical composition of precipitation derived from Pío XI ice core, Southern Patagonia Icefield

Prof. Dr. M. Schwikowski / PSI & Uni Bern
December 2010

MASTER THESIS

Bernadette Hammer

Production and distribution of long-lived radionuclides in a lead-bismuth target from ISOLDE

Dr. D. Schumann / PSI
Prof. Dr. A. Türler / PSI & Uni Bern
December 2010

AWARDS

Nadzeya Homazava
Award for the Doctoral Thesis
Development of a novel micro-flow capillary technique online hyphenated to the inductively coupled plasma mass spectrometry for the spatial- and time-resolved investigation of local corrosion
Faculty price of the Faculty of Sciences, University of Bern, February 2010.

SUMMER STUDENTS

Morgane le Floch
HONO uptake on aerosols
University of Orleans, France
April - August 2010

Eva Bühlmann
Stable isotope ratios and ion concentrations in an ice core from the Central Andes
Universität Bern
August - September 2010

Nora Hänni
Isotherme Vakum-Thermochromatographie mit dem leichteren homologen von Element 114: Blei
Universität Bern
July – September 2010

Yannick Suter
Optimierung der Trennungsparameter für „Rostfreier Stahl“
Universität Zürich
July – August 2010

Daniel Infanger
Optimization of radiolabeling reactions of peptides with positron emitters
Universität Bern
August – September 2010

Luca Erhart
3-wöchiges Berufspraktikum zur chemischen Analyse von Gletschereis
Kantonsschule Wettingen
October 2010

VISITING GUESTS AT PSI 2010

25–26 January
Joshua L. Dixon, Sunset Laboratory Inc., Hillsborough NC, USA
A new laboratory OCEC analyzer with NDIR detector

02-03 March
Silvia Lehenberger, TU München, Germany
Experiment ^{177}Lu and ^{161} Tb

02-03 March
Christoph Barkhausen, TU München, Germany
Experiment ^{177}Lu and ^{161} Tb

19 March
Lukas Gutzwiller, Federal Office of Energy, Bern, Switzerland
Swiss climate and energy policy after Copenhagen

23 March
Sebastian Crespo, IANIGLA, Mendoza, Argentina
Discussion of future collaboration on glacier mass balance in the Argentinian Andes

01-26 March
Manabu Shiraiwa, Max Planck Institut, Mainz, Germany
Experiment PROTRAC protein aerosol nitration

21-26 April
Manabu Shiraiwa, Max Planck Institut, Mainz, Germany
Experiment PROTRAC protein aerosol nitration

29 April – 07 May
Tatyana Papina, IWEP SRRAS, Institute for Water and Environmental Problems, Barnaul, Russia
First results from the Mongolian ice core

29 April – 01 May
Matthew Brown, Fritz-Haber-Institut, Berlin, Germany
Discussion of collaboration NAPP at SLS

29 April – 19 May
Elena Mitrofanova, IWEP SRRAS, Institute for Water and Environmental Problems, Barnaul, Russia
Preperation of ice samples for diatom analyses

30 April
Rienk Schnittenberger, ETHZ, Zurich, Switzerland
^{14}C measurements for the investigation of soil dynamics

10-31 May
Yuefang Li, Cold and Arid Regions Environmental and Engineering Research Institute, Lanzhou, China
Interlaboratory comparison of trace element analysis in ice

28 May
Matthias Schädel, GSI, Darmstadt, Germany
From seaborgium to element 114 - experimental techniques and their application in superheavy element research at GSI

28 May
Alexander Yakushev, TU München, Germany
COMPACTible chemistry with elements 108 and 114

05-08 June
Irene Wientjes, IMAU, Utrecht, The Netherlands
Analysis of ^{14}C in ice from Greenland

13 July
Uwe Morgenstern, GNS, Lower Hutt, New Zealand
Tritium and ^{32}Si dating of ice and groundwater

19-20 August
Hendrik Bluhm, Chemical Sciences Devission, Lawrence Berkeley National Laboratory, Berkeley, USA
Ambient pressure XPS für environmental science and Diskkssion NAPP@SLS Design, Zusammenarbeit

06-10 September
Julia Even, Institut für Kernchemie, JohannesGutenberg-Universität, Mainz, Germany
Experiments at Mrs. Piggy, Univ. Bern

07-08 September
Gino Casassa, Centro de Estudios Cientificos, Valdilvia, Chile
Discussion of future projects in Patagonia

04-05 October
Federico Robledo, Ciudad Universitaria, Buenos Aires, Argentina
Discussion of potential collaboration regarding ice core data

29 October
Jon Abbatt, University of Toronto, Canada
Oxidation of organic aerosol: hupaction particle compostition, hygroscopic, and redox cycling potential

04 November
Dominik Fleitmann, Inst. of Geological Sciences and Oeschger Centre for Climate Change Research, Uni Bern, Switzerland
Paleoclimatic significance of chemical and physical parameters in stalagmites

19 November
Timothy I. Eglinton, ETH Zurich, Switzerland
The dynamics and mechanics of organic matter cycling within and between terrestrial and marine environments

10 December
Thomas Leisner, Institute of Technology, Karlsruhe, Germany
Aerosol cloud interaction: Laboratory studies

12-18 December
Carmen Riquelme, University Uppsala, Sweden
Training on ice core cutting and ion chromatography

PAUL SCHERRER INSTITUT

LABOR FÜR RADIO- UND UMWELTCHEMIE DES PAUL SCHERRER INSTITUTS UND DER UNIVERSITÄT BERN

31.12.2010

UNIVERSITÄT BERN

PSI — **Prof. Dr. Andreas Türler** — **Uni Bern**

Angela Blattmann (Secretary / 80 %)

Catrina Veraguth (Secretary / 40 %)

Prof. Dr. Margit Schwikowski (Deputy)

SURFACE CHEMISTRY
Dr. Markus Ammann
Dr. Thorsten Bartels-Rausch
Dr. Adèla Krepelovà
Dr. Markus Lampimäki
Mario Birrer
Yulia Sosedova [1]
Veronika Zelenay [1]
Thomas Ulrich [1]
Sepp Schreiber [1]
Goran Grzinic [1]

ANALYTICAL CHEMISTRY
Prof. Dr. Margit Schwikowski
Leonhard Tobler
Dr. Anja Eichler (50%)
Dr. Gabriela Gramlich (50%)
Roman Bentz
Jonas Schmid (20%)
Sabina Brütsch
Silvia Köchli
Pierre-Alain Herren [1]
Isabella Mariani [1]
Isabel Schuck [1]
Alexander Zapf [1]
Fang Cao [1]
Pavlina Pavlova [1]
Eva Bühlmann [2]

ENVIRONMENTAL RADIONUCLIDES
PD Dr. Sönke Szidat
Edith Vogel
Florian Krättli
Simon Fahrni [1]
Yanlin Zhang [1]

HEAVY ELEMENTS
Dr. Robert Eichler
Dr. Rugard Dressler
Dave Piguet
Alexander Vögele
David Wittwer [1]
Stefan Söllradl [1]

RADWASTE ANALYTICS
Dr. Dorothea Schumann
Dr. Jörg Neuhausen
Dr. Marin Ayranov
Sabrina Lüthi
Tanja Stowasser (50%)
Stephan Heinitz [1]
Matthias Rizzi [1]

RADIONUCLIDE DEVELOPMENT
Dr. Konstantin Zhernosekov
Dr. Alexander Hohn (ZRW)
Holger Dorrer [1]
Maruta Bunka [1]

[1] Graduate student
[2] Master student

AUTHOR INDEX

AFFILIATION INDEX

BAG	Bundesamt für Gesundheit BAG, Abteilung Strahlenschutz, CH-3003 Bern, Switzerland
CEA-Saclay	DSM/DAPNIA/SPhN, Bat.703, CEA-Saclay, 91191 Gif-sur-Yvette cedex, France
CECS	Centro de Estudios Cientificos, Valdivia, Chile
CERN	European Organization for Nuclear Research, CERN CH-1211, Genève 23, Switzerland
CIC	Niels Bohr Institute, Centre for Ice and Climate, Juliane Maries Vej 30, DK-2100 København, Denmark
CWU	Central Washington University, Department of Geological Sciences, 400 E. University Way, Ellensburg, WA 98926, USA
EAWAG	Eidgen. Anstalt für Wasserversorgung, Abwasserreinigung und Gewässerschutz, Überlandstrasse 133, CH-8600 Dübendorf, Switzerland
EMPA	Forschungsinstitution im ETH-Bereich, Überlandstrasse 129, CH-8600 Dübendorf, Switzerland
ETHZ	Eidgen. Technische Hochschule Zürich, CH-8092 Zürich, Switzerland
Friedrich Schiller Univ.	Friedrich-Schiller-Universität Jena, PF 07737 Jena, Germany
FLNR Dubna	Flerov Laboratory of Nuclear Reactions, Joliot Curie 6, 141980 Dubna, Russia
FS INVENTOR	FS Inventor AG, Muristr. 18, CH-3132 Riggisberg, Switzerland
FZD	Helmholtz-Zentrum Dresden-Rossendorf, Bautzner Landstr. 400, 01328 Dresden, Germany
FZ Jülich	Forschungszentrum Jülich GmbH, Leo-Brandt-Str., D-52428 Jülich, Germany
GFA	Large Research Facilities (GFA), Paul Scherrer Institut, CH-5232 Villigen PSI, Switzerland
GNS	GNS Science, PO Box 30-368, Lower Hutt 5040, New Zealand
IDPA-CNR	Institute for the Dynamics of Environmental Processes e CNR, University of Venice, Dorsoduro 2137, 30123 Venice, Italy
Inselspital	Klinik und Poliklinik für. Nuklearmedizin, Univ.-Spital Bern, 3010 Bern, Switzerland
ILL	Institut Laue-Langevin, 6, Rue Jules Horowitz, BP 156 - 38042 Grenoble Cedex 9, France
IMAU	Institute for Marine and Atmospheric Research Utrecht, Utrecht University, Princetonplein 5 3584 CC Utrecht, The Netherlands
Institute of Tibetian Plateau Research	No. 18 Shuangqing Rd, Haidian District, Beijing, P. R. China, 100085
IRCELYON	Institut de recherches sur la catalyse et l'environnement de Lyon, Université Lyon1 and Centre national de la recherche scientifique, 69622 Villeurbanne cedex, France
IRS Hannover	Institut für Radioökologie und Strahlenschutz, Herrenhäuser Str. 2, 30419 Hannover, Germany
IWEP	Institute for Water and Environmental Problems, Siberian Branch of the Russian Academy of Sciences, 105 Papanintsev Str., RU-Barnaul 656099, Russia
KFKI	Atomic Energy Research Institute, Konkoly-Thege 29-33, 1121 Budapest, Hungary
KUP	Climate and Environmental Physics, Physics Institute, University of Bern, Sidlerstrasse 5, CH-3012 Bern, Switzerland
LAC	Laboratory of Atmospheric Chemistry, Paul Scherrer Institut, CH-5232 Villigen PSI, Switzerland
LBNL	Lawrence Berkeley National Laboratory, Berkeley, CA 94720, USA

LGGE	Laboratoire de Glaciologie et Géophysique de l'Environnement, (UMR 5183), 54 rue Molière, 38402 - Saint Martin d'Hères cedex, France
LOG	Fachbereich Logistik, Paul Scherrer Institut, CH-5232 Villigen PSI, Switzerland
Massey Univ.	Massey University (Albany Campus), Private Bag 102904, North Shore MSC, Auckland, New Zealand
MPI-CH	Max-Planck-Institut für Chemie (Otto-Hahn-Institut), Joh.-Joachim-Becher-Weg 27, 55128 Mainz, Germany
NES	Nuclear Energy and Safety Research Department, Paul Scherrer Institut, CH-5232 Villigen PSI, Switzerland
NPI	Norwegian Polar Institute, N-9296 Tromsø, Norway
NUM	Research with Neutrons and Muons**,** Scherrer Institut, CH-5232 Villigen PSI, Switzerland
OCCR	Oeschger Centre University of Bern, Zähringerstrasse 25, CH-3012 Bern, Switzerland
PNNL	PNNL: Pacifc Nortwest National Laboratory, Richland, WA, USA
PTB Braunschweig	Physikalisch-Technische Bundesanstalt (PTB), Bundesallee 100, D-38116 Braunschweig, Germany
PSI	Paul Scherrer Institut, CH-232 Villigen PSI, Switzerland
SLF	Institut für Schnee- und Lawinenforschung, Flüelastr. 11, CH-7260 Davos, Switzerland
SLS	Swiss Light Source, Paul Scherrer Institut, CH-5232 Villigen PSI, Switzerland
SWAN	SWAN Isotopen AG, Freiburgstrasse 18, 3010 Bern, Switzerland
TU Wien	Technische Universität Wien, Karlsplatz 13, 1040 Wien, Austria
Univ. Auckland	The University of Auckland, Private Bag 92019, Auckland 1142, New Zealand
Univ. Bern	Departement für Chemie und Biochemie, Universität Bern, Freiestr. 3, CH-3012 Bern, Switzerland
IPS Univ. Bern	University of Bern, Institute of Plant Sciences, Altenbergrain 21, CH-3013 Bern, Switzerland
Univ. Colorado	NCAR Earth System Laboratory and CIRES, University of Colorado, Boulder, CO, USA
Univ. Dresden	Technische Universität Dresden, D-01062 Dresden, Germany
Univ. Fribourg	Av. de l'Europe 20, 1700 Fribourg, Switzerland
Univ. Innsbruck	Innrain 52, A-6020 Innsbruck, Austria
Univ. Latvia	University of Latvia, 19 Raina Blvd., Riga, LV 1586, Latvia
Univ. Maine	Climate Change Institute and Department of Earth Sciences, University of Maine, Orono ME 04469, USA
Univ. Tallinn	Institute of Geology, Tallinn University of Technology, 10143 Tallinn, Estonia
Univ. Venice	University of Venice Ca' Foscari, Environmental Science Department, Calle Larga Santa Marta 2137, IT-30123 Venezia, Italy
Univ. Vienna	University of Vienna, Dr.-Karl-Lueger-Ring 1, 1010 Wien, Austria
Uni Zürich	University of Zurich, Winterthurerstr. 190, CH-8057 Zürich, Switzerland
UoT	University of Toronto, 27 King's College Circle, Toronto, Ontario, Canada M5S 1A1
UU	Department of Earth Sciences, Uppsala University, Villavägen 16, S-752 36 Uppsala, Sweden
Victoria Univ. Wellington	Victoria University of Wellington, PO Box 600, Wellington 6140, New Zealand

Paul Scherrer Institut, 5232 Villigen PSI, Switzerland
Tel. +41 (0)56 310 21 11, Fax +41 (0)56 310 21 99
www.psi.ch